Thesis for the Master of Science

Degree Program: Space Science and Technology

Impact of Climate and Land Cover Change in Urban Heat Islands

Supervisor:	Prof. Dr. Annette Ladstätter-Weißenmayer
Secondary Supervisor:	Dr. Adrian Fessel
Submission Date:	13.05.2024

Linus Andrae	Hegelstraße 24
	28201 Bremen
Matriculation Number:	6015384

Universität Bremen

Abstract

Urban Heat Islands (UHIs) pose a growing health risk by exacerbating heat stress for residents of urban areas. Due to the increased prevalence of extreme weather events, urbanization and heat waves and as a cause for higher energy consumption, UHIs become more relevant as a topic for city planners and policy makers to consider. Identification of areas most impacted or at risk require a data backed tool set to aid urban planning. This work investigates the impact and influence of rising temperatures and land use changes in cities on the severity of the UHIs within them. In this case study different methodologies where combined and extended to find UHIs within the city of Bremen. The introduction of a statistical measure reduces seasonal effects on severity of UHIs. The study shows that sealed surface types are dominant in strong UHIs (with more than 3σ above average temperature of the surrounding rural area). The data indicate an increase in size and a combining of surface urban heat islands with rising temperatures. More research could give insight in how this impacts air temperatures and if vegetation corridors within affected areas could limit and mitigate this effect.

Keywords: Urban Heat Islands, Climate Change, Land Use/ Land Cover, Image Processing, K-Means

Contents

List of Figures

List of Tables

Acronyms

DWD Deutscher Wetter Dienst. 25, 49, 53, 61

ESA European Space Agency. 2

HI Heat Index. 16, 17, 61

LST Land Surface Temperature. v, vi, 14, 35, 36, 40, 41, 48, 59

LU/LC Land Use/ Land Cover. iv, v, 4–6, 28, 32, 33, 42, 60, 62, 63

ML Machine Learning. 18

NDVI Normalized Differential Vegetation Index. v, 15, 35, 36, 42–44, 60

SUHI Surface Urban Heat Island. 5, 6, 8, 9, 13, 25, 26, 28, 49, 60

TOA Top of Atmosphere. 14, 48, 49

UHI Urban Heat Island. i, iv–vi, ix, 1–9, 11–15, 25–28, 38, 39, 45–49, 53, 57–61, 63

USGS United States Geological Survey. v, 3, 49

VOC Volatile Organic Compounds. 10, 11

WBGT Wet Bulb Globe Temperature. 17, 61

Glossary

Area Of Interest A area that contains the city or structure to be investigated. 62

Dilation An image processing operation that extends objects by adding pixel to the outside of an object. 34

Environmental Protection Agency U.S. Government organisation tasked with protection of the health of humans and the environments. 1

Erosion An image processing operation that reduces the size of objects by removing pixels at the border of the object. 34

Inter-Agency Standing Committee The *Inter-Agency Standing Committee* is an UN Organisation coordinating different bodies of the United Nations. 1

Mean Squared Error Algorithm to calculate the difference between two sets of data (see eq. (9)). 31, 33

Sentinel-3 A Pair of Satellites, that are part of the Copernicus constellation. Using 21 spectral channels with a resolution of 300 m per pixel. 3

Structural Similarity Measure Algorithm to calculate the similarity in Images (*Zhou Wang et al. 2004*). 31, 33, 45

Acknowledgements

This master thesis would not have been possible without the help of countless of people around me, to some of whom I would like to show special gratitude.
First I wish to thank my girlfriend and family for supporting me and listening to my complains and allowing me to work long hours during the final phases of this work, who always supported me and helped in lightening my spirit during the thesis. I'd also like to thanks all family members and friends that helped me by proofreading and supporting me while writing this thesis. I would not have come so far without the support and privilege of having this supportive people at my side.

My deepest gratitude goes to my principle supervisor Prof.-Dr. Annette Ladstätter-Weißenmayer, that sparked my interest in the topic of UHI during the lecture *Biogeochemistry* and introduced me to the cooperation partner OHB Digital Connect GmbH. She also help me in countless meetings with answers to my questions, interesting ideas and general support for the thesis. She also provided me guidance for my career and her advocacy have profoundly impacted the successful completion of this work and my academic career.

Further I'd like to thank my secondary supervisor Dr. Adrian Fessel who helped me immensely with the development of the image processing pipeline and always had helpful suggestions and ideas on how to overcome problems and limitations when working on the processing software and deepen my understanding in machine learning and remote sensing. He always had helpful suggestions and supported my work in many different ways and gave many insightful guidances to how to handle all kinds of problems.

I would also like to thank the nice people at OHB Digital GmbH especially Daro Krummrich that helped me with lots of organisational support and lots of very smart advice and support during the time of writing, he always had my back and my best interest in mind. He and all colleagues at OHB always had helpful tips and advice when I had any questions. I'd also like to thank all the numerous scientists working in this field and dedicating whole careers on providing insides into our everyday live and environment and on whoms publications I was able to base this work on.

1 Introduction

The investigation of Urban Heat Islands are a very important topic in times of climate change and urbanization.
Urban environments have been the interest of studies for a long time, but increases in frequency and intensity of extreme weather events and heat waves are significantly more likely to happen (*Uhe et al. 2016*). These are expected to appear with intensities that were nearly impossible without the impact of climate change (*Bador, Terray, and Boé 2016*). This is well understood and can be attributed to anthropogenic climate change on larger scales, but local effects and impact of climate change on a small scale is harder to simulate and understand. The major issue is that the missing impact of localized phenomena such as weather, terrain and urban climate are not covered by climate models, making prediction of extreme heat waves with high accuracy difficult (*Van Oldenborgh et al. 2022*). Studying and understanding the local urban climate has a long history, including the understanding of Urban Heat Islands (UHIs) and impacts of urban atmospheric pollution on humans and the greater atmosphere. Together with research the need for tools and data processing platforms are demanded by different organisations (such as the Inter-Agency Standing Committee (Extreme heat *2022*) and the Environmental Protection Agency (Launching a Cross-Agency Temperature Network *2024*)) to prepare affected areas and organisations for heat mitigation in urban areas.

1.1 An historical overview of urban heat research

The scientific investigation of the urban climate and the influence of human settlements and activity on the local atmosphere and temperature has been studied for more then 200 years. *Howard 1833* investigated the climate of London in a study from 1819 to 1827 and a similar study was conducted in Paris in the 1850s by *Renou 1862*. The first mobile measurement campaigns around the topic of urban climate were conducted by *Peppler 1929* and *Tollner 1932* and investigated the spacial distribution of temperatures within urban areas in the 1920s in Germany and Austria. This type of measurement were repeated in multiple cities around the globe at the time.
The term UHI was coined in the 1960s in publications regarding case studies in London (*Chandler 1961*) and Montreal (*Oke 1968*). During this time the influences and understanding of the interaction between the human industrial activity, the land change by urbanisation and industrialization and the influence of these factors on temperatures was investigated by numerous case studies using fixed or mobile weather stations. Health problems within industrial areas or incidents like the 1930 Meuse valley fog catastrophe, in which exhaust gases, including fluorine gas, combined with an inversion weather condition, forming a cloud over the area causing the death of at least 60 people (*Nemery, Hoet, and Nemmar 2001*).

The *Great Smog of London* in 1952, a similar event lasting four days, causing 4000 direct deaths and between 10000 and 12000 deaths from consequences of the fog in the months after (*Bell, Davis, and Fletcher 2004*), triggered scientific interest in the interaction between human settlement, pollution and meteorological phenomena on human health and the environment. The investigation of incidents like this using scientific methods shaped the idea of an man made urban climate.

To understand the urban meteorology in three dimensions the first use of balloons, helicopters and air planes to measure vertical temperature profiles were documented in the 1950s (*Duckworth and Sandberg 1954*). These studies focused on the atmospheric heat distribution over urban areas and resulted in the development of physical energy transport models for these atmospheric urban heat islands. These models required a deeper understanding of the surface properties and the temperature distribution within the urban area.

Then newly available remote sensing devices, such as infrared imagers, made it possible to observe the urban environment from above and detect temperature hot spots using airborne and satellite images.
First investigations regarding the feasibility of this approach were proposed in the late 70s (*Watson 1975*, *Carlson, Augustine, and Boland 1977* and *Block 1978*) but the resolution of satellite images were insufficient for detailed investigations of UHIs.
A first study using satellite infrared imagery were conducted in 1978 using the NOAA 5 Satellite (with a spacial resolution of 1km (*Matson et al. 1978*)).
Multiple studies in the 70s and 80s used images taken from planes or helicopters to aid the investigation of smaller scale effects within the urban surface temperature distribution (e.g. *Landsberg 1979*, *Ljungberg and Norberg 1980* and *Foster, Ormsby, and Gurney 1981*).
With advances in satellite technology, the resolution and data availability increased significantly. The Landsat program started in 1975 and with the launch of *Landsat 4* in 1982 thermal infrared data of the whole planet were continuously provided. The infrared resolution that allowed pixel sizes between 60 m (*Landsat 7*) and 120 m (*Landsat 4* and *Landsat 5*), made investigations of smaller patterns within urban areas possible.
Many different satellites have been launched since, closing gaps in spectral, spacial and temporal coverage, with different resolutions for different use cases. Relevant for investigation of the urban climate are the ASTER and MODIS instruments on the Terra satellite, providing a high revisit time and are useful for land cover monitoring. The ASTER instrument provides thermal data with high spacial resolution and a large dataset was created from ASTER data of the land surface properties (this dataset is used, among others, in the creation of the Land Surface Temperature product form the Landsat 8 and 9 satellites). The European Space Agencys (ESAs) Copernicus satellites provide high spacial

resolution visible data (Sentinel-2) as well as surface temperature (Sentinel-3).

The increased revisit frequency of roughly two weeks made remote satellite data a more

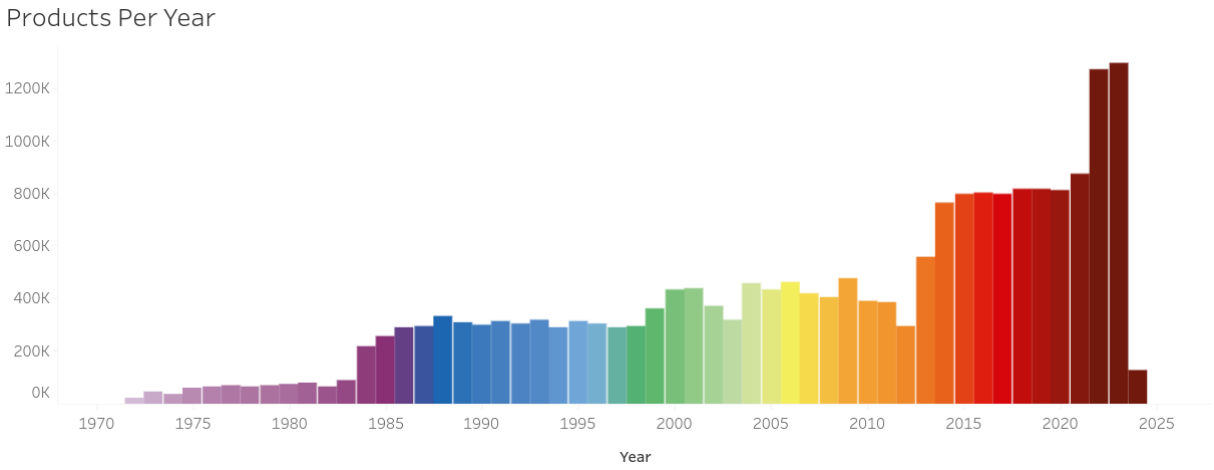

Figure 1: Number of Landsat Products per year over time (as of Feb. 2024) by the USGS (*U.S. Geological Survey 2024*)

useful and widely used tool in the research on urban meteorology and urban heat islands. Over the past 30 years, the amount of available remote sensing data skyrocketed, Landsat 8 and 9 alone produced over 6 million images since the start of operation in 2013. Figure 1 shows the number of scenes taken by the Landsat satellites per year. The rise in availability on the one hand makes it easier for researchers and companies to use the data, requiring increased computing and storage availability, to manage the increased data amount. This offers the possibility of creating scientific studies covering a wide range of cities over time, using the same sensor and tools.

In *Sobrino and Irakulis 2020* a methodology to compare UHIs using Sentinel-3 images was proposed and a broad study of UHIs severity in cities around the world was conducted. Over the past years the number of scientific papers investigating the issue from multiple angles increased significantly (ct. *Piracha and Chaudhary 2022, P. 3*).

In conclusion, the advancement of remote sensing technology, particularly the availability of infrared imagers and satellite imagery, has revolutionized the study of UHIs. From the early investigations and roots of the field in meteorology and public health the research field expanded touching urban development, climate science, atmospheric chemistry and medicine as well as social sciences.

The abundance of data provided by satellites like Landsat 8 and 9 now allows researchers to conduct long duration, high resolution studies. Analysing urban surface temperature distribution with unprecedented detail and accuracy. The increase in data availability has not only facilitated research on urban meteorology and heat islands but has also presented new challenges in terms of data management and analysis that require the creation of performative analysis software and methods to extract, monitor and analyse urban areas

during change.
Despite these challenges, the potential for conducting comprehensive studies across various cities using consistent sensor data and combining multiple sensor sources allows a deep understanding and continuous monitoring of the urban environment. The coming years promise even more missions that can be used for detecting urban heat islands, with nearly daily coverage and higher spacial resolution (e.g. ESAs LSTM mission with 50 m resolution and a 4 day revisit time *CEOS 2024*). Together with fusion approaches to combine different datasets to reduce error and increase spacial resolution (as done in e.g. *Camps-Valls and Bruzzone 2009*), monitoring services, heat warning systems and verification of implemented mitigations in cities by creating long term analysis of urban areas are about to become feasible.

The next step in advancing the comprehension of UHIs involves gaining a deeper understanding of how various parameters contribute to the formation and intensity of UHIs. With the wider adaption and interest in to the introduction of countermeasures to UHIs and climate change resilience techniques in different cities, continuous monitoring of UHIs and the urban climate is necessary to judge effectiveness of the taken countermeasures. To do this efficiently, statistical parameters and indices are crucial in order to assess the effectiveness of the mitigation strategies.

1.2 Research Question

In this thesis, the impacts of land cover, land cover changes such as urbanisation, and rising average temperatures due to anthropogenic climate change on the UHI phenomena are investigated. The specific questions posed are:

1. What definition can be used to define UHIs comparably?
2. What is the influence of LU/LC change on the size of urban heat islands?
3. How significant is the impact of urbanisation on UHIs, both in terms of absolute and relative temperature changes?
4. What is the effect of rising average temperatures on the UHIs effect?
5. What indices can be used or created to categorize and rate UHI intensity?

The first question tackles the problem that the UHI phenomenon and its definition was refined over time. For answering the question different types of UHIs (see section 2.1) have to be distinguished and methods for measuring them found. The goal is to find a definition that allows investigation and detection of UHIs in a comparable way, to allow global measurement and comparison between cities and regions.
The second and third question investigates the impact urbanisation and surface sealing

on the intensity and size of urban heat islands. This can help in urban planning and mitigation of effects of UHIs in areas at risk.
The goal of the fourth questions is to answer how much the rise of local temperature and the global mean temperatures due to climate change is affecting the intensity and size of UHI effect in cities. The fifth and last question shall answer what indices that are already given can be used to describe heat islands or if there is the need to create a new index for measuring intensity and human impact of UHI effects within cities.

1.3 Methodology

To address the outlined research questions, multispectral satellite images are used to extract temperature and surface information. This data is used and processed and urban areas are extracted. The data is compared with measurements from ground based stations and statistical analysis is conducted to answer the questions posed above.

1.3.1 Data Sources

Multi-spectral visible and thermal infrared satellite images are used to measure and identify Surface Urban Heat Islands (SUHIs) and analyse land surface temperature. The used satellite data product is described in section 2.1.5. The LU/LC data is referenced against a LU/LC product for validation.
For air temperature data the data of weather stations within the area of interest are used, more details can be found in the section 5.3 and section 6.3.

1.3.2 Procedure

The satellite data (s. section 2.1.5) is selected using filters and manual selection to find cloud free images of the area of interest in the time period that was selected for analysis. The dataset is downloaded and the area of interest is extracted to reduce the data footprint. This dataset is also used to classify the land cover to allow short term land cover analysis using machine learning algorithms for classification. For the further analysis a time series of LU/LC is created for the city of Bremen.
From the dataset a longitudinal analysis of UHIs intensity over time is created. For the selected days where satellite cover is available, temperature data and other sources are used to create indices to measure heat stress and other parameters for assessing UHIs intensity at different days. This data can then be used to create projections of UHIs development based on the findings from SUHI measurements and LU/LC analysis. Section 3.2 explains the used processing steps in detail.

1.4 Structure of the Thesis

In the introduction as well as in section 2, previous work and an overview of the current understanding of the UHI effect and research in this area is given. Section 4 explains the used adaptation of the proposed methodology by *Sobrino and Irakulis 2020* to create a definition of SUHIs that is usable for comparing UHIs in different cities. Section 5 explains how the measurements and investigations of the impact of LU/LC changes by build up where done. In section 6 the impact of changing temperatures an increase of extreme weather phenomena on the intensity and seasonal variety of UHIs was investigated. After these the section 7 combines the findings of the previous chapters, shows which further studies could investigate the UHI phenomena and where this research could be improved.

2 Background

2.1 Urban Heat Islands

Urban Heat Islands (UHIs) are areas with increased temperature in urban areas. Due to increase in global temperature as well as increased occurrence of extreme weather and longer periods of heat waves, this phenomenon will likely increase in intensity and will also occur in cities at higher latitudes (*Sachindra et al. 2016*, *Wilby 2008, p. 904*). UHIs are a spacial phenomenon that occurs on different scales and intensities, this makes observation using remote sensing data a good and widely used approach (*Weng 2003*).
UHIs are distinguished into surface and atmospheric UHIs as discussed in the sections below. The major background effect behind UHIs is the change in energy transfer of solar radiation on urban surfaces. Compared to rural areas, the urban environment has

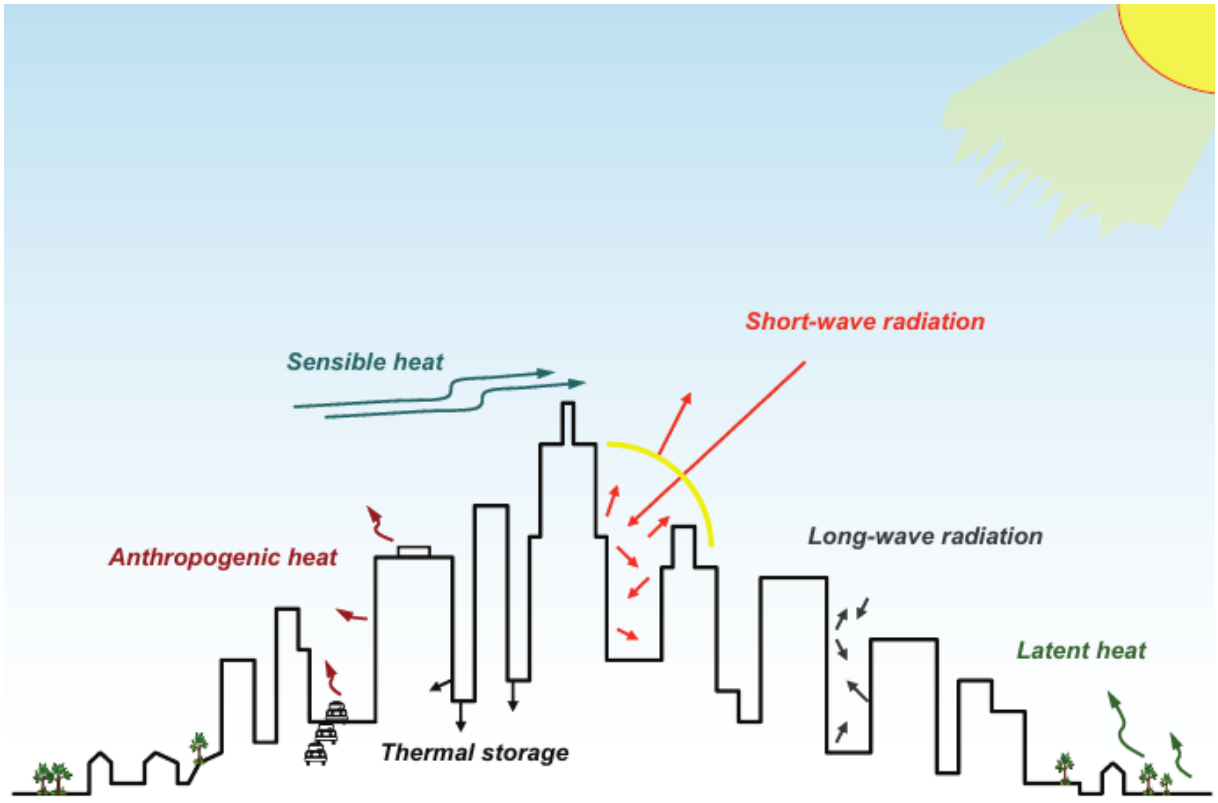

Figure 2: The Urban Energy Budget (, Reprinted from *U.S. Environmental Protection Agency (EPA) 2008, Fig. 7*)

additional reflective surfaces, creating additional energy transfer increasing the fraction of the incoming short wave solar radiation that is not reflected back towards the atmosphere (*U.S. Environmental Protection Agency (EPA) 2008, p.12*). Due to lower vegetation cover and higher sealed surfaces the amount of latent heat due to evaporation and transpiration is lower. The fraction of infrared radiation that is trapped within the urban area, especially if the sky view factor is low, is higher.

An additional influx of thermal energy is anthropogenic emission from industrial production. The guiding equation is the equilibrium of incoming solar radiation and the outgoing upwards radiation. The incoming radiation (R_n) is matched by

- Latent heat transfer of evaporation and transpiration (lE)
- Sensible heat transfer due to wind and upwelling warm air (H),
- Storage in surfaces (S)
- Metabolic conversion by photosynthesis (M)

This gives eq. (1) with R_n being positive and all other terms negative.

$$R_n + lE + H + S + M = 0 \tag{1}$$

In rural areas, lE and M are bigger due to vegetation, while the S term is larger due to surface properties mentioned above. H depends strongly on urban morphology, so urban or rural areas can have higher sensible heat transfer rates.

Since the phenomenon is known for a long time, mitigation strategies have been proposed to reduce the impact on well-being and intensity of the UHIs and are touched upon in section 2.1.4. Section 4 will go into more detail of the definition of UHIs for comparison within the scope of monitoring and remote sensing.

2.1.1 Atmospheric Urban Heat Islands

Atmospheric UHIs are sections with increased air temperatures within an urban area. These are more dependent on weather and local topology and are in part caused by the slower cooling rate of build up land, responsible for SUHIs. The main factors in forming UHIs is the thermal storage capacity of materials used in urban areas like concrete, asphalt and steel, that have a high heat capacity and heat up quickly during the day and emit the stored thermal energy as sensible heat with a delay (eg. during the night (*Prathap Ramamurthy et al. 2014*)). High surface sealing and lack of vegetation reduce surface water availability and diminish evaporation and the cooling effect of latent heat causing more thermal energy to be available as sensible heat. Another factor is the heat produced by human activity such as industrial processes and combustion engines. As a consequence of higher temperatures, active cooling devices (such as air conditioners) are more frequently used for buildings and vehicles, converting electrical or chemical energy to thermal energy stored in the urban atmosphere. The emitted thermal energy of these heat pumps further increases the surrounding temperature, reinforcing the effect.

2.1.2 Surface Urban Heat Islands

SUHIs are areas of higher surface temperatures within urban areas compared to rural areas due to the materials used and heat from mobility, electrical appliances, heating and cooling as well as less vegetation and higher sealed surfaces that reduce surface water availability (*U.S. Environmental Protection Agency (EPA) 2008, pp. 7–12*). The SUHIs are a small scale phenomenon that has a high seasonal variability and is most intense in summer. SUHIs are an important factor for the development of atmospheric UHIs due to the following factors:

- Surface material radiates off the stored heat during the night, increasing urban air temperature
- Surface types are susceptible to regulatory influence allowing direct implementation of countermeasures by local government and direct action of citizens.
- Surface materials are one major factor in the development of UHIs shown in section 5.

Since atmospheric UHIs can not be directly observed using remote sensing data and are therefore not in focus of this work, the terms UHI and SUHIs are used interchangeably in later sections of this document.

2.1.3 Air pollution and Urban Heat Islands

Air pollution has been a documented problem for the quality of life since the start of the industrialisation. While in the 19th and first half of the 20th century the major problem came from unfiltered exhaust, burning coal and wood for heating and heavy industry. The major pollutants in urban areas in the 21st century come from car exhaust, industrial processes and by-products of industrial agriculture (*Leung 2015* and *McDuffie et al. 2021*). Especially large urbanized areas are susceptible to air pollution due to increased concentration of combustion and industrial activity on a small area (*Kanakidou et al. 2011*). One major pollutant with a significant health impact is tropospheric ozone, that is produced in larger quantities within environments with elevated temperature (see *Ebi and McGregor 2008*).

Ozone in the troposphere is mainly produced when (anthropogenic) NO_x emissions from fossil fuel burning and Volatile Organic Compoundss (VOCs) from anthropogenic or natural sources react with oxygen under UV influence in a photochemical reaction. The creation of ozone is dependent on UV intensity (and therefore insolation) and temperature, increasing between 2.2 and 3.2 ppbv/°C depending on NO_x and VOCs availability. Recent studies found that reduction of NO_x and VOCs concentration, reduces O_3 temperature dependence (*Otero, Rust, and Butler 2021*). Sources of VOCs are mainly of natural origin (*Kansal 2009*), anthropogenic sources are vapours and fumes from solvents and mainly originate from industrial processes while the main natural source of VOC are trees. Trees and other plants release VOCs like isoprene and terpenes as a protective mechanism against temperature stress and to protect from insects and pests. The usefulness of these VOCs for trees varies over the year. This gives the VOC and the resulting O_3 emission a high seasonal variability (see Figure 3). The resulting tropospheric ozone, is

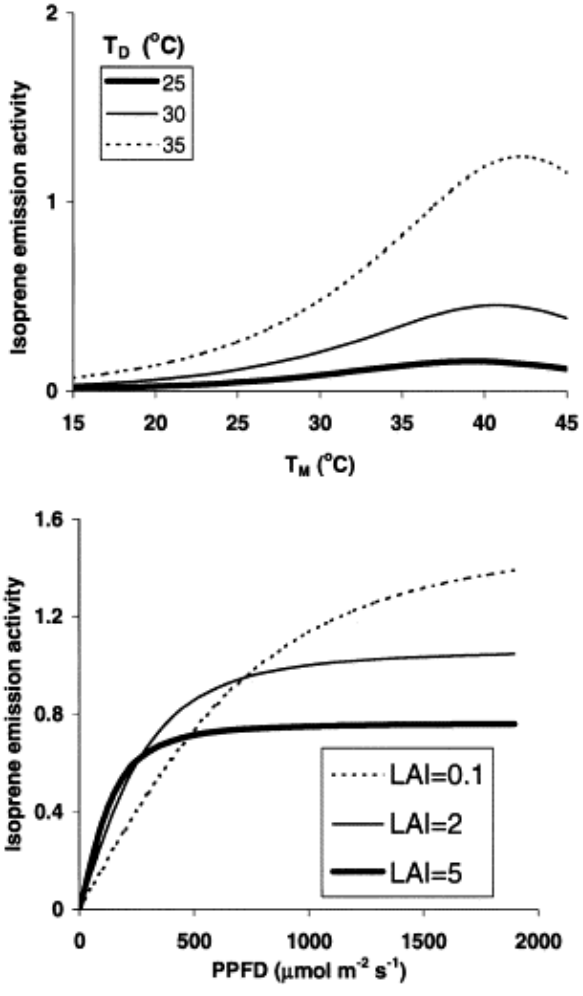

Figure 3: Temperature dependence of isoprene emission of 15 minute (T_M) and 15 day (T_D) mean temperature, with permission from *Guenther et al. 2000*

a major health concern, it is directly toxic to humans and is shown to cause lung damage by oxidative stress in the lung lining tissue (see *Mudway and Kelly 2000*). With rising global temperatures the number of days with temperatures causing heat stress in trees (e.g. with a temperature above 30 °C shown in Figure 3) has been increasing even at higher latitudes (Figure 4 shows the German average of days exceeding 30 °C growing from 1950 from an average of 5 to 11.3 in 2023). Due to the effect of UHIs causing a further increase

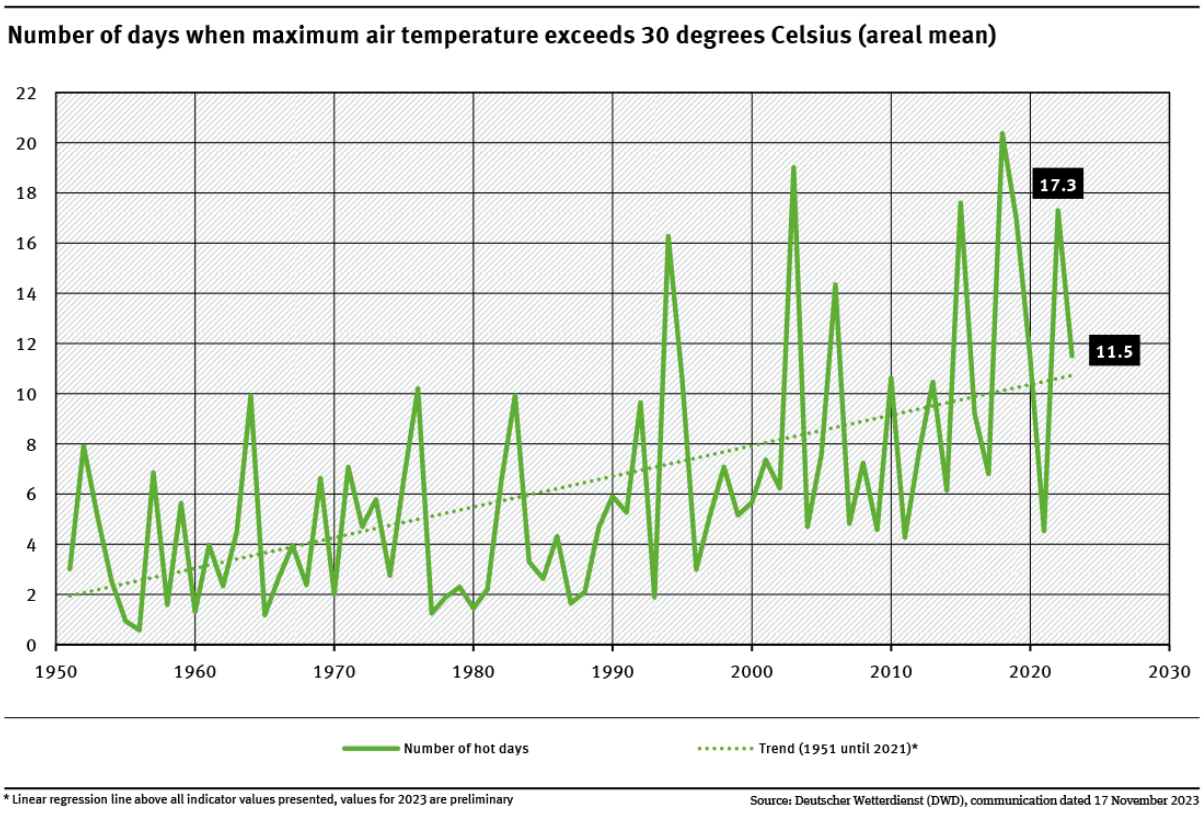

Figure 4: Days with a maximum temperature of more then 30 °C in Germany (Reprinted from *Wilke 2023*)

in temperature within urban areas, there is an expected increase of tropospheric ozone levels due to higher VOCs emission from urban and sub-urban trees due. This increases air pollution increases mortality and causes other negative health consequences within urban areas (shown in *Ebi and McGregor 2008*).
Studies have shown, that reduction of UHIs by urban greening reduces the amount of ozone by 5–8% (*Fallmann, Forkel, and Emeis 2016, p.209*).

2.1.4 Mitigation techniques for Urban Heat Islands

There are multiple adverse effects and possible mitigation techniques for the reduction of UHIs (e.g. *Nichol 1994* and *Stewart 2011*) some of which are natural phenomena. Advective cooling can be observed when the temperature gradient generates airflow from the cooler

surrounding areas towards the hot areas within the city, cooling it down according to the second law of thermodynamics (*Haeger-Eugensson and Holmer 1999*).
Urban areas with no close water body and with low average wind speed are more likely to be affected by urban heat islands (*P. Ramamurthy and Bou-Zeid 2017*). Since water reduces the severity of heating, due to sea breezes as well as latent heat transport and acts as a thermal capacity, dampening heating effects. Higher temperatures due to UHIs cause stress to animals and humans, increasing health risks due to heat stroke and increased surface level ozone concentration (see *Santamouris 2020*).
The attempt to reduce urban heat build-up and the associated heat related health problems in cities is older than scientific work on this field of study. In hot areas around the globe different methods were used to create spaces with cooler temperatures for rest and work. All over the Mediterranean, houses are painted white to increase albedo of roof surfaces, decreasing heat build-up. In newer studies, this traditional painting pattern has shown to be an efficient counter to high solar intensities (*Fayad, Maref, and Awad 2021*).
Another method of larger scale cooling is the increase of vegetation to increase latent heat transport and water availability. Two basic physical principles make water well suited for cooling and energy transfer. Water has a latent heat of vaporization of $2440kJ \cdot \mathrm{kg}^{-1}$ at 25 ° C and the capacity of water vapor in higher temperature air is increasing exponentially. Saturation vapor concentration increases from $\approx 17.5\mathrm{g} \cdot \mathrm{m}^{-3}$ at 20 ° C to $\approx 52\mathrm{g} \cdot \mathrm{m}^{-3}$ at 40 ° C. This means that, given surface water availability, high amounts of water can be vaporized and will carry away higher amounts of thermal energy in higher temperature condition. Reducing temperature in the surrounding area. Active evaporative cooling was used and studied in arid climates over the past decades, showing effective at low air humidity providing 10 to 15 K cooling during high heat hours (*Vanos et al. 2022*).

While high relative humidity, at high temperatures, has significant health risks (see section 2.4.2), evaporation reduces temperature. *Pontes et al. 2022* developed a comfort zone, based on the Heat Index, founded on field measurements and previous research. This could be used to find an optimum between increase in relative humidity and air temperature e.g. by limiting the use of moisture based active cooling or adding evaporation control covers as already shown effective in areas with high insolation *Ghazvinian et al. 2021.*
Green roof concepts, green facades, parks or street trees all show effective in reducing temperatures within the urban environment (see *Dimoudi and Nikolopoulou 2003; Feyisa, Dons, and Meilby 2014; Gartland 2008; Prathap Ramamurthy et al. 2014*). The study by *Fallmann, Forkel, and Emeis 2016* mentioned in section 2.1.3 also showed that urban greening has a more beneficial effect compared to high reflective surfaces. Due to the increase in back scattering of high energy radiation of reflective surfaces, ozone is created during high insolation, providing additional health risks. The same simulation showed that

urban greening can limit boundary layer mixing due to reduced thermal updraft caused by lower turbulent kinetic energy, increasing pollution levels at street level. This problem can be solved by employment of established methods for reduction in urban pollution, e.g. increase of public transport and regulation or taxation for high pollution vehicles and industries.

Adding water bodies inside the city as well as "sponge-city"-concepts are also promising approaches to mitigate heat islands (*He et al. 2019*). Increasing the water available can also be archived using different, less sealed surfaces, such as grass pavers or permeable pavements, that cause less run-off (*U.S. Environmental Protection Agency (EPA) 2008, p. 7*).

2.1.5 Landsat 8 & 9 Dataset

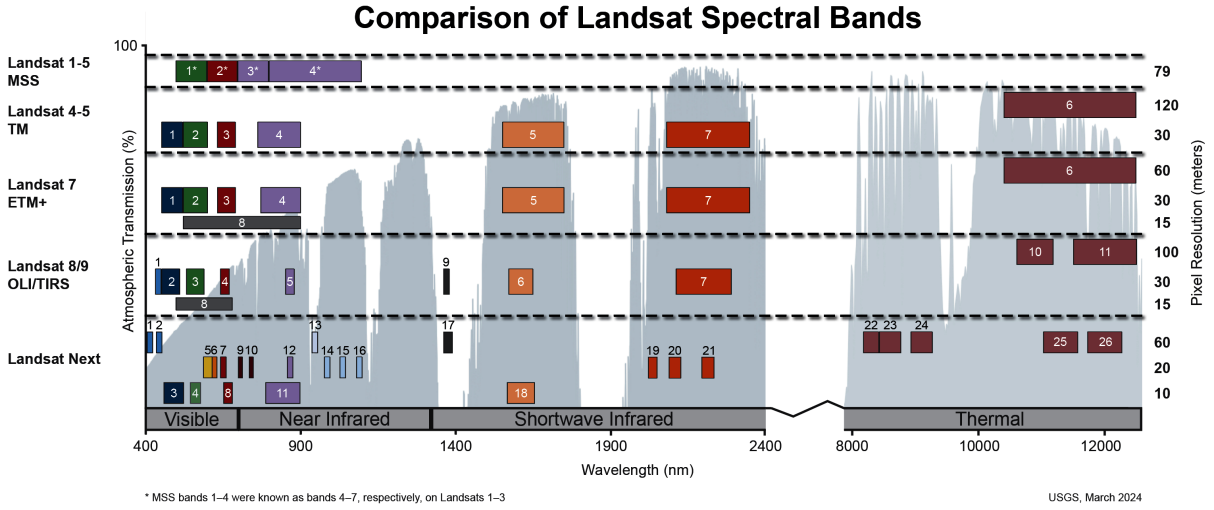

Figure 5: Landsat 8 and 9 instrument spectral bands (second to last row) compared to other Landsat missions(*USGS 2014*)

Using remote sensing data to detect and analyse SUHI requires devices that are able to detect thermal infrared radiation. Satellites that are equipped with thermal infrared sensors, are able to detect upwelling emission from the surface within the $8\mu\ m < \lambda < 12\ \mu m$ range. Instruments that were previously used for measuring UHIs are Landsat, MODIS, ASTER and Sentinel-3. In the following steps data from the Landsat 8 and Landsat 9 satellites were used. Landsat 8 and Landsat 9 both have a TIRS (Thermal Infrared Sensor) and an OLI (Operational Lands Imager) instrument on board that measure in two and nine bands respectively. Since the start of Landsat 9 the availability of scenes increased and the shorter revisit times allow a denser mapping and reduced risk of cloud cover.

The OLI covers a wavelength of 0.43 μm to 1.83 μm separated into 9 bands with a resolution of 30 m per pixel (see Figure 5). For the calculation of thermal infrared emission of the Earth's surface the TIRS instrument contains two bands within the thermal infrared

covering wavelength between 10.6 μm and 12.51 μm with a resolution of 100 m. Both satellites have a revisit time of 14 days.

2.2 Land Surface Temperature

Land surface temperature is the temperature at which an object emits infrared radiation according to plank's law (*Liang and J. Wang 2020*). Using remote sensing methods this quantity can not be directly observed since the satellite is observing Top of Atmosphere (TOA) brightness temperature. This temperature can be transformed to a LST using atmospheric correction and correction for the emissivity of the ground. The conversion factor is data source dependent and can be found in section 6.2.2.

2.3 Air Temperature

Urban heat islands that directly impact human health are the atmospheric UHIs in the urban canopy layer. These are defined by the air temperature from street level up to roof height. The air temperature within the urban area is warmed differently from the air

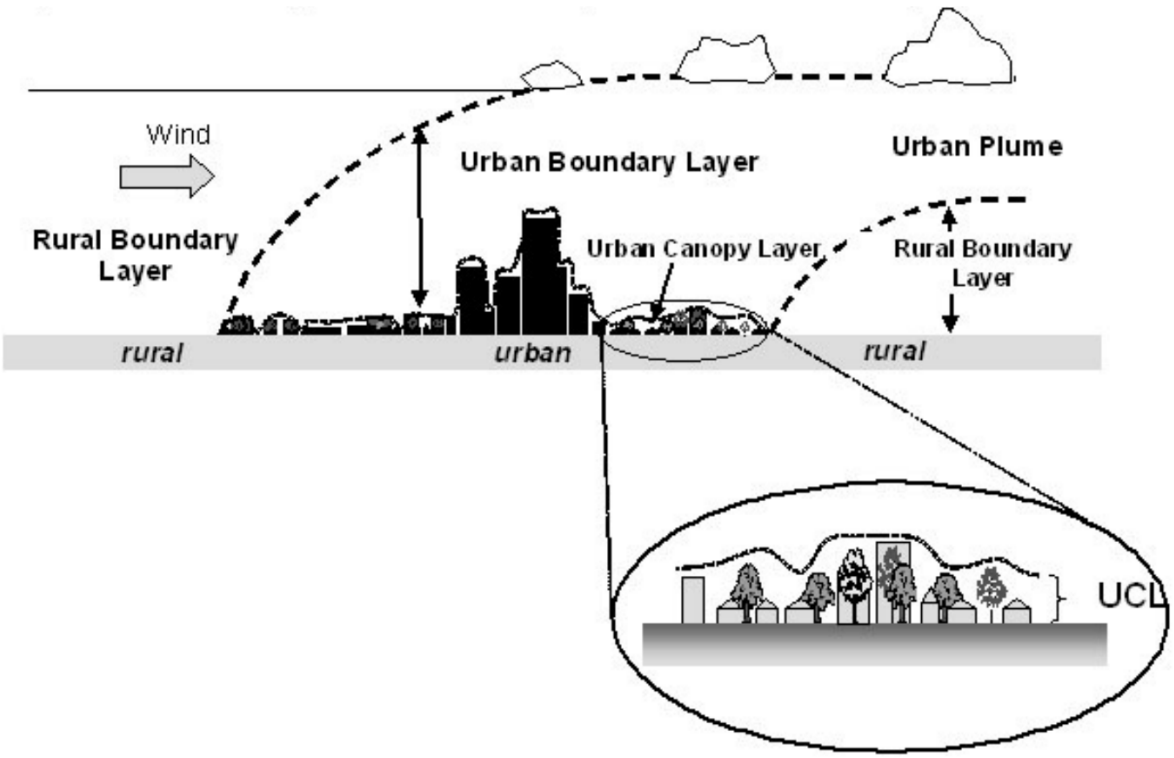

Figure 6: Overview of the Urban Atmosphere (*Fabrizi, Bonafoni, and Biondi 2010, Figure 1*)

temperature outside the urban area, due to higher thermal mass that buildings and sealed surfaces have and lower latent heat transport. During the day the air temperature is lower than the surface temperature (*U.S. Environmental Protection Agency (EPA) 2008*),

during the night the hot surfaces radiate off the energy heating the surrounding air. There are multiple additional factors impacting urban air temperature. Combustion from traffic and industrial processes produce heat as a by-product heating the surrounding air. HVAC systems also produce heat, when cooling buildings. This further increases the air temperature, increasing cooling need within the urban area, creating a positive feedback loop.

2.4 Indices

Many different indices are used for analysis of images or parameters in remote sensing, atmospheric physics and meteorology. The following sections introduce the indices that where used to analyse the UHIs within this work.

2.4.1 NDVI

The following section is a slightly reworked version of a section from the pre-thesis master project (Andrae 2023, see)

The NDVI is an widely used index using the difference of the red and near infrared bands

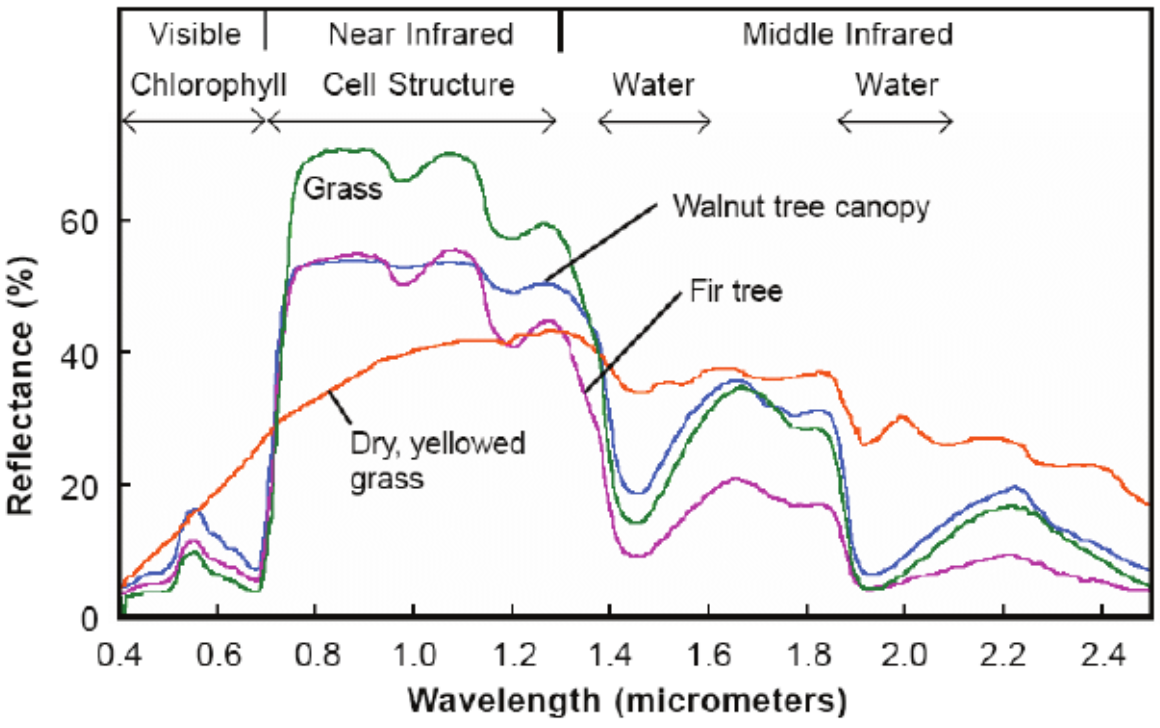

Figure 7: Absorption spectrum of green vegetation (*Smith 2012, P. 5*)

to determine the amount of green vegetation.

$$NDVI = \frac{Red - NIR}{Red + NIR} \tag{2}$$

For Landsat 8 and 9 data, channel 4 (red 0.640 μm – 0.670 μm) and channel 5 (near infrared 0.850 μm – 0.880 μm) where used. As shown in Figure 7 healthy plants reflect near infrared and there is a sharp rise in reflectance between the two used channels at around 0.700 μm. By using the difference of the two color bands on opposite sides of the edge, the NDVI provides an inside how much healthy green vegetation is present in each pixel.

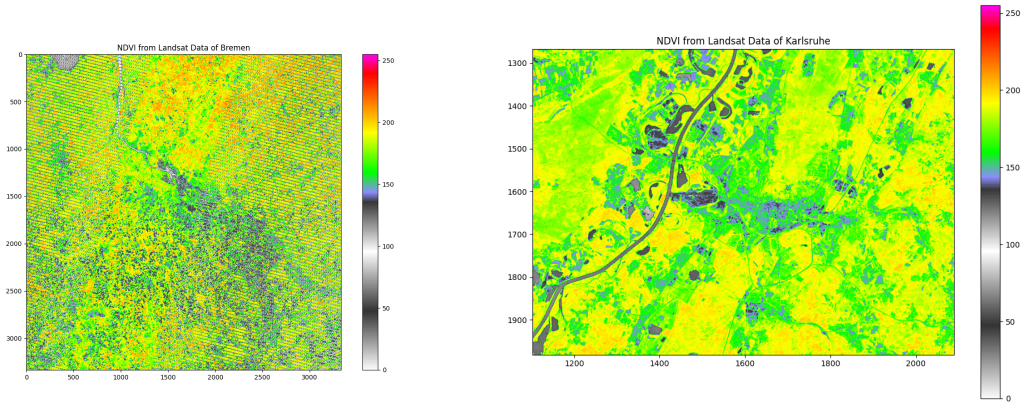

(a) NDVI of Bremen (Bands 5 and 6) using Landsat 7 data on 2019–07–23

(b) NDVI of Karlruhe (Bands 4 and 5) using Landsat 8 data on 2023–06–07

Figure 8: NDVI Images from the different satellites

2.4.2 Heat Index

The Heat Index (HI) is a temperature index that takes sultriness into account and rates the impact of temperature and air humidity of the human body. The output of this temperature scale (given in °C) is the apparent temperature, depending on relative air humidity. The defined range is between 20 °C and 50°C dry bulb temperature and up to 90% relative humidity (*Steadman 1979, p. 862*). The HI is based on a model human and takes wind chill and clothing into account, to produce a apparent temperature of the model human. The HI can be used as a good reference for non-extreme conditions. Its biggest downside is the missing account for direct insolation on body temperature and comfort. *Schoen 2005* created an polynomial approximation for the heat index table developed by Steadman (*Steadman 1979*), with ±0.7 ° C for temperatures above 27 degrees that was used for rating heat island severity.

$$HI = c_1 + c_2T + c_3R + c_4TR + c_5T^2 + c_6R^2 + c_7T^2R + c_8TR^2 + c_9T^2R^2 \tag{3}$$

with T being the wet bulb globe temperature and R being the relative humidity. c_1 to c_9 are factors for correction depending on temperature, wind chill and where taken from *Cassano 2010*. For extreme conditions the HI shows an underestimation during heat waves (*Romps and Y.-C. Lu 2022*), limiting the usefulness for these scenarios.

2.5 Wet Bulb Globe Temperature

To account the impact of insolation on the human body and the effect on heat stress exacerbated on the human body when high heat and insolation are present at the same time, the Wet Bulb Globe Temperature was developed. Working under heat stress poses a serious health issue, for this the Wet Bulb Globe Temperature (WBGT) was defined as EN ISO 7243:2017 (*ISO 2024*) as work place safety standard, calculating the thermal load on the human body. Heat exchange between the human body and the environment is dominated by evaporation of secreted sweat. The efficiency of this process is determined by the vapor pressure, that is influenced by the temperature and humidity difference. The simpler HI is a way of calculating this impact while not taking radiant heat into account, the WBGT does incorporate this effect into this calculation. It was specially developed to help create safety for workers that work long hours outside with little or no shade, like construction or agricultural workers or soldiers.

3 Image Processing

Using remote sensing data for scientific purposes requires a

a systematic

b reproducible and

c verifiable

way of extracting patterns and information from the available dataset.
The field of image processing and machine learning has developed a wide range of tools that are used in many different fields over the past decades.

3.1 Machine Learning

The term machine learning describes a sub-set of artificial intelligence research, focusing on algorithms that use statistical models to find correlations using different weights to approximate data. Machine Learning encompasses a wide range of techniques, including supervised, unsupervised and reinforcement learning, as well as more specialized topics such as deep learning and symbolic regression(*Rodrigues 2023*). In the context of remote sensing, machine learning methods have been utilized for tasks such as classification, biomass and soil moisture retrievals, and crop growth monitoring. Flexibility and comparably lower computational requirements of machine learning methods allow processing of large amounts of high-dimensional data and handle non-linear problems, enabling efficient analysis of remote sensing data (*Maxwell, Warner, and Fang 2018*).
Physics-Informed Machine Learning allows integration of base truth to circumvent "hallucinations" or false results, that can occur in other Machine Learning (ML) techniques and aims to guide machine learning models towards solutions that are physically plausible. Examples of applications of machine learning in physics include system identification, control, and analysis, as well as the development of physics-informed digital twins. ML, offering powerful tools for data analysis, modelling and gaining deeper understanding of remote sensing and atmospheric research data. These approximations can be stored and be used to detect the same features within new but similar data. For this analysis the k-means algorithm was used. In the next sections the image processing steps are described from a technical perspective and the underlying mathematical frameworks are discussed.

3.2 Data Processing Pipeline

An image or data processing pipeline is a chained list of processing steps, allowing to feed different data through the same algorithm. Many different data processing and machine learning lib use these to allow flexibility and modularity of the steps in data processing (e.g. the used Scikit-Learn (*Pedregosa et al. 2011*), Keras (*Keras Development Team 2024*) or

Gluon (AutoGluon *2024*)). The data processing was done using a *scikit-learn* pipeline for data analysis as well as multiple other lib listed in section 8.2.3. In Figure 9 the overview of the different steps within the data processing can be seen.

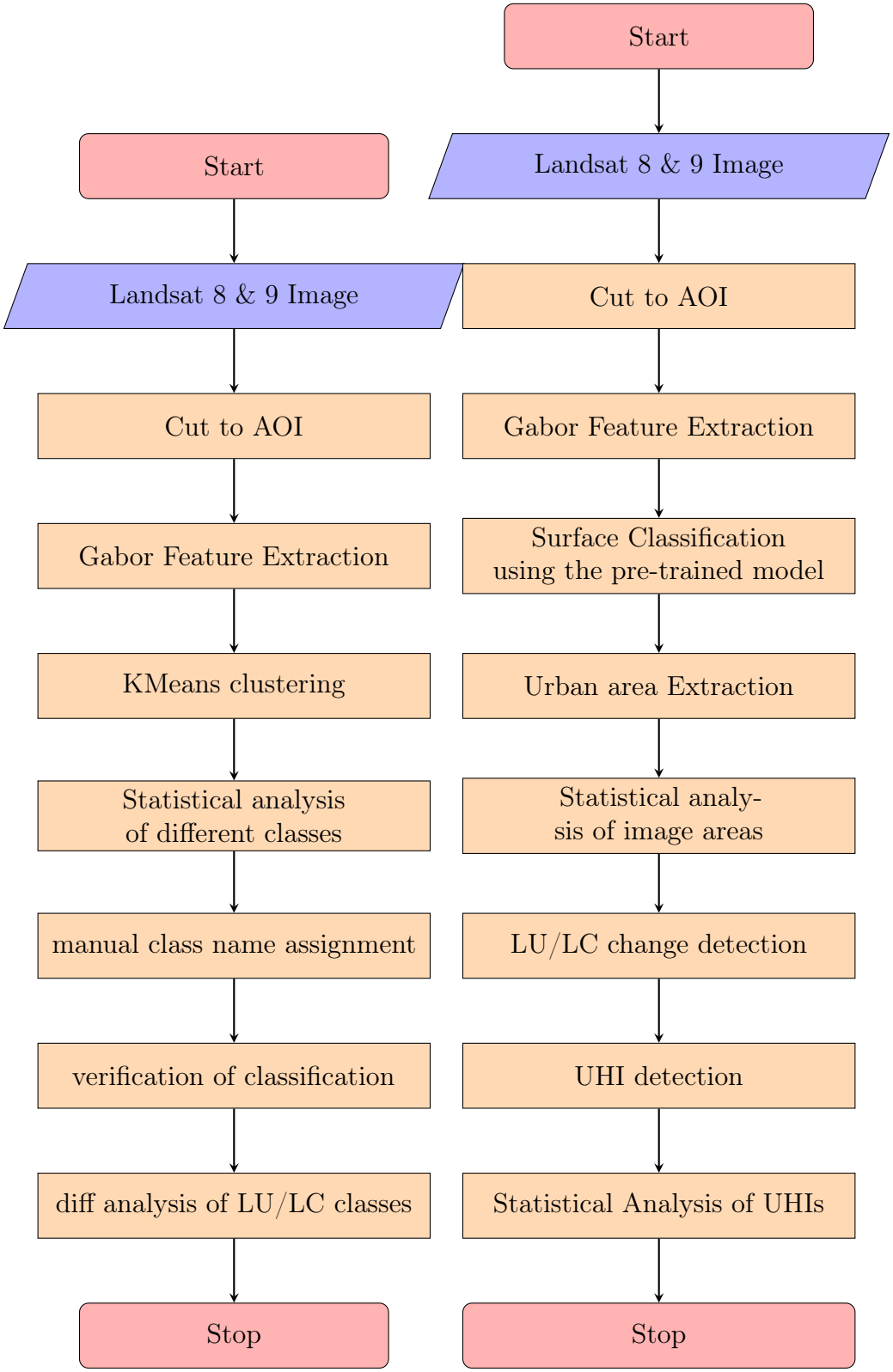

(a) Processing pipeline for training the model

(b) Data Processing pipeline with the trained Model

Figure 9: The image processing overview

3.3 Gabor Feature Detection

The Gabor filter is a linear filter using a convolution of an image with a wavelet created by rotating a sine modulated Gaussian. This kernel type is also called the *gabor wavelet*. Figure 10 shows an example of a single Gabor filter kernel. In image processing, this algorithm is used as a feature extraction algorithm, to extract and analyse texture and structures of different sizes within the image (*Cerdan 1993*). By rotating the kernel and changing the frequency, different textures are extracted from the image.

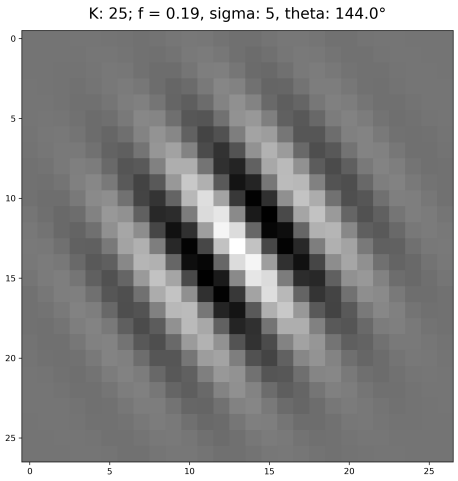

Figure 10: Example kernel with 26×26 pixel kernel size

Mathematically the Gabor-filter is defined by

$$g(x, y; \lambda, \theta, \phi, \sigma, \gamma) = \exp\left(-\frac{x'^2 + \gamma^2 \cdot y'^2}{2\sigma^2}\right) \cdot \exp\left[i\left(2\pi\frac{x}{\lambda} + \phi\right)\right] \tag{4}$$

With $x' = x\cos(\phi) + y\sin(\phi)$ and $y' = -x\sin(\phi) + y\cos(\phi)$.
The **x** and **y** parameter determine the kernel size, this parameter should be chosen based on the image size and expected structure length.
$\boldsymbol{\gamma}$ is the aspect ratio of the kernel, with $\gamma = 1$ the kernel is round, for smaller γ the kernel becomes a more eccentric ellipse.
$\boldsymbol{\phi}$ is the angle of phase shift of the sine component of the kernel.
$\boldsymbol{\theta}$ is the angle of rotation of the kernel, detecting differently oriented features.
$\boldsymbol{\lambda}$ is the wavelength of the sine wave.
$\boldsymbol{\sigma}$ is the standard deviation of the Gaussian distribution.
To detect different structures of different scales within the image, a filter bank can be created by combining multiple filters and varying ϕ, σ and θ.
After the convolution of the image with the filter bank, the resulting set of detected features can be used as an input into different algorithms. Figure 11 shows the binary output of different kernel sizes and rotations on a satellite image of Bremen. It can be seen that the different structures such as fields (seen in Figure 11b and Figure 11e) or larger structures and water bodies (seen in Figure 11a and Figure 11c) are extracted from the image. The output of the filter is an tensor that contains a binary image sized matrix per filter. Each layer provides meta information for each pixel, if it is part of a larger scale texture or pattern. This meta information is used to add additional features for the surface classification (section 5.1.1) using k-means to allow better classification.

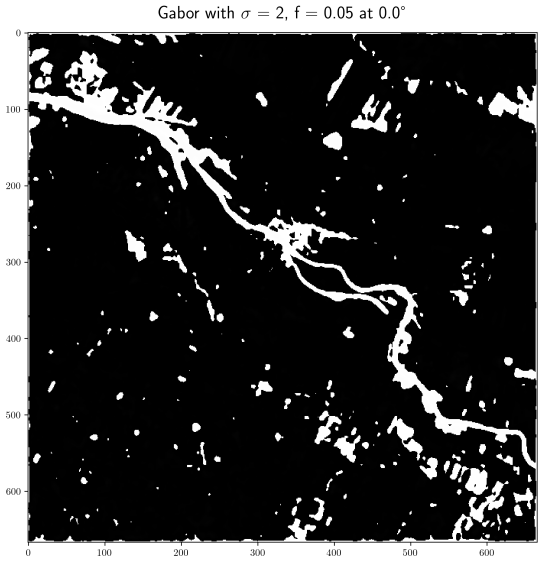

(a) Kernel with $\sigma = 2$, f = 0.05 and 0 ° rotation

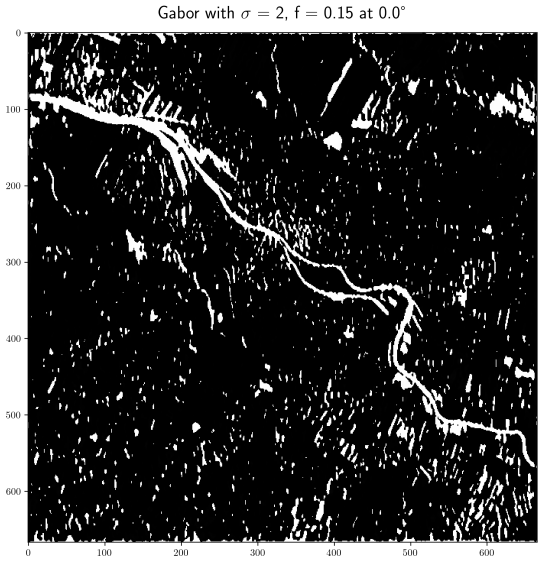

(b) Kernel with $\sigma = 2$, f = 0.15 and 0 ° rotation

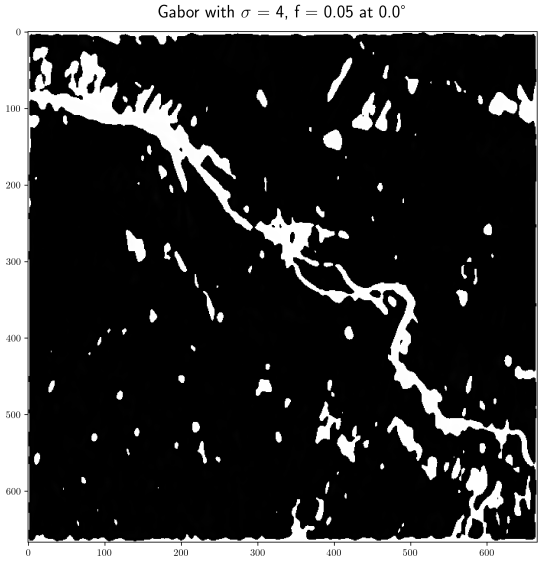

(c) Kernel with $\sigma = 4$, f = 0.05 and 0 ° rotation

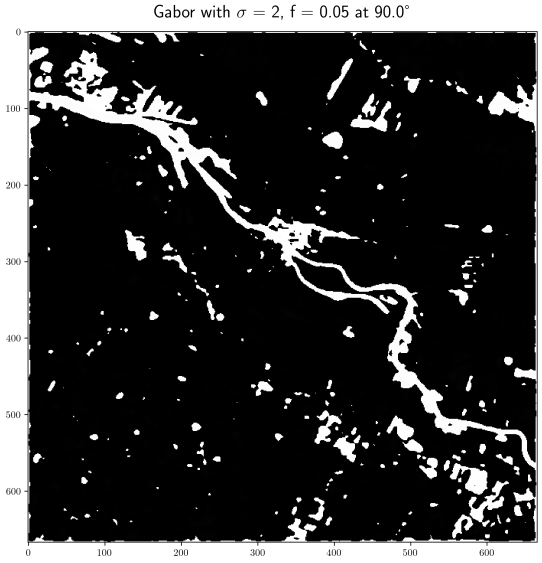

(d) Kernel with $\sigma = 2$, f = 0.05 and 90 ° rotation

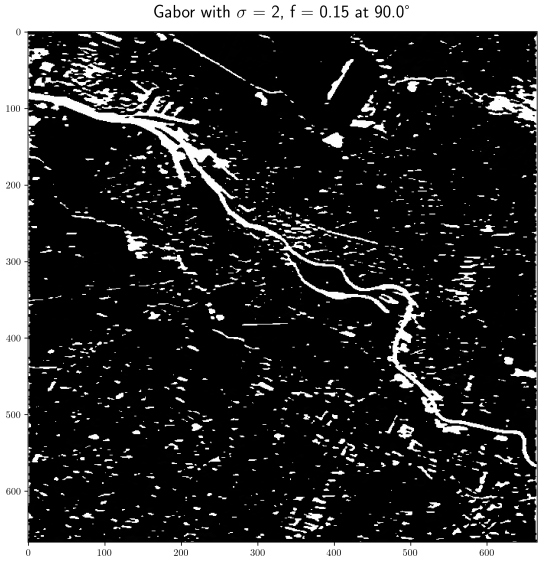

(e) Kernel with $\sigma = 2$, f = 0.15 and 90 ° rotation

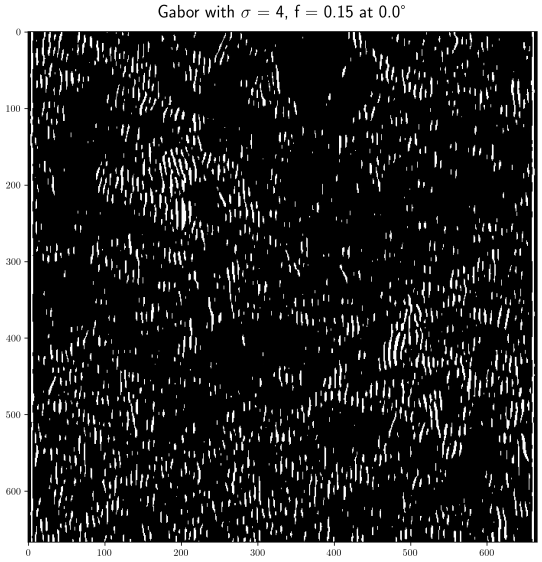

(f) Kernel with $\sigma = 4$, f = 0.15 and 0 ° rotation

Figure 11: Result of convolving differently oriented Gabor wavelets with an Landsat-8 image of Bremen

3.4 K-Means Clustering

K-means clustering is an unsupervised machine learning algorithm that is used to partition n observations into k clusters. Each observation belongs to the cluster with the nearest mean, serving as a prototype of the cluster. This method has many applications in data mining, image processing and pattern recognition.
The algorithm consists of three steps:

1. **Initialization**: Choose k initial centroids from the data points.
2. **Assignment**: Assign each data point to the nearest centroid, forming k clusters.
3. **Update**: Recalculate the centroids as the mean of all data points in the cluster.

This process is repeated until a maximum number of iterations or minimal changes in centroids is reached (*Sinaga and Yang 2020*).
There are multiple algorithmic implementations of K-Means, the specific algorithm used for classification used the Lloyd-Algorithm. Mathematically a set of observations $(x_1, x_2, \ldots, x_n)$, where each observation is a d-dimensional real vector. K-means clustering aims to partition the n observations into k ($\leq n$) sets $S = \{S_1, S_2, \ldots, S_k\}$ so as to minimize the within-cluster sum of squares.
The objective is to find:

$$arg\ \min S = \sum_{i=1}^{k} \sum_{x \in S_i} \|x - \mu_i\|^2 \tag{5}$$

where μ_i is the mean of points in S_i. The k-means clustering algorithm has been successfully used for surface classification using the feature enriched multi band satellite data (e.g. *Burrough, Gaans, and MacMillan 2000*). Figure 16 shows the result of clustering land surface types. The pre-trained model is stored to disk and can be used to classify similar images again. Since the class labels are not consistently applied, the labels need to be reassigned to the correct cluster. For this the cluster-centres from the trained k-means are saved as a array of n-tuples for each class, where n is the number of features used for training.

3.4.1 Label Reassignment

The distance from the cluster centres of the initial training dataset and the centres of the newly classified data is calculated. To get consistent mapping of class names to classification id, the minimal distance is not sufficient since an assignment of multiple classes to one original class has to be minimal. To mitigate this issue the *Hungarian Algorithm* is used, minimizing an overlying metric and creating a bijective assignment. The distances are then minimized using the sum of distances of all cluster centres as optimization metric.

$$\min = \sum_{i} \sum_{j} C_{i,j} X_{i,j} \tag{6}$$

This ensures that the minimum distance is used and an optimal reassignment takes place, even if cluster centres shift between images.

4 Comparable Definition of Urban Heat Islands

The definitions of SUHIs in literature are varying slightly and do not take into account that most definitions do not allow easy comparison between different areas or times. Local studies often use a single reference measurement station and use the absolute temperature difference as a measure of intensity. Others use the surface temperature of surrounding rural areas like forests as a reference. The definition of the U.S. EPA (*U.S. Environmental Protection Agency (EPA) 2008*) and the German Weather Service (Deutscher Wetter Dienst (DWD)) both define SUHI as an area of increased temperature between the urbanized areas compared to the surrounding.
Different studies analysing UHIs use different reference temperatures. The first goal of this work is defining a systematic reproducible approach to measure UHI intensity.

4.1 Approach

As a starting point the method of *Sobrino and Irakulis 2020* was adapted, where SUHI where compared in different cities around the world using Sentinel-3 images. For each city a buffer zone was calculated around the city border, using the average temperatures of the different areas as a comparison point. This was then used to identify and measure the intensity of heat islands within the city area.
This work uses the same basic approach but Landsat 8/9 data was used. In *Sobrino and Irakulis 2020* urban adjacent, future urban adjacent and peri-urban areas are defined as buffers. These where adapted by removing the urban growth projection (since the scope of the paper was the investigation of SUHIs in 2050 that does not match the goal for this work). The urban area is identified by detecting land cover classes indicating a larger area of build up classes. These areas are then converted into a polygon that is extended by buffer zones as shown in Figure 14. The classification was done using the same dataset. Larger urban areas are removed from within the reference temperature area. For the processing of the images and techniques for surface classification see section 5.1.1. Additionally, an approach is discussed where the relative (statistical) intensity is used compared to the absolute temperature difference to compensate for seasonal temperature spread within certain areas.

4.2 Definition of Urban Heat Islands

The following UHI definition is proposed and used throughout this document.

An SUHI is an area with increased surface temperature within an urban space. It is defined as having a temperature at least 3 standard deviations above the average temperature of the adjacent rural buffer zone. The rural buffer zone measurement is corrected for temperature influence of larger settlements.

For comparability a statistical metric is used, since the absolute intensity as well as the daily temperature spread varies with the seasons and is easily altered by water bodies or other thermal masses in the image.
The proposed threshold of at least three standard deviations above the average temperature was chosen since this gave consistent results over the seasons.
The reference measurement is calculated using the surface temperature of the peri-urban buffer zone and removing all larger urban areas within it. The removal will get rid of the temperature influence of other cities or larger industrial sides close to the area of interest. The mean temperature and variation within the peri-urban area is then calculated and used as reference. Depending on the season the temperature distribution will vary. Due to the definition using the standard deviation, the detection of UHIs is coupled to the range of temperatures observed within the image. During processing single outlier areas as well as clouds, cloud shadows are removed. Holes within the urban area are closed, this allows to include parks and other urban green areas to be processed and only includes larger areas of elevated temperatures as urban heat islands. This will increase robustness of UHI detection to reduce the influence of single hot surfaces (such as solar panels or industrial tanks) during detection.

4.2.1 Urban Buffer Zones

To generate the different temperature statistics, buffer zones must be created. This is done by defining multiple areas using eq. (7).

$$\begin{aligned} W_U &= \frac{A_U^{\frac{1}{2}}}{4} \\ W_P &= \frac{6 \cdot A_U^{(\frac{1}{2} - W_U)}}{4} \end{aligned} \tag{7}$$

Where A_U is the urban area, extracted from the classification (see section 5.2.1), W_U is the suburban buffer zone and W_P the peri-urban area. These definitions were used in *Sobrino and Irakulis 2020* and were initially developed in the 90s for modelling urban development and are used in different areas of urban planning and analysis (*Alkan-Bala and Üstüntaş 2014, see*). These models follow the idea that cities have an influence space surrounding

them and grow in all directions if not obstructed by borders or natural barriers. The practical implementation used the results of the classification for urban area detection and buffer zone creation and is described in more details in section 5.2.1.
The heat island is then defined as area that is more then 3σ above the mean temperature of the surrounding area W_P, while the surrounding area is defined as a fixed buffer based on the size of the urban area and clean the area of larger settlements.

4.3 Conclusions

The definition of UHIs using reference regions and a statistical threshold for identifying areas is a methodology that has multiple advantages compared to using absolute values and single reference points. The impact of seasonal and geographic variations in temperature spread as well as weather and other metereological effects are reduced, since the peri urban area has a mixed composition.

5 Impact of Land Cover Changes on Urban Heat Islands

One of the key factors influencing the intensity and distribution of UHIs is land cover change. Change in LU/LC is primarily driven by urbanization and associated human activities. Soil and surface properties impact the emissivity, thermal conductivity and heat capacity of an area. Increases in the sealed surface fraction reduces surface water availability (see section 2.1). This is changing the energy flow, increasing the heat build-up within the urban area.
This section examines the relationship between land cover change and UHIs effects using LU/LC detection based on the previously classified Landsat images. The first part of this section begins with an overview of how land cover changes influence heat build-up within the urban environment. Followed by how LU/LC can be detected using Landsat data and how surface classification was done within this work.
This section then goes into detail how the classification of land cover was conducted using Landsat 8 and 9 images, the analysis of spatial and temporal patterns of UHIs in relation to the detected land cover classes follows. To answer the question 2 of the influence of land cover change on intensity and size of UHIs, statistical analysis is conducted on the UHIs within the area of Bremen.

5.1 Impact of Land Cover/ Surface Type on Heat Build-up

The change of the urban surface properties is one of the major factors causing SUHIs. Multiple studies have shown that land cover has a significant impact on land surface temperature and UHIs (e.g. *Karakuş 2019*, *Weng, D. Lu, and Schubring 2004* and *Stewart 2011*). This is mainly caused by the physical thermal properties of the different materials found in the different land cover classes. Areas with urban characteristics contain higher amounts of metal, stone and concrete, materials with a high thermal mass combined with a higher absorption at short wavelengths (dependent on surface coatings). Build up surfaces have lower water availability for evaporation and thus more heat is heating up the material itself. Forests and other vegetated areas are permanently cooled by evaporative cooling and transpiration of trees, increasing vapor content and heat capacity of the air.

5.1.1 Classification

The methodology employed for land cover classification involved the multi-step process utilizing satellite imagery, feature enhancement and machine learning techniques shown in Figure 9 and described in section 3.2. The primary data source for classification were 8-band Landsat images, which provided a comprehensive spectral view of the area to be classified. To augment the dataset and enhance the classification accuracy, Gabor filtering (see section 3.3) was applied to the Landsat images. As input, the Gabor filtered

multispectral data of satellite images from two dates were used. The multi band image was loaded and cut to match the study area and reduce processing time by reducing data size.
The analysis used the following parameters:
The Gabor filter used for feature engineering was varied using different σ, θ and f values. Due to computational restrictions the number of rotations (θ) was limited to 5, a value of 4 yielded in best results. For ease of variation the σ_x value was varied while the $\sigma_y = \frac{\sigma_x}{2}$, giving a 2:1 kernel ratio (shown in Figure 12).
For $\sigma_x > 2$ the classification degraded showing stripes very large patterns were detected, a value of $\sigma_x = 1$ resulted in a kernel size of 7×7 pixel and good results. The usable frequencies are limited by the size of the kernel and the image resolution shown in Figure 12. Due to the low resolution, a large kernel size would detect features that are repeated with a features size in the range of 200 m that do not occur in large quantities in urban areas. Larger kernel sizes with higher frequencies would increase detection capability for images with higher resolution. Figure 12 shows the used kernels for classification.
The filter bank with these kernels act as an edge and structure detection algorithm.
In structured areas with fields or buildings on a street raster, the filter amplifies the structures, for smaller structures the filter detects edges for change in building material. The detection is working due to the different specific albedo of the different frequency bands, depending on material properties. The result of the convolution of all bands of the image with the Gabor filter was then used as feature vector. By variation of parameters, a minimal error to the reference data was achieved using 4 rotations, an asymmetric kernel with a 2:1 ratio, two frequencies and two sigma sizes (see error calculation below). Since the classification was done using a reproducible randomness, the parameters influencing the result where:

- the selected images
- the number of classes to find by the k-means algorithm
- the parameter of the Gabor filter

The images were not changed for finding the best filter settings, the number of k-means clusters was varied as well as the parameters of the Gabor kernels. One limit of the Gabor filter parameters (rotation, size and frequency) was given by the resulting increase in processing time, since the resulting feature vector for each band is set as

$$N_{feat} = |\theta| \cdot |\sigma| \cdot |f| \tag{8}$$

with an increase of any parameter the dataset size increased significantly, creating a limit of the parameter variation. The 1833×1833 pixel sized image of Bremen (covering a

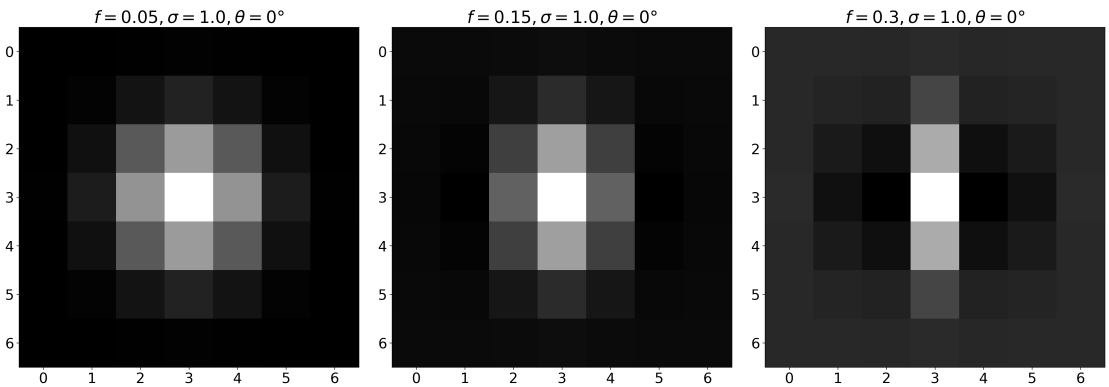

(a) Kernel 1 (b) Kernel 2 (c) Kernel 3

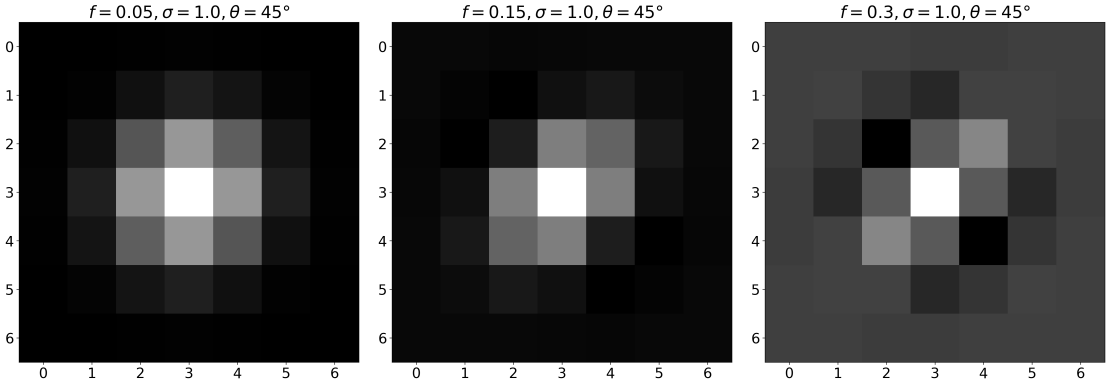

(d) Kernel 4 (e) Kernel 5 (f) Kernel 6

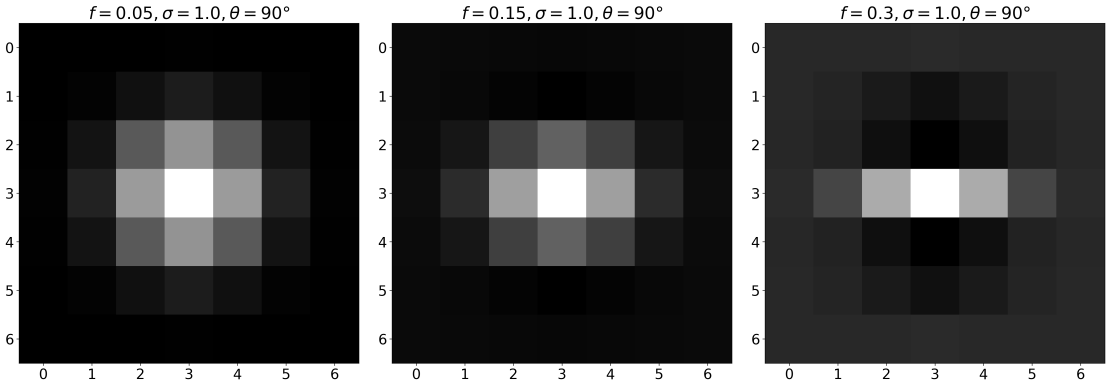

(g) Kernel 7 (h) Kernel 8 (i) Kernel 9

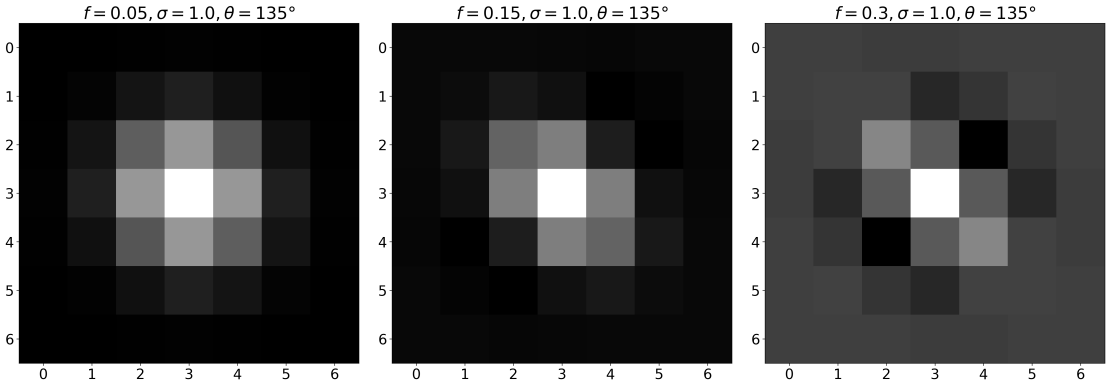

(j) Kernel 10 (k) Kernel 11 (l) Kernel 12

Figure 12: Filter bank of 12 Gabor filters with 4 rotations and a $\sigma_x = 1$, $\sigma_y = 0.5$ and $f = 0.15, 0.35$ and 0.4

square of ≈ 55 km around the city centre), has a size of 13 MB per Band[1]. The optimal sigma was found using systematic variation to be between 1.0 and 1.5. The frequencies of the sine wave where varied between 0.05 and 0.5. A trade-off between computation time and results was found using 3 frequencies shown in Figure 12.
This step was crucial in extracting and emphasizing spatial patterns and textures, thereby facilitating more distinct classification of land cover types. For classifying surfaces the k-means unsupervised machine learning algorithm was used. The number of classes was varied between 8 and 12 classes, giving best results in terms of minimal Mean Squared Error and highest Structural Similarity Measure when using 11 classes. The quality of the feature vectors was judged by the output of the classification that is covered below. The feature enhanced data of images of Bremen were used of multiple years to create the unsupervised k-means clustering model. The classified image has 11 classes that are shown in table 1.

Table 1: Land Cover Classes Identified

Class Number	**Land Cover Type**	**ESRI Class**
1	Water	Water / Flooded Vegetation
2	Vegetated Residential	Build Area
3	Clouds / PV	Build-up[2]
4	Fields & Meadows	Crops
5	Agricultural	Crops
6	Industry	Build Area
7	Residential	Build Area
8	Bare Soil, Rock	Bare
9	Vegetated Residential (moist)	Build Area
10	Industry Halls	Build Area
11	Forest / Dense Vegetation	Trees & Crops

[1]After feature detection the resulting dataset would be 107 MB per Band resulting in around 1.2 GB for each 8 band Image for each time point within the used classification training dataset.
[2]Analysed images do not contain clouds over the urban areas

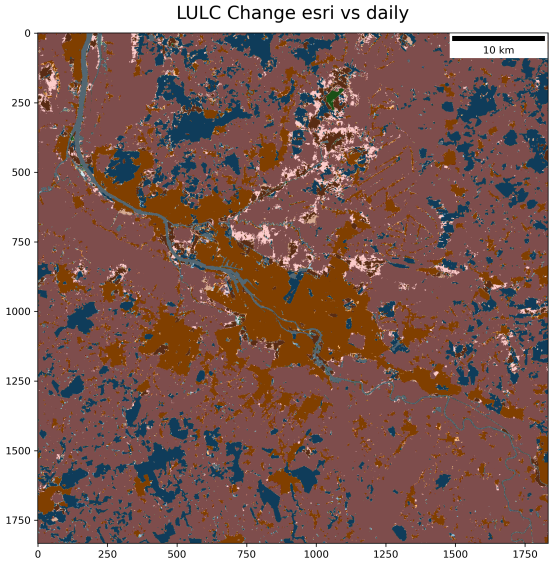

Figure 13: Change between reference product and k-means LU/LC classification

In Figure 13 this difference is shown between the 2019 LU/LC and 2022 LU/LC. The major differences are all seen outside of the city area and can be attributed to changes on agricultural land, e.g. harvesting or change in vegetation type. During the available time neither classification nor reference data showed significant land use changes within the urban area of Bremen. The majority of changes occurred at the interfaces between two classes that are caused by errors in georeferencing, naturally occurring changes in vegetation growth and uncertainties due to spacial resolution. Due to the missing LU/LC changes within the given time frame, the analysis of the impact of land cover changes could not be completed. In section 7.8 possible areas with LU/LC errors are listed as areas to be studied in the future.

5.2 Validation of Classification results

The model was validated using the Sentinel-2 10 m Land Use/Land Cover product (*ESRI LULC 2024*). Since the reference data uses 8 classes, the used classes where mapped to the best fitting class as indicated in table 1. Clouds, cloud shadows and snow/ice where not used for training and verification and removed for the analysis, since reference images do not contain clouds and images were selected to not contain ice, snow and clouds within relevant areas. The Esri 10m-LU/LC Dataset was obtained using the ESRI land cover explorer (*Zhang 2024*) and scaled to the 30 m resolution of the Landsat images. It can be seen from the difference between the LU/LC classification and the main difference in categorization is along the edges between different class patches. This can be explained by differences in the categorization approach, where the reference dataset is using averages for the whole year while the classification for the data is done at a single point in time. This can lead to an over detection of vegetation or water classes due to season or weather impact on the single point in time classification. A simple comparison of difference can be done by calculating the Mean Squared Error for each classification of the image using eq. (9), where m and n are the sizes of the image and reference image respectively. Where I and K images with the pixel values at index i and j.

$$MSE = \frac{1}{m \cdot n} \sum_{i=0}^{m-1} \sum_{j=0}^{n-1} \left[I\left(i,j\right) - K\left(i,j\right) \right]^2 \tag{9}$$

The score given by this gives and rough estimation of the difference between the images and the trained model was then used to classify other cities and datasets from different times. Part of the training data as well as different time data from the same area was used and Feature enhanced using the same Gabor-Filter bank.

$$SSIM = \frac{(2\mu_x\mu_y + c_1)(2\sigma_{xy} + c_2)}{(\mu_x^2 + \mu_y^2 + c_1)(\sigma_x^2\sigma_y^2 + c_2)} \tag{10}$$

μ are the mean values of each image, σ is the variance of each image and σ_{xy} the covariance of each image. c_1 and c_2 are stabilizing constants derived from the dynamic range of the image*Z. Wang, Simoncelli, and Bovik 2003, Equation 6*. For the SSIM the scikit-image implementation was used (*Walt et al. 2014*). Structural Similarity Measure returns a value between 1 (identical images) and -1 (inverted images) with 0 for images with no similarity (*Z. Wang, Simoncelli, and Bovik 2003*). The Structural Similarity Measure of the images was calculated as 0.98 $\pm$0.001 showing very high similarity.
The classification labels were assigned, based on the proximity of the cluster centres of the training data, to the cluster centres of the K-means fit (see section 3.4.1). This approach ensured that each land cover class was consistently labelled independent of the area of study.

5.2.1 Urban Area Extraction

The resulting classified image was then processed to extract urban areas. The algorithm used the classes 1, 2, 6 and 11 from table 1 to detect areas that can be considered urban. The areas were processed, using dilation and erosion, to isolate core urban areas. For small gaps between parts of the city, covered by vegetation (parks or railways), dilation was used to bridge gaps and close small holes. Small thin links, such as highways, between larger areas are cut, to create separate urban areas. After preprocessing the areas were enumerated and all areas that cover at least 1% of the selected image section where used to create buffer zones. Buffer zones were defined as described in section 4.2.1. The result for the urban area of Bremen can be seen in Figure 14.

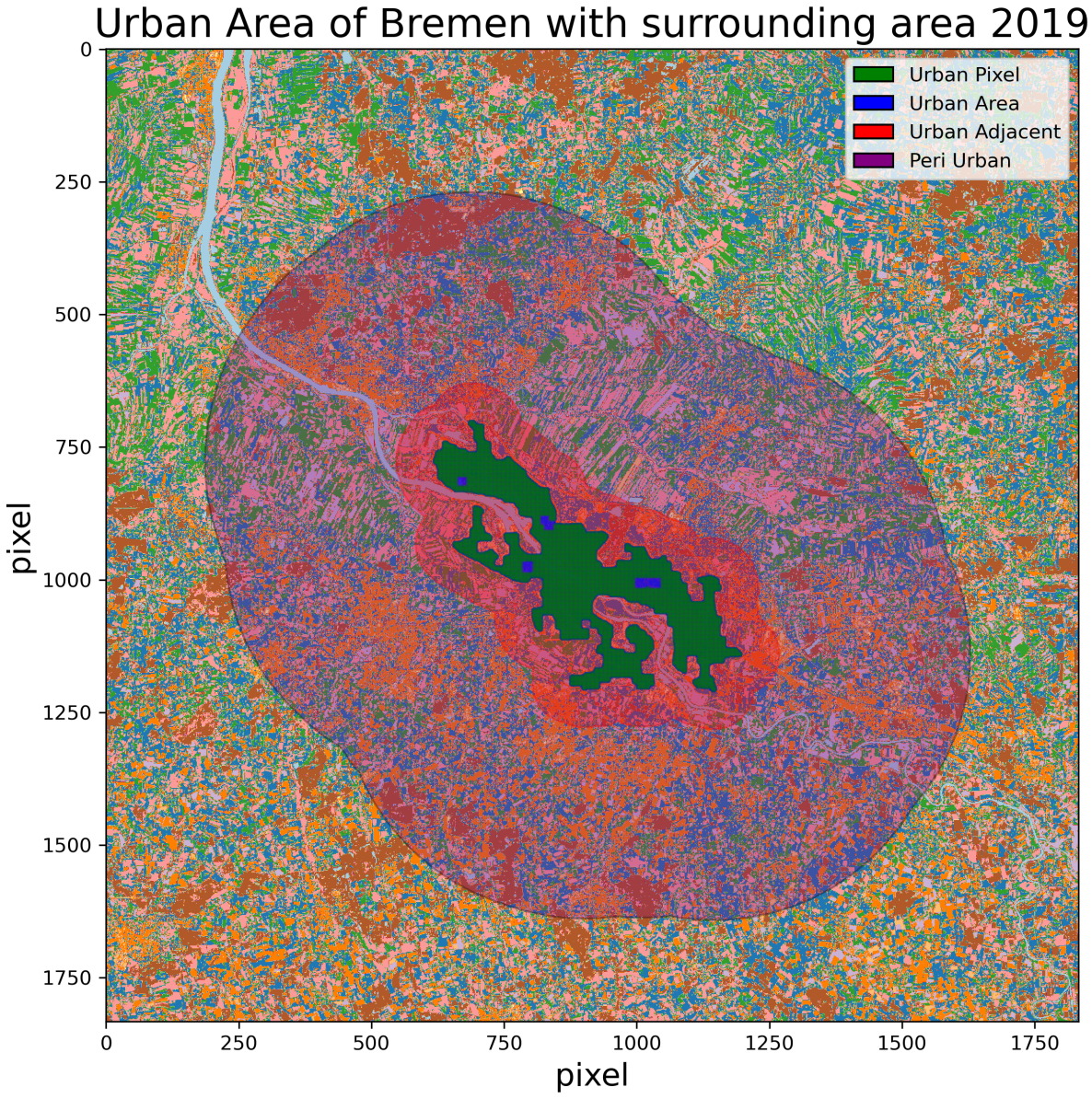

Figure 14: Urban Area of Bremen, with buffer zones for Adjacent and Peri Urban Area

5.3 Analysis

The results of this classification can be seen in Figure 15.

In Figure 16a and Figure 16b the different pixel values and the measured LST and NDVI

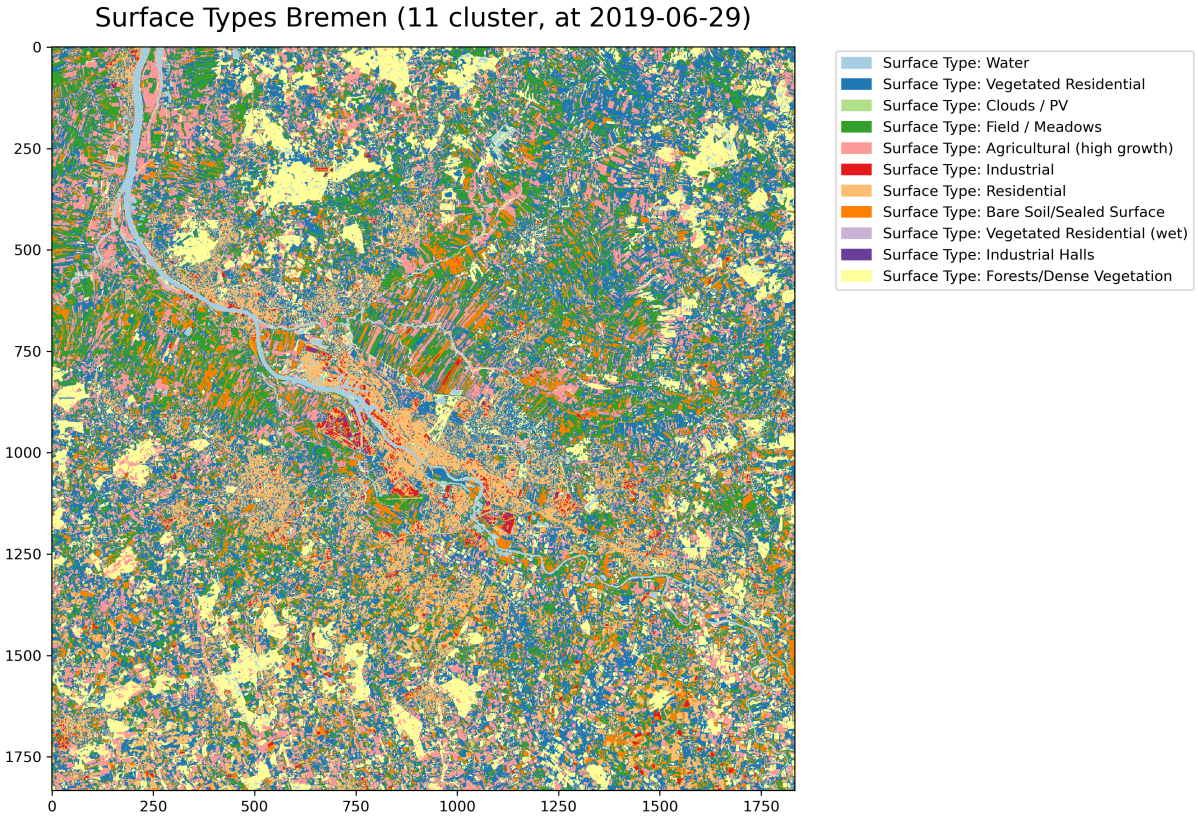

Figure 15: Classification result

values are plotted of the classified results. Especially the *Water* and *Dense Vegetation* classes are distinctly separated from the rest of the clusters within the NDVI and LST plane. The scatter plot also shows that the principle components of the classifications are not simply NDVI and LST but the added feature dimensions play a significant role in separation of classes.

The urban area shown in Figure 14 yielded a usable output shape following the Bremen city borders, this was manually verified using the visible images and third party visible satellite images.

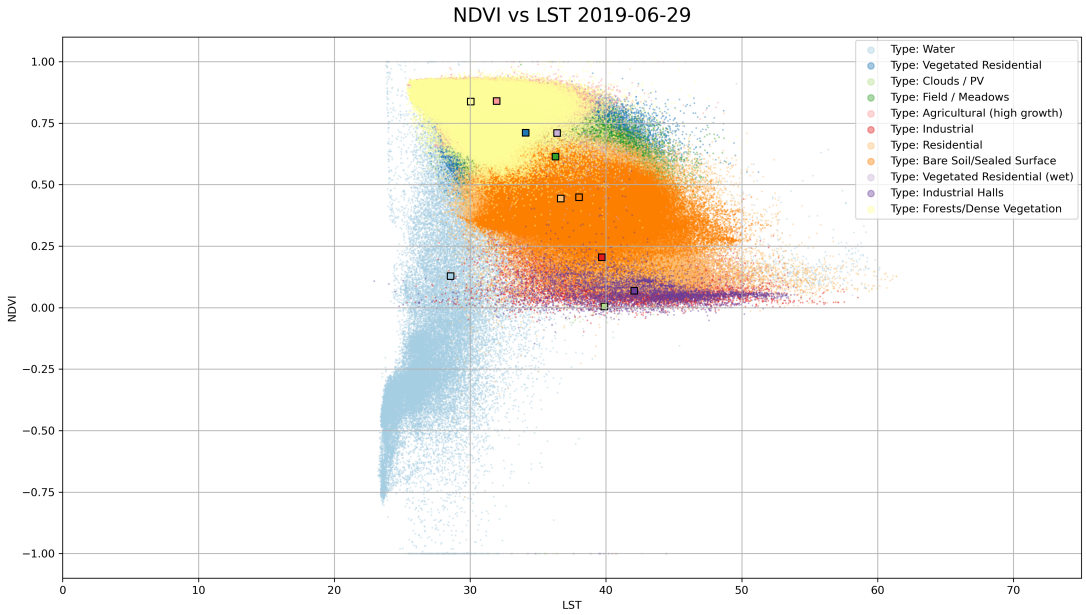

(a) Classification distribution on a day with higher temperatures

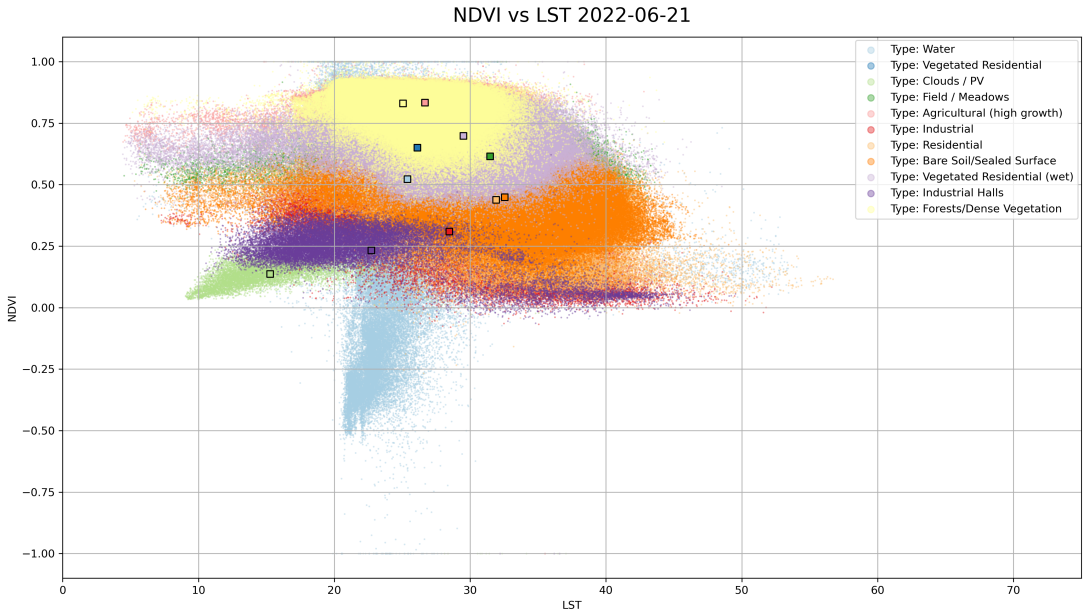

(b) Classification distribution on a day with lower temperatures

Figure 16: Result of clustering plotted with NDVI and LST values and cluster centres (coloured squares)

Figure 17 shows the classification of pixels within the peri urban area. It can be seen, that the pixel of the peri urban area has a mixed surface classes dominated by vegetation classes. Parts of these are removed (*Residential*, *Vegetated Residential*, *Industrial & Industry Halls* and *Bare Soil*) if in a linked area of more than ≈ 25 ha of size, to remove other larger settlements that could distort the measurement. This distribution matched the expected peri urban distribution, prior to removal of close by larger settlements.

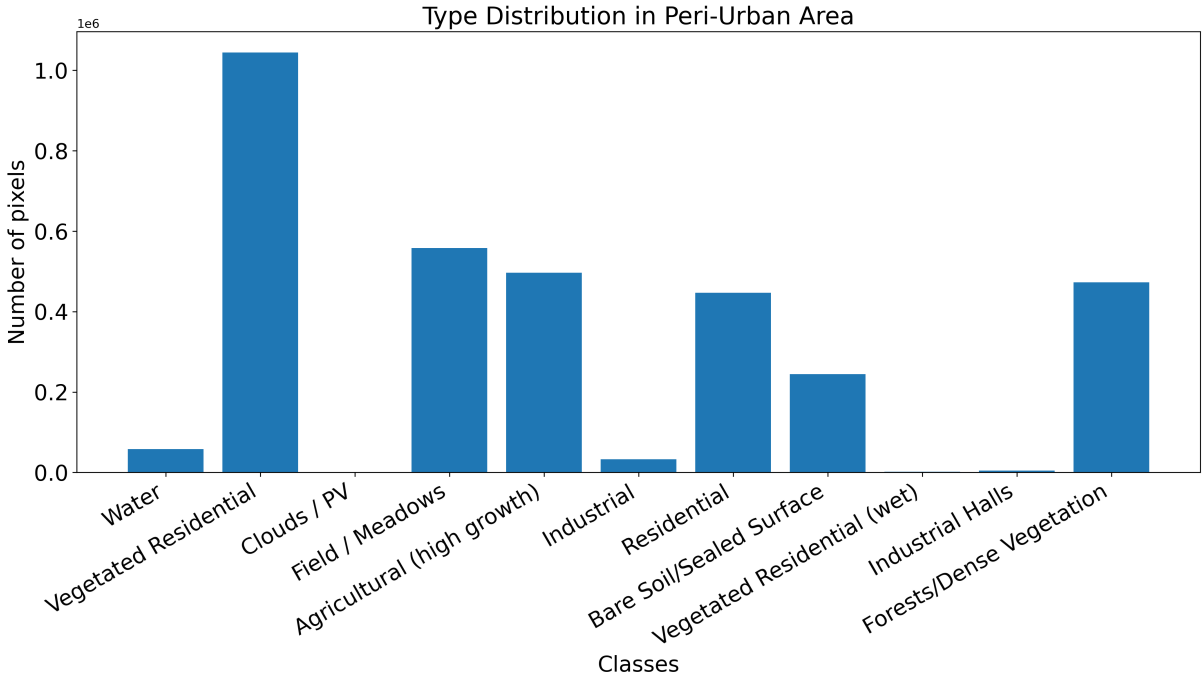

Figure 17: Distribution of surface types within the peri urban area (prior to filtering)

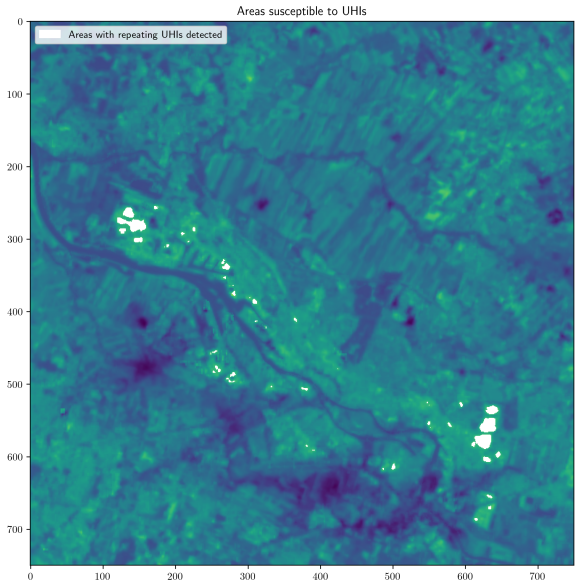

Figure 18: Areas with UHIs detected in both times

The temperature values of the different areas are calculated by overlaying the masks on the thermal band of the Landsat data. The average temperature and variance is calculated for the peri urban and the urban area. Using the average temperature, UHIs are detected using the definition from section 4.2 within the area defined by the urban mask. The areas that are above the threshold are then detected within the urban mask, the resulting UHIs are shown in Figure 19. The white area is the urban mask of Bremen and the detected UHIs, are circled in black. Some areas extend to the suburban area around, thus looking cut in this visualisation. Figure 18 is a differential image marking the areas affected by UHIs in both times. The white areas are sections where UHIs were detected at both times. The found areas could be further investigated, if health risks or high heat have negative side effects within these areas.

In Figure 20 and Figure 21, the temperature distributions within the different classes is shown. Confirming previous research, classes with high vegetation and water are lower in temperature. The 2022 day was colder, with mixed cloud cover, explaining the significantly lower temperature of PV / Cloud classes. The variance of the temperatures of the colder day is lower showing a higher difference in mean temperature between classes. The PV / Clouds class also included some cumulus clouds outside of the city area further decreasing the temperature values within this class.

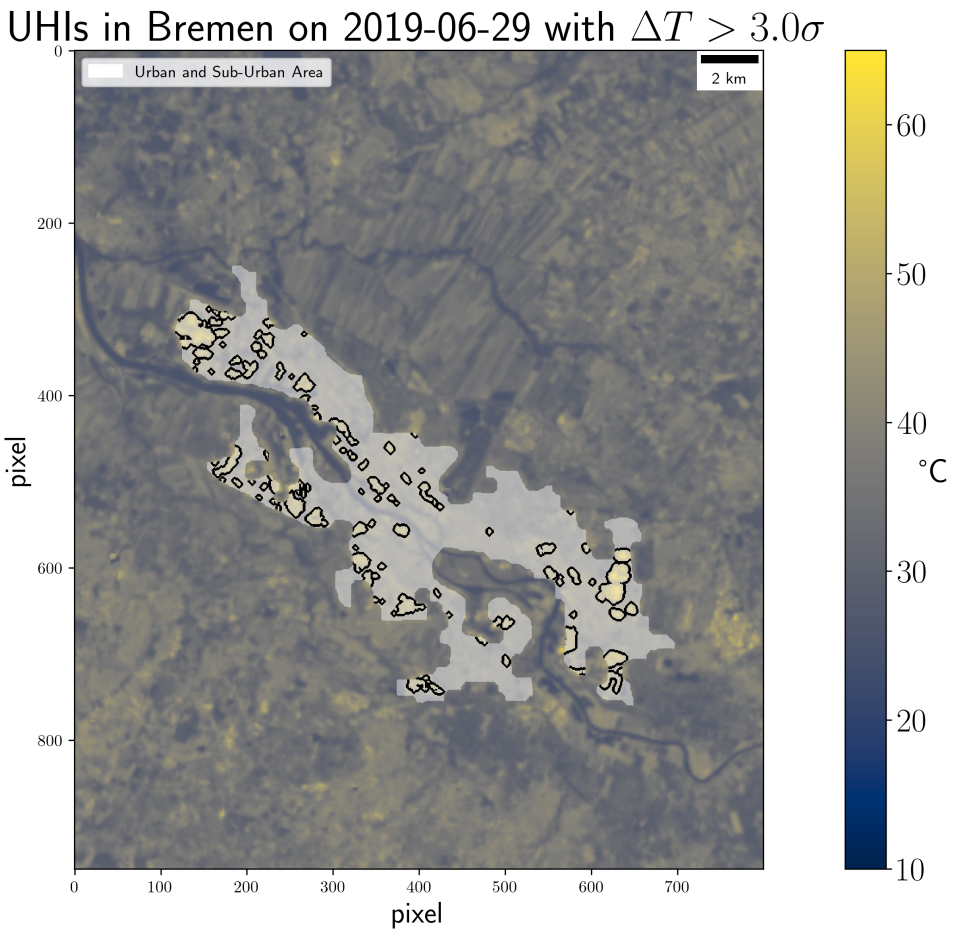

(a) Map of the detected UHIs in June 2019

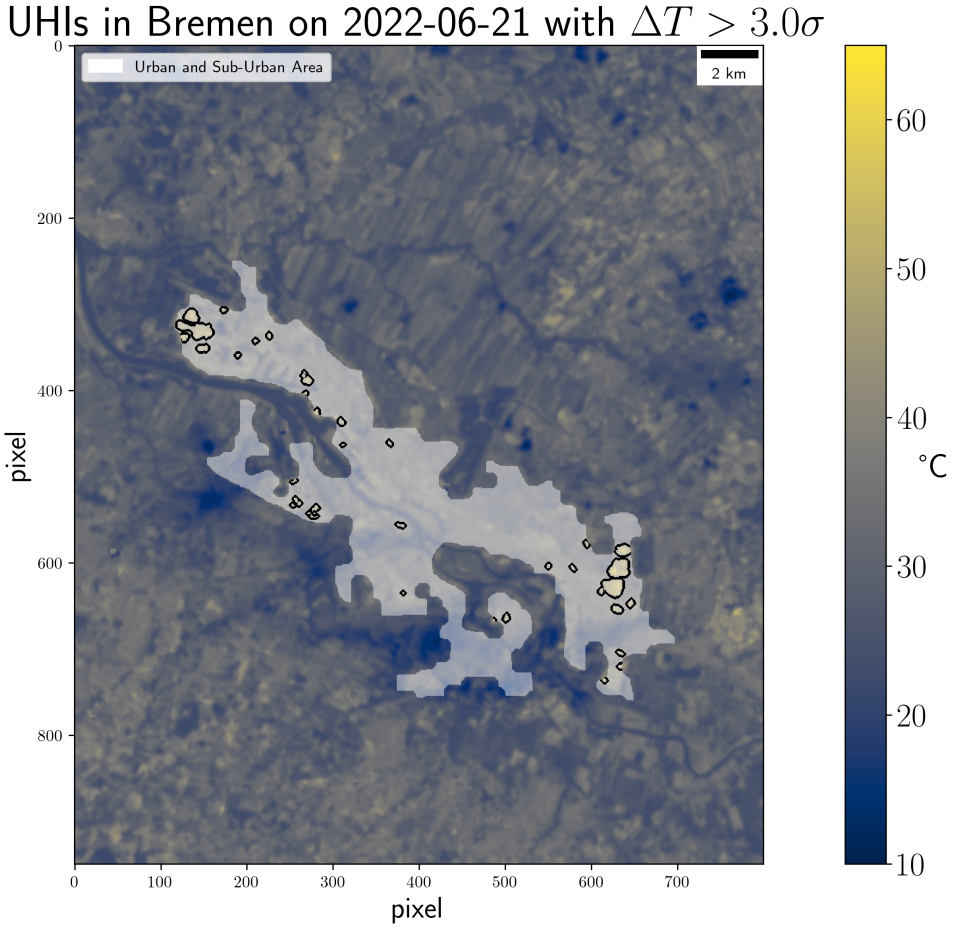

(b) Map of the detected UHIs in June 2022

Figure 19: Overview of Bremen UHIs at different times

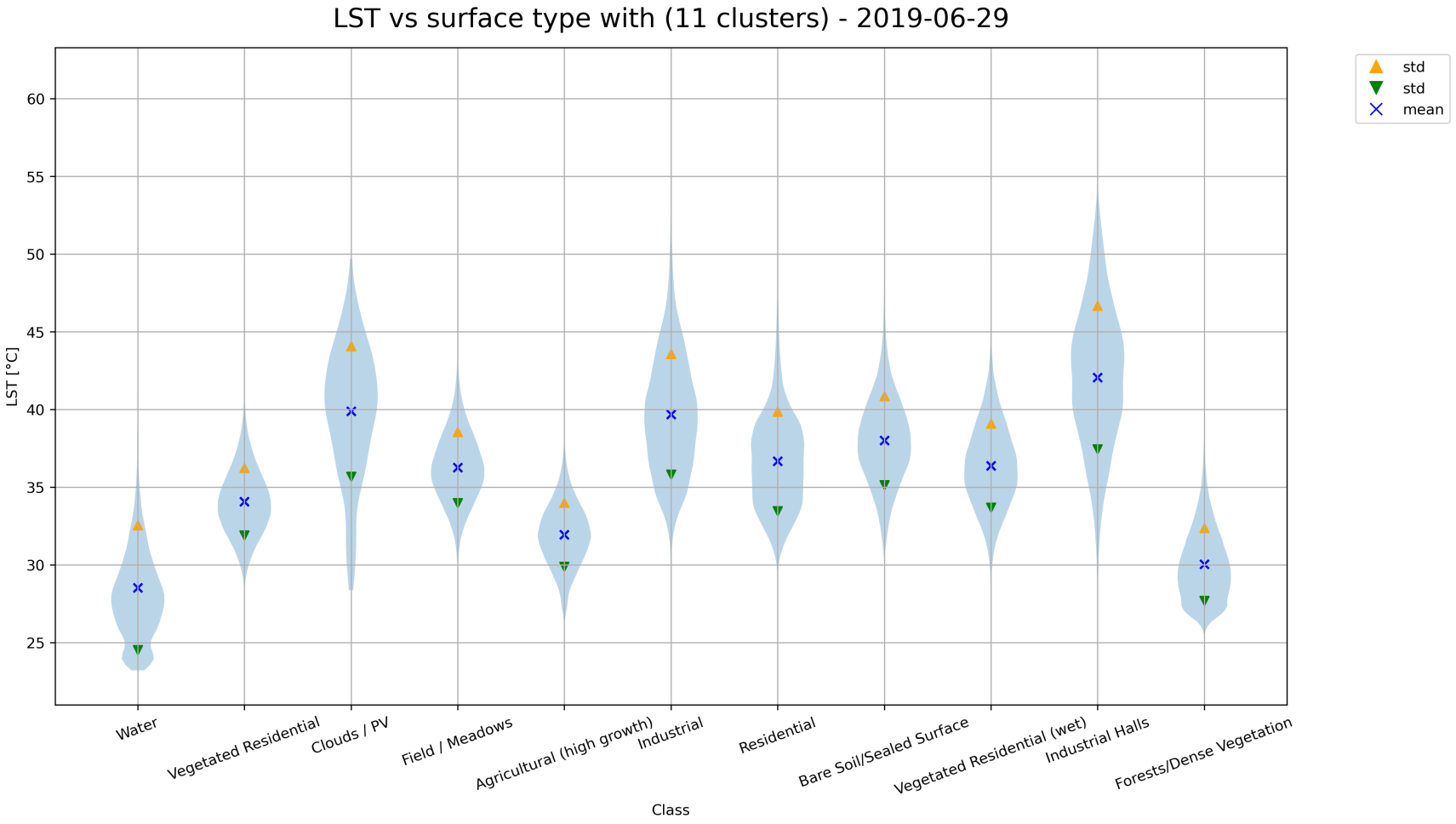

Figure 20: Distribution of pixel LST [°C] values per class June 2019

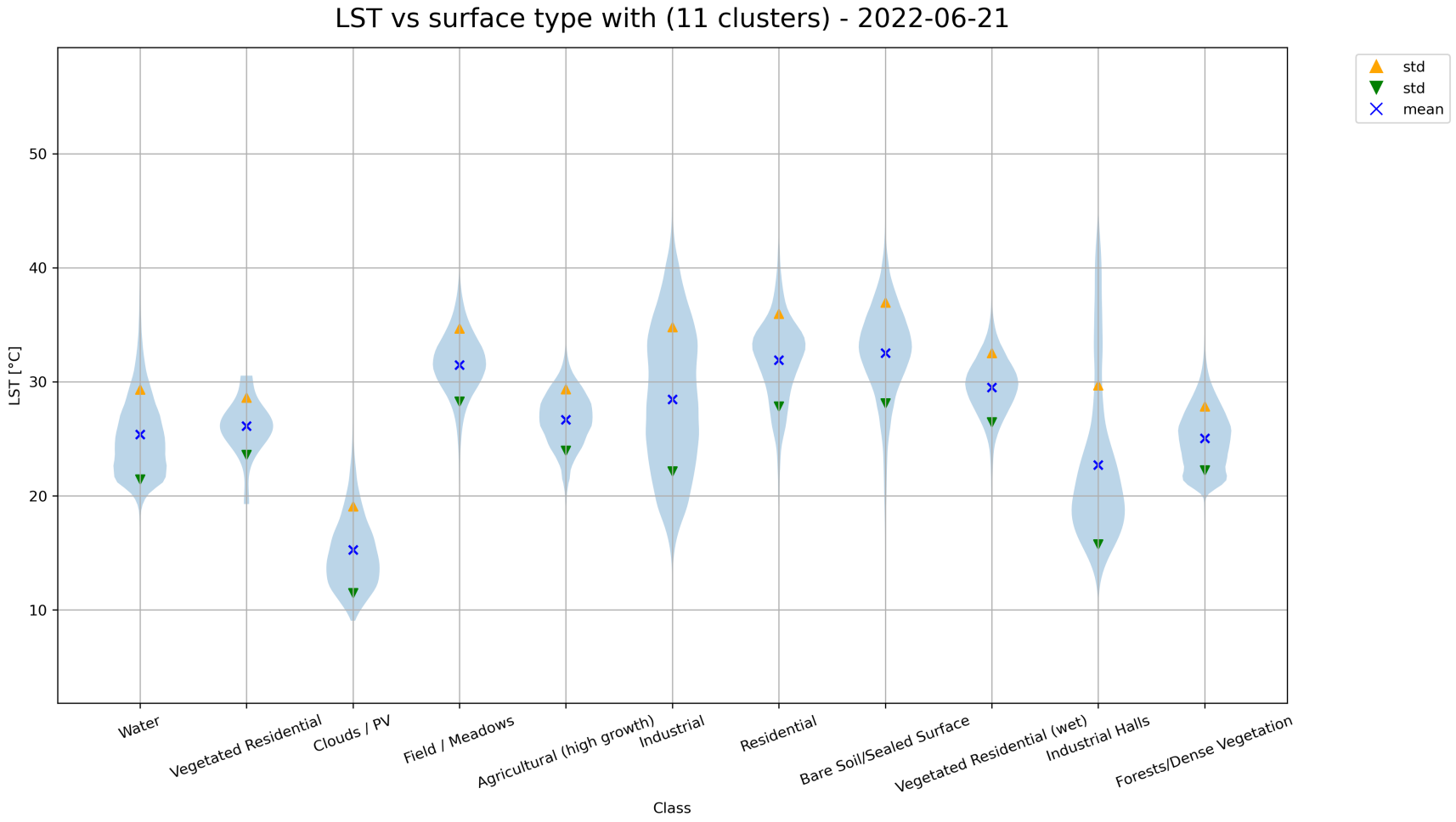

Figure 21: Distribution of pixel LST [°C] values per class June 2022

Figure 22 and Figure 23 show the NDVI values of the same classes. One unexpected observation is the wide spread of the water class over the whole range of the NDVI, where it is expected to be ≤ 0. This can be explained by the fact that the highly vegetated riverbank areas are also classified as water based on the additional features, changing the NDVI values assigned to this class. To calculate the diff between LU/LC at different points in time, a median filter is applied to reduce single pixel changes at class interfaces.

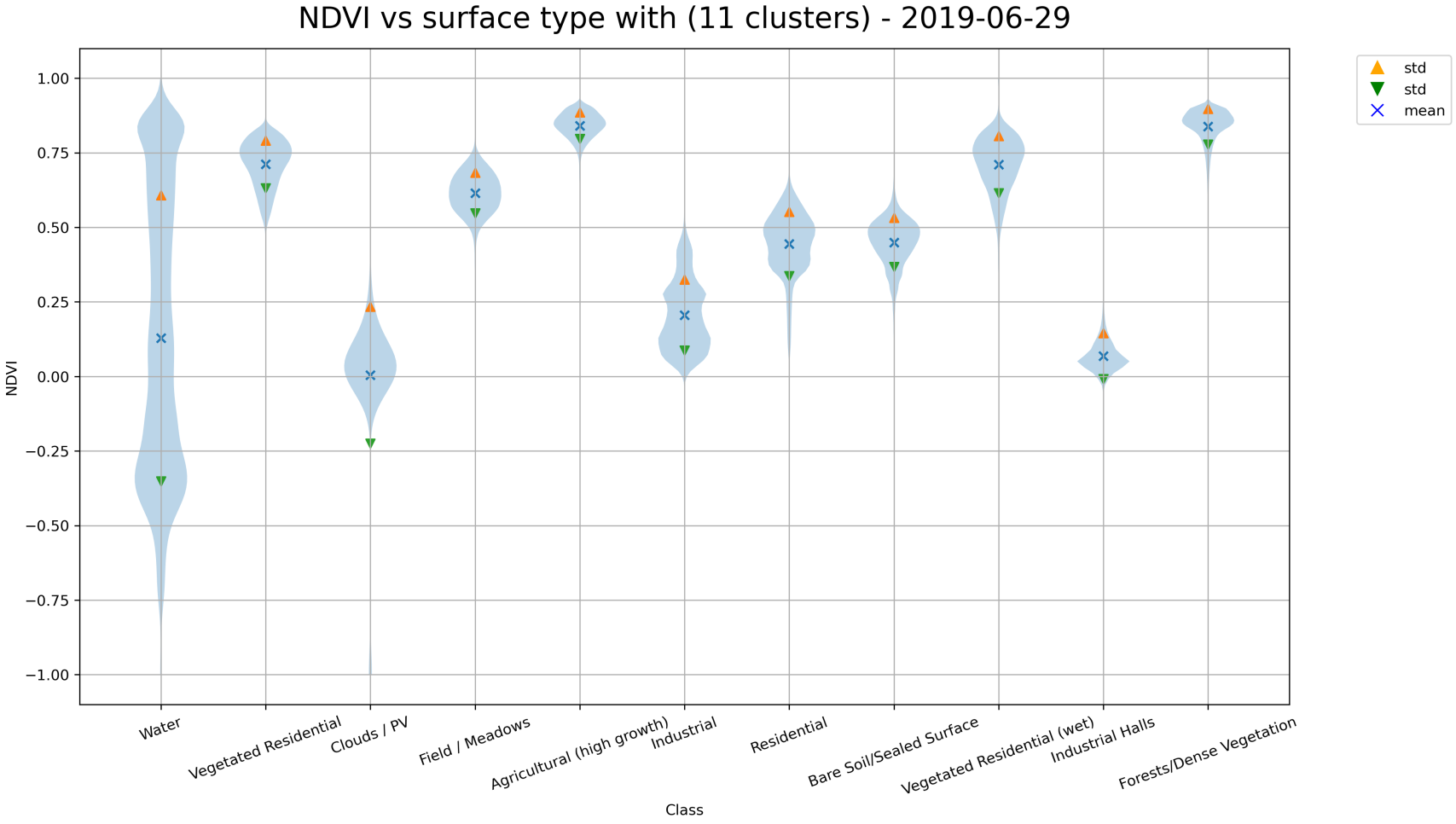

Figure 22: Distribution of pixel NDVI values per class 2019

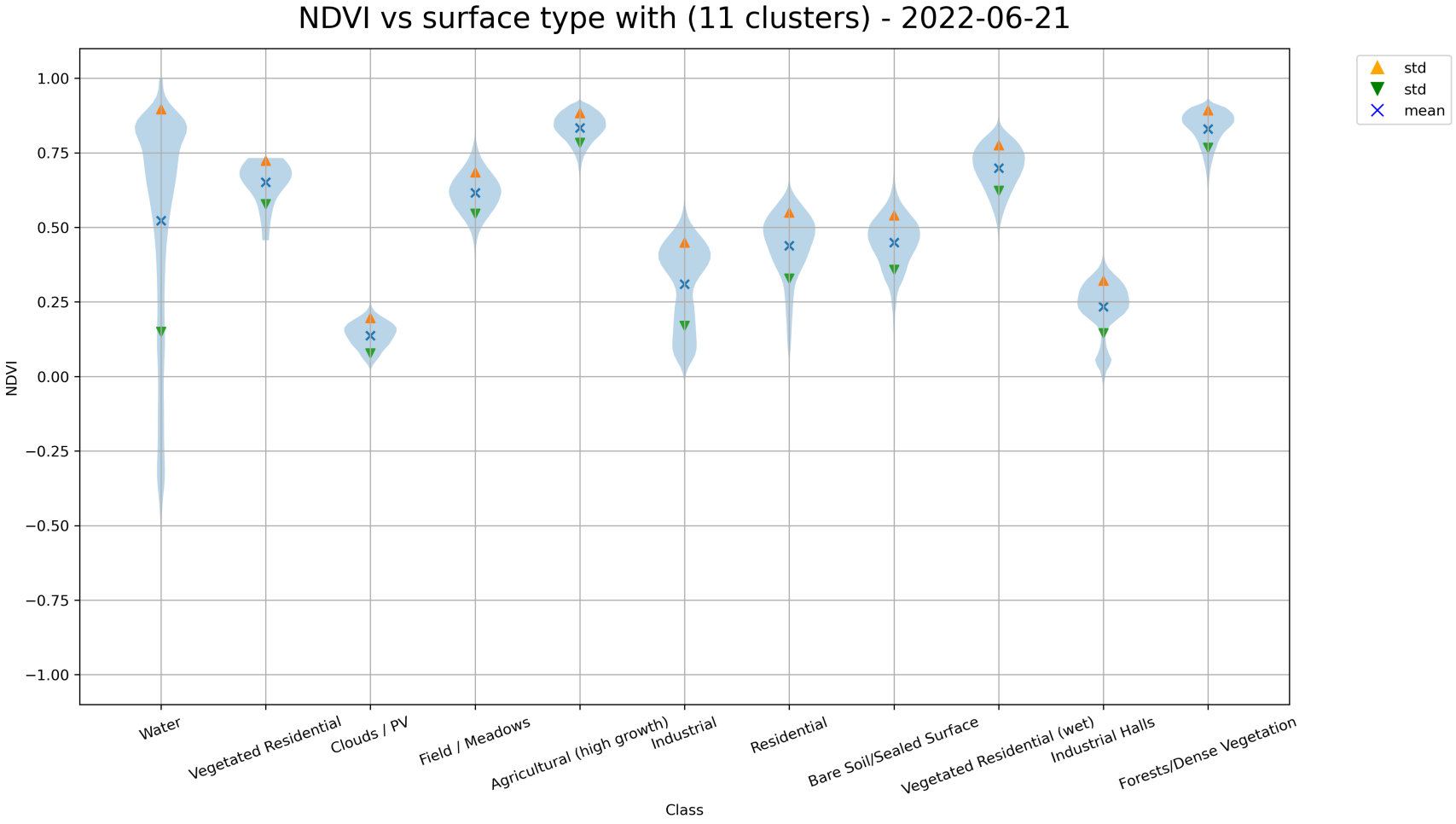

Figure 23: Distribution of pixel NDVI values per class 2022

Each detected UHI was further investigated by detecting the dominating class within the UHI area. The separated classes are plotted against UHI T_{max} in Figure 24 Industrial and sealed surfaces are the most common class found within areas affected by UHI. Very few UHIs classes were dominated by any class associated with high vegetation classes. The image shows, that the residential area includes the hottest UHI while Industrial UHI have a higher average max temperature.

5.4 Conclusions

The usage of Landsat imagery, with a Gabor filtering, K-means based classification constituted a robust methodology for land cover classification. The filter parameters on the Gabor filter were optimal with an absolute MSE of 0.3 $\pm$0.05 (class values 0 = water, 1 = urban and 2 = non-urban) for two years of classification, which is an error of 10%. Using the more detailed Structural Similarity Measure, the index is 0.98 $\pm$0.001 showing very high similarity (1 would be identical images, -1 inverted images and 0 for no similarity). These metrics were found highest with a filter bank of 12 asymmetric 7×7 px kernels, using 3 frequencies, 4 rotations and a sigma of 1.0 and 0.5) in x- and y- direction respectively (see Figure 12). The number of classes that are distinguishable varies by season and is limited by computing power, one possible improvement is the use of *reducing machine learning algorithms*, that identifies the principle components that have less variance between seasons. Additionally using parallelization by means of libraries such as *dask* (*Dask Development Team 2022*), allow bigger filter banks and additional steps to the pipeline to increase output quality. Another simple way that was not utilized was to incorporate the QA layer provided by the Landsat L2 data product, that provide per pixel probability values for water and cloud detection, that could remove outliers in the water and cloud classes and therefore provide higher quality results for the other classes. One way of increasing accuracy of the results is an increase in resolution, that allows the Gabor filter bank to have a wider range for usable values. In Figure 12 it can be seen that the first kernel of each rotation is nearly identical, due to to missing resolution. This would allow to detect smaller features. Another improvement might be the implementation of weights for the feature and original image values. Due to the missing changes within the image time frame no impact on the urban heat islands within Bremen due to urbanization or construction can be seen. The analysis of the classes dominant in the UHI clearly show that the surface type does have an significant influence on the creation of urban heat islands. Industrial and sealed surfaces are the most common class found within areas affected by UHI. No UHIs had an majority of pixels associated with high vegetation classes, confirming previous findings.

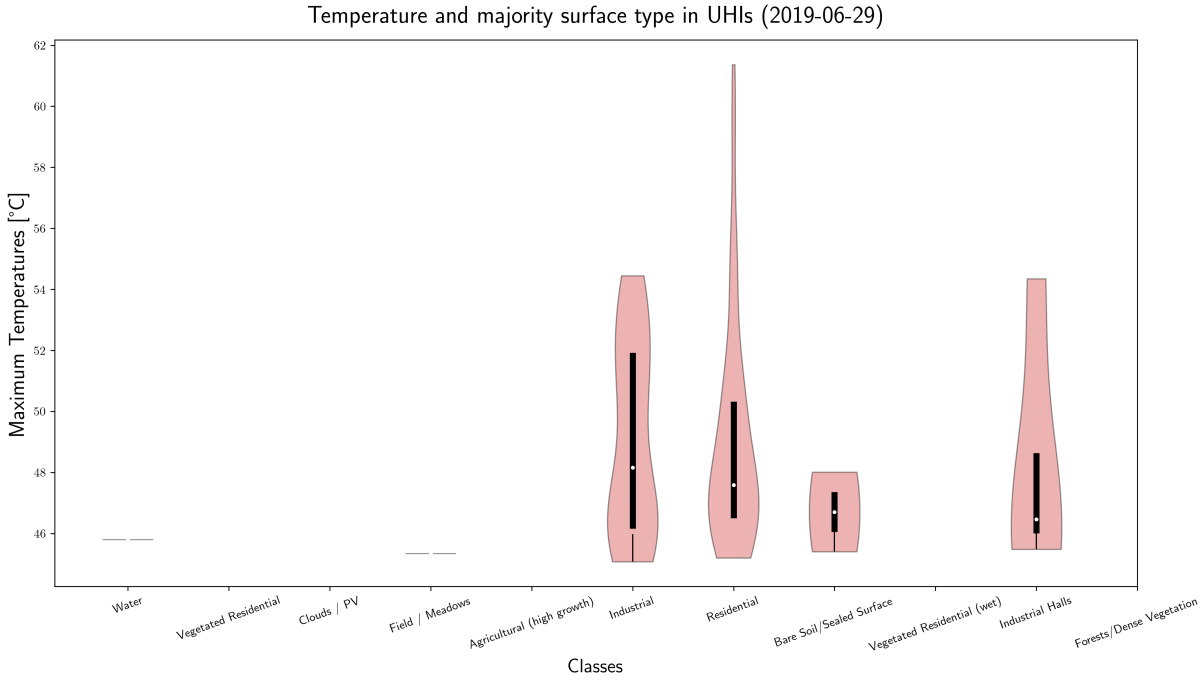

(a) 2019

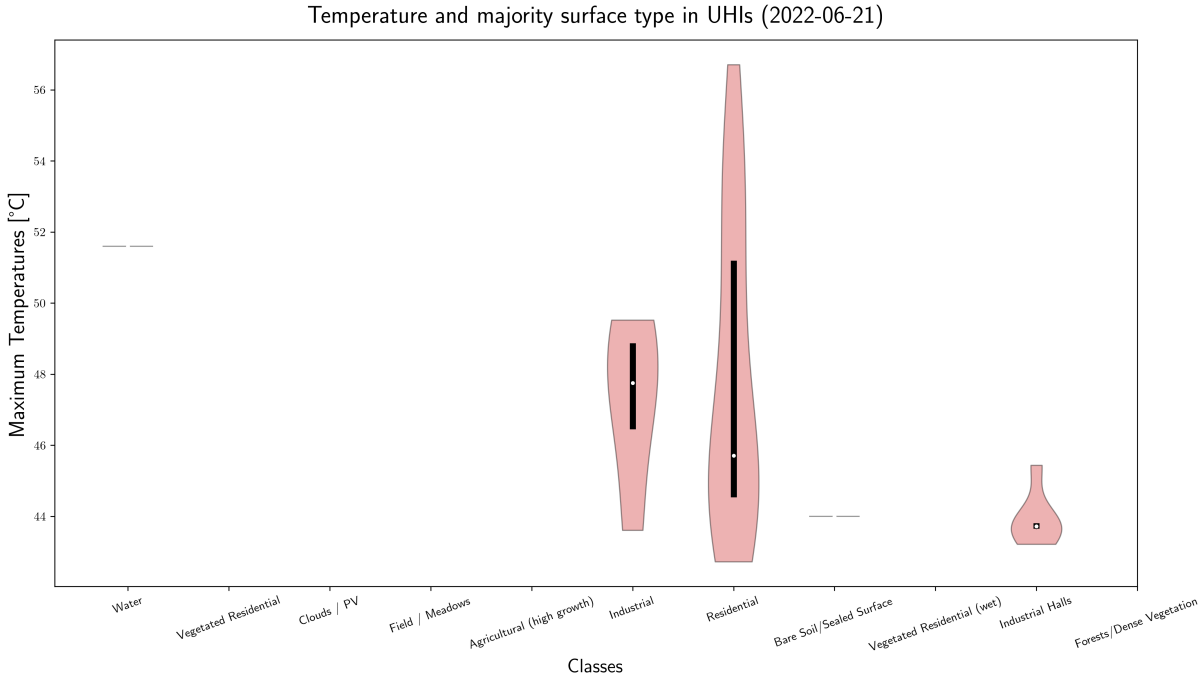

(b) 2022

Figure 24: Analysis of the majority classes within areas of UHIs and the associated temperature distribution

6 Impact of Climate Change on Urban Heat Islands

6.1 Introduction

The interaction between global and local climate is a complicated process that has multiple parameters, and is not yet fully understood or directly measurable (see section 1). While rural areas and the global south is most effected in terms of temperature increase and drought, the excess mortality of heat waves is greatest within city areas (*Gabriel and Endlicher 2011*). During high temperatures the threshold of negative health effect shows to be lower in northern European cities compared to Mediterranean cities (*Baccini et al. 2008*). The negative health consequences and increased mortality is affecting elderly the most and the excess mortality is an immediate effect (*Baccini et al. 2008*). In western Europe the climate is governed by a transitional climate, with attributes from maritime and continental climate. The summer is, compared to southern Europe, milder and not regularly affected by burning and heat waves. The temperatures in major European cities have increased at a similar pace than the global mean temperatures. In Bremen, the 5-year-average temperature has risen from 1990 (13.79° C) by 1.4° C to 15.20° C in 2020. The change over the past 20 years in monthly averages is shown in Figure 25.

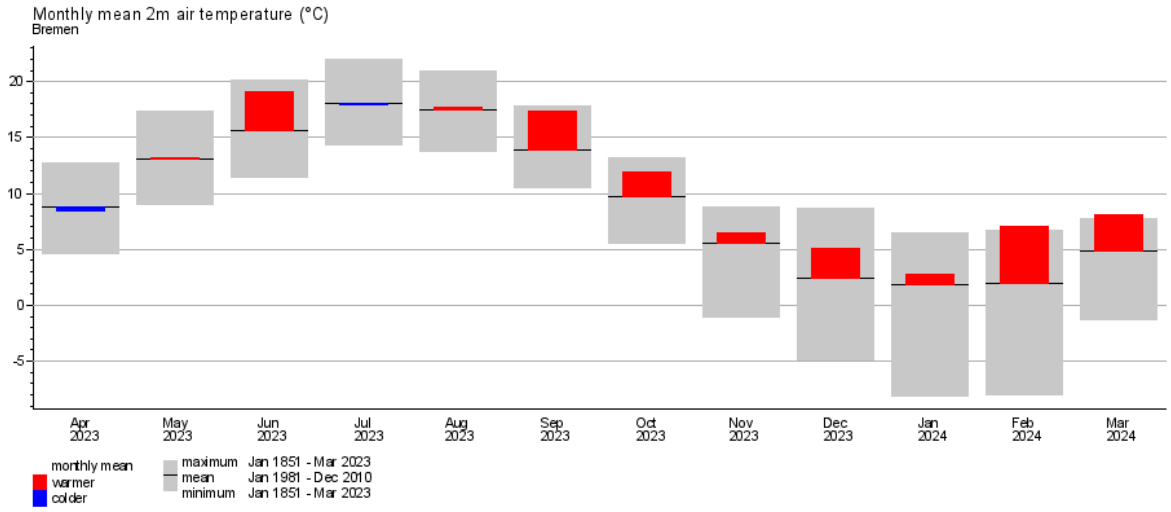

Figure 25: Change of monthly air temperature average compared to average of 1981–2010 (*Deutscher Wetter Dienst 2024a*)

6.2 Methodology

Measurement of the impact of rising temperatures have to be done after correcting for other variables such as urban development and meteorological impact factors such as wind and rain. To achieve this, a time series of land surface temperatures and UHIs from 1990 to 2022 was created using Landsat 7 and Landsat 8 and 9 data. Data from two weather stations in the areas were used to calculate the trend of mean temperature over the time.

The UHIs data was then correlated with the air temperature data of the local measurement stations and corrected for size increases of UHI impacted by land cover change in the previous step. This way all UHIs that would be impacted by urbanisation or change of surface type were excluded from the analysis.

6.2.1 Data Handling

One of the challenges arising during the processing of multiple images were the large amount of data of the images and feature bands. To reduce the memory footprint of the processing chain, xarray (*Hoyer and Hamman 2017*) was used. Xarray allows lazy loading from disk, this only loads parts of the complete dataset. Another feature of xarray that was used are labelled data. Each loaded image used latitude and longitude as coordinates allowing to accessing sub areas by reference coordinates. Another axis was added for the time dimension, so that each area could be stored in a single data file, but access is done loading only the relevant data for a specific time or a selected time frame.

For this step the following data was loaded from the previous dataset:

- Band data from the area of interest (Band 1 to 10)
- Classification label, a layer with the numerical classifications assigned to each pixel
- Urban mask, a layer with urban, suburban and peri-urban areas
- UHIs, for each time step a layer, masking urban heat islands

6.2.2 Land Surface Temperature Calculation

The LST can not be measured directly by a satellite but must be calculated from the upwelling thermal infrared radiation and corrected for the atmospheric perturbation. For Landsat 7 and Landsat 8 data is provided in different processing levels. For analysis of past data that has already be processed the level 2 data can be used, that provides land surface temperature and has been calculated from the level 1 data. To derive the level 2 data from level 1 data, Top of Atmosphere (TOA) brightness is used, corrected for stray light (Landsat 8 specific, see (*Zanter 2019, p. 67*)) and instrument distortion. Geometric and geographic terrain-correction (*Zanter 2019, p. 44*) is applied, resulting in an geolocalized image. The TOA temperature data is calculated according to eq. (11), where K_1 and K_2 are band specific conversion factors from the meta data file and L_λ is the spectral radiance at the TOA in $\frac{W}{m^2 \cdot srad \cdot \mu m}$ e.g. the Band 10 Channel.

$$T = \frac{K_2}{\ln\left(\frac{K_1}{L_\lambda} + 1\right)} \tag{11}$$

To get the level two data from these TOA measurements the value is corrected for emissivity of the ground using measurements from the *ASTER GED* database (see *USGS 2014*).
The temperature is also corrected for atmospheric interference using local reference stations. The USGS uses reference stations, atmospheric models and independent reference measurements from other satellites to calculate the surface temperature. The surface temperature product has an accuracy of $\pm 1K$ overall and other uncertainties are marked in a quality assurance file provided for each image.
To convert the image file containing 16 bit, unsigned integers into a temperature eq. (12) is used. The scaling and offset factors are specific to the product and were taken from *Earth Resources Observation And Science (EROS) Center 2013, Table 6-1.*

$$T_C = T_K - 273.15 = \mathrm{DN} \cdot 0.00341802 + 149.0 - 273.15 \tag{12}$$

Where DN is the *Digital Number* (a 16 bit integer) stored in the image file, the multiplication factor as well as the 149.0 offset are provided in the meta data file and in the Landsat user manual (*Earth Resources Observation And Science (EROS) Center 2013*). The accuracy of the resulting temperature value is given by the user manual as also ± 1 K.

6.2.3 Local temperature rise

For investigating a city, the next ground based measurement stations was used as reference. This data was correlated with the SUHI intensity as well as the measured temperature data from the times of the satellite data acquisitions. For German cities the stations of the DWD are used, these have very accurate readings and a long archive of measurements. One indicator interesting in the research on UHIs is the number of days with very high temperatures. There are multiple threshold days that are used to classify seasons in comparison to the average. Hot days (defined by the DWD as days with a maximum temperature over 30 °C), summer days (maximum temperature over 25 °C) and tropical nights (days with daily minimal temperature over 20 °C), are tracked by meteorological organisations (*Deutscher Wetter Dienst 2024b*). Another measurement to visualize a rise in average temperature is the amount of frost days (where the minimal temperature is below 0 °C). The Figure 26 and Figure 27, show the development of these indicators for Bremen over the past 82 and 32 years respectively.

Table 2: Bremen weather data using data from *Deutscher Wetter Dienst 2024a*

	Extremly Cold	**Average**	**Extremly Warm**
	min	mean	max
Annual average °C (Jahr)	7.2 (1940)	9.4	11.1 (2020)
Abs. T °C (Jahr)	-23.6 (Feb. 1940)		37.6 (Aug. 1992)
Summer days ($T_{\max} \geq 25$ °C)	4	27.7	78
Hot days ($T_{\max} \geq 30$ °C)	0	4.9	22
	max	mean	min
Frost days ($T_{\min} < 0$ °C)	105	70.8	24
Ice days ($T_{\max} < 0$ °C)	54	14.9	0

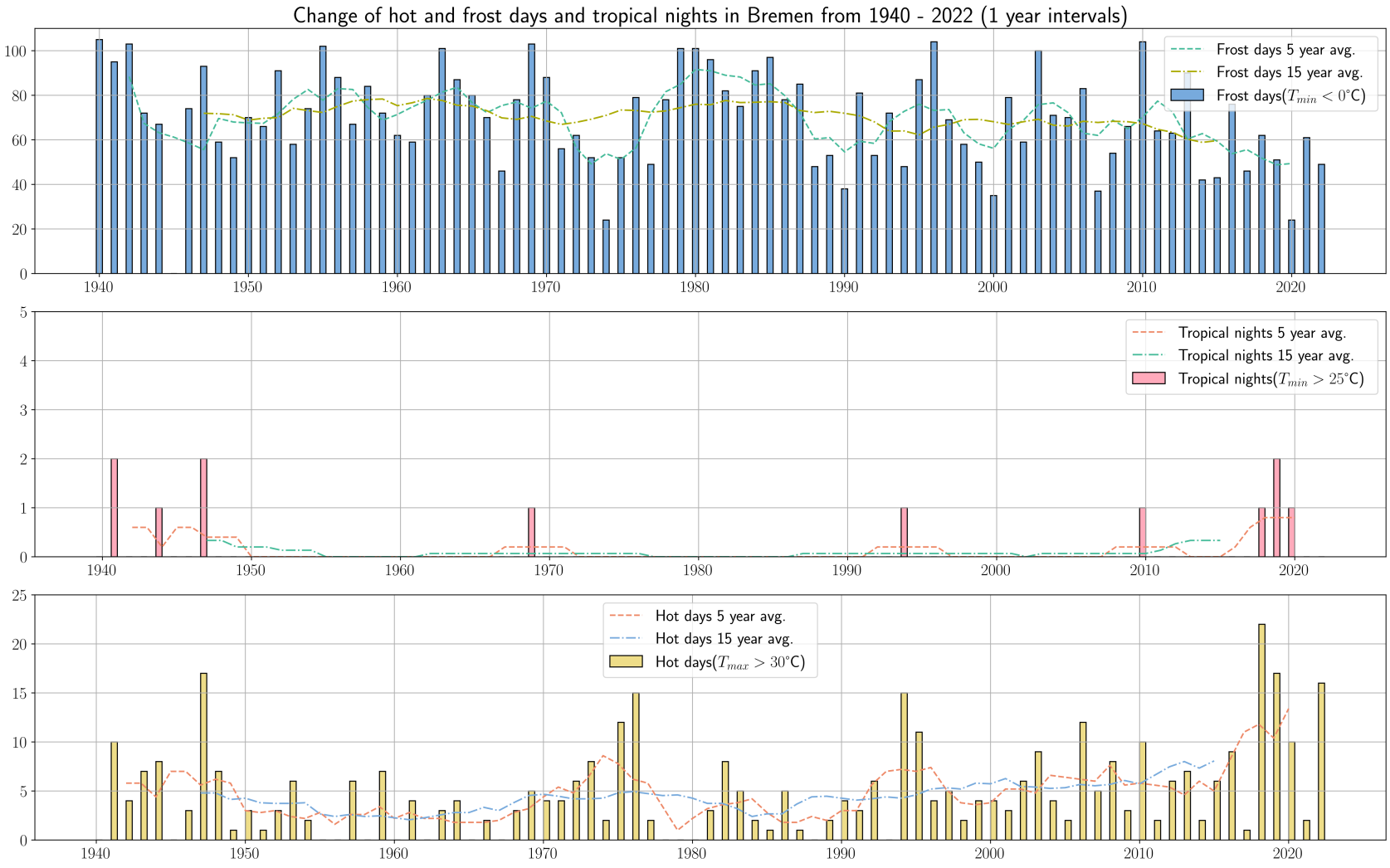

Figure 26: Number of cold and hot days over time in Bremen, Germany 1940-2022

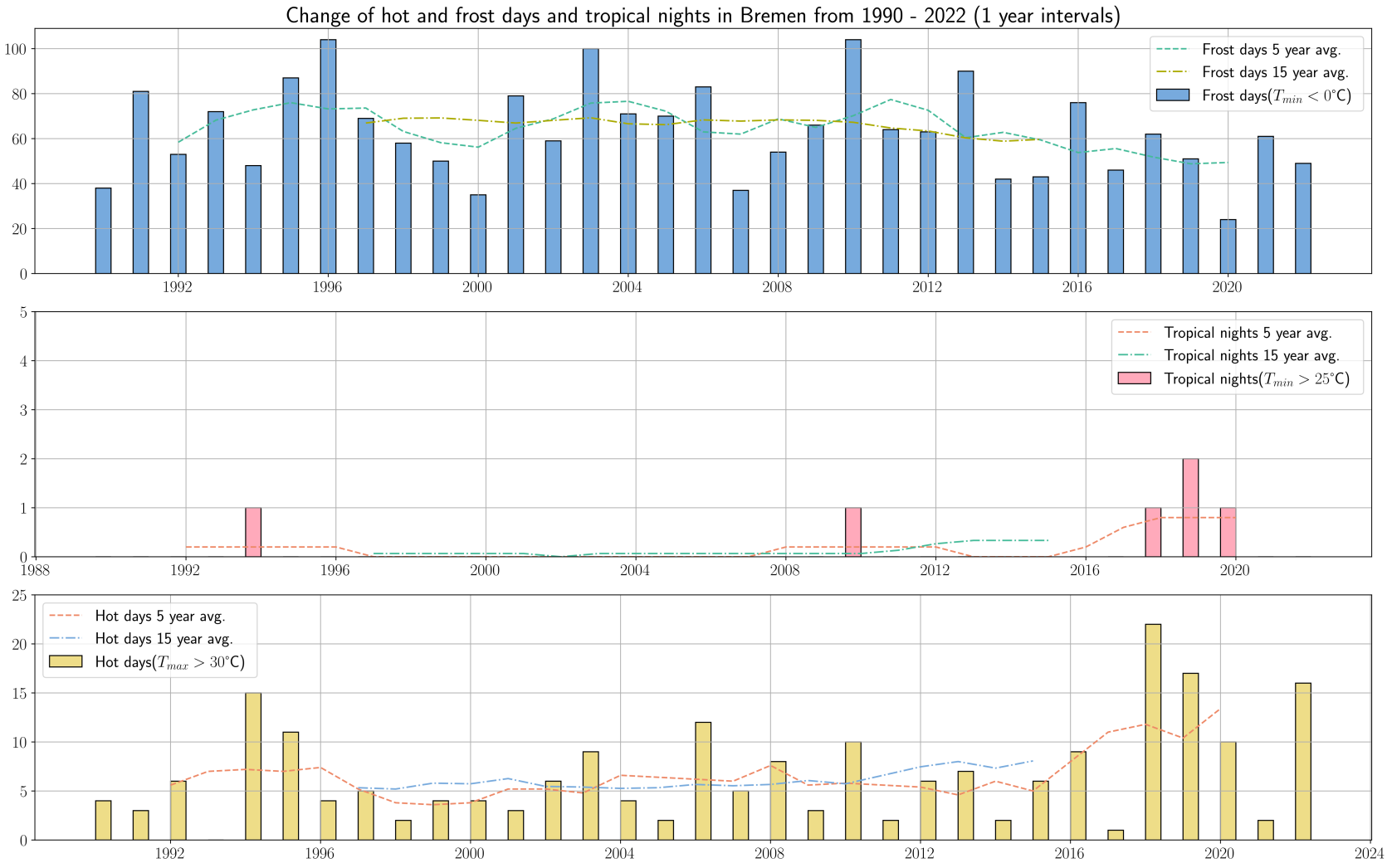

Figure 27: Number of cold and hot days over time in Bremen, Germany 1990-2022

6.3 Analysis

Bremen was selected as the base area of the study, to be able to verify classification results using personal local knowledge. The study area covers the city centre of Bremen and an area of 27 km in all directions covering an area of approximately 3000 km^2. The study area is at sea level elevation and has a temperate-oceanic climate according to the *Köppen and Geiger 1930* classification. An overview of the climate of Bremen is shown in table 2. The development of threshold days over time are shown in Figure 26, the strongest change can be seen in Figure 27 and the downward trend in frost days. Together with the increase in tropical nights over the past five years and the increased appearance of hot days for the past 3 years after 6 decades with no or one hot day per decade, this fits the trend of global rise in temperatures.

The weather station in Bremen is located at the airport on the edge of the city area. For comparison of air temperature with a more rural area the DWD weather station "Worpswede-Hüttenbusch" located roughly 30 km north-north-east of the weather station and is located in a rural area (see Figure 28). To verify that the measurements of the

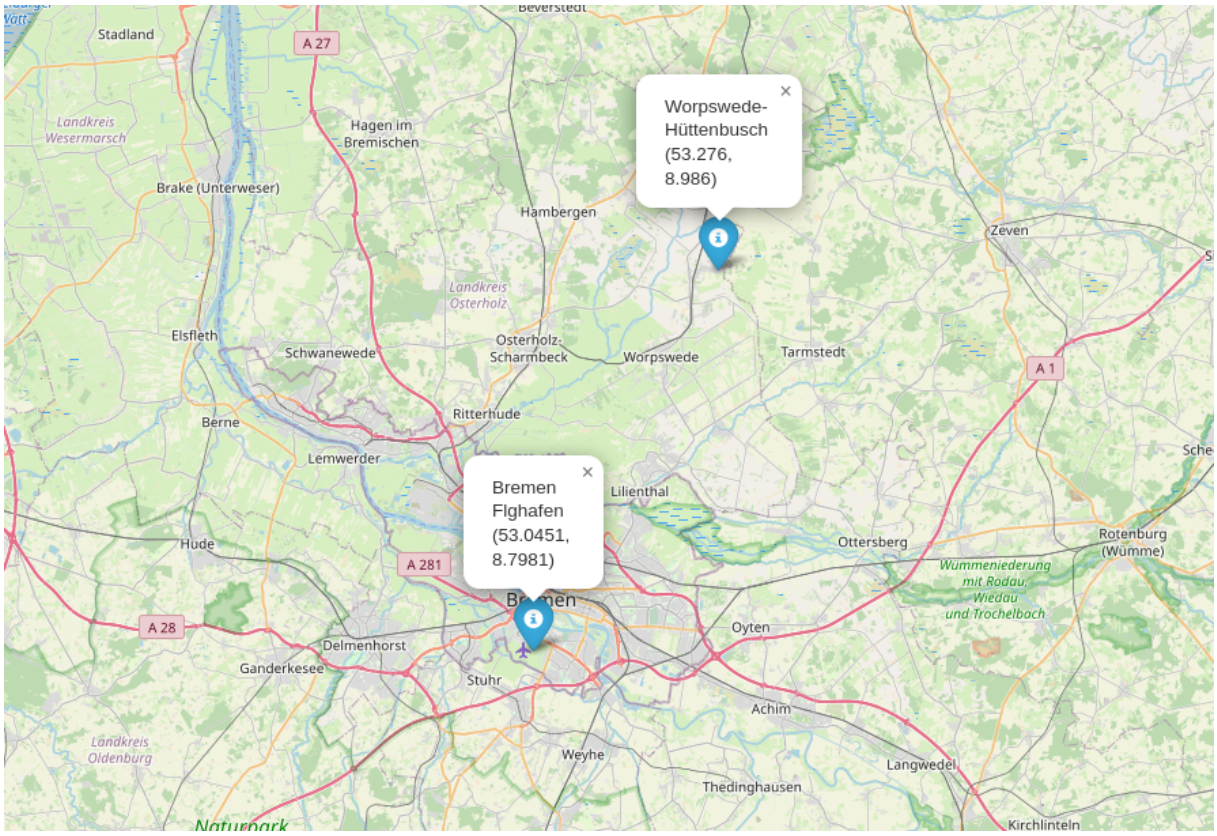

Figure 28: Location of the weather stations in Bremen and the rural reference station in Worpswede-Hüttenbusch

urban and rural stations, the difference in daily measurement values of both stations is shown in Figure 30 and Figure 31. It can be seen that the atmospheric UHI over Bremen

is affecting the Bremen airport station. In the period from April to October in 2015 the daily mean temperature was 0.6 ° C lower at the rural station. In the same period in 2022 the daily mean temperature was 0.85 ° C lower at the rural station. The Stations are calibrated to provide comparable weather data with high levels of accuracy (error smaller ±0.2° C (*LES 2024*)). Figure 29 shows the offset of minimum, maximum and mean temperature daily temperature over the year. This indicates that the atmospheric heat island of Bremen is affecting the airport weather station.

Figure 30 and Figure 31 exemplary show the lack of usable satellite imagery for Bremen

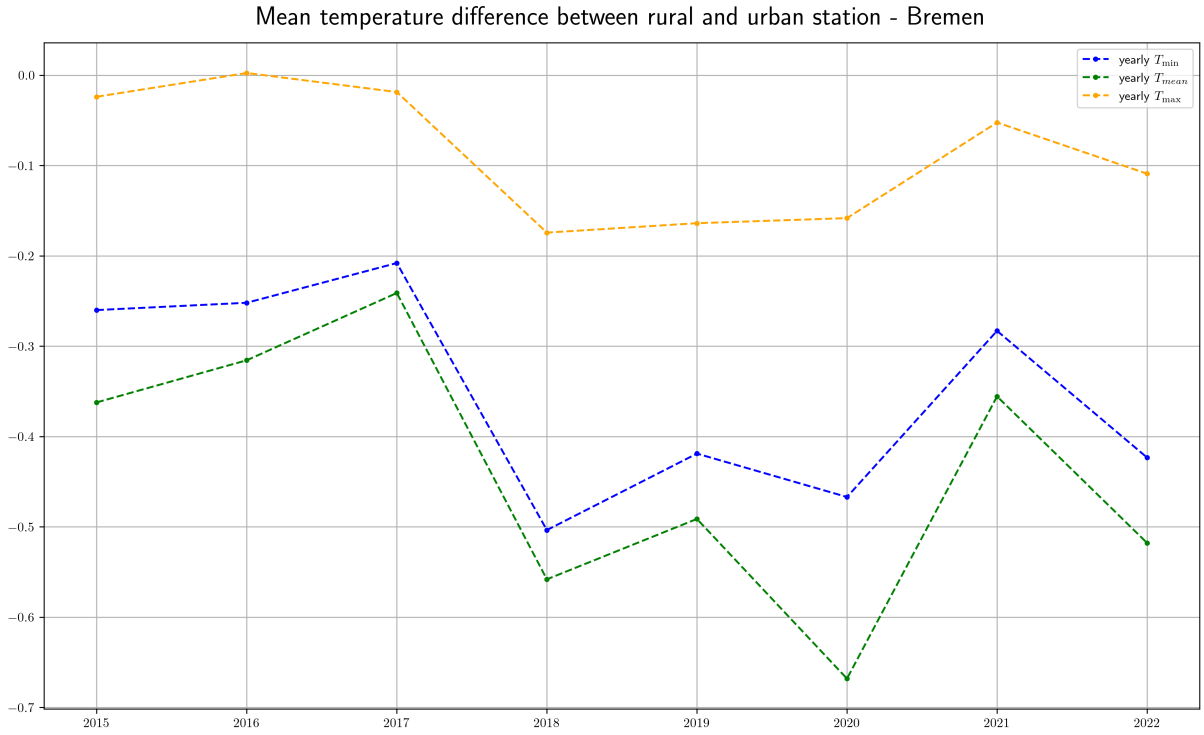

Figure 29: Mean yearly station offset urban rural station

in green. Especially finding cloud free cover of the area with similar seasonal and weather patterns was difficult.

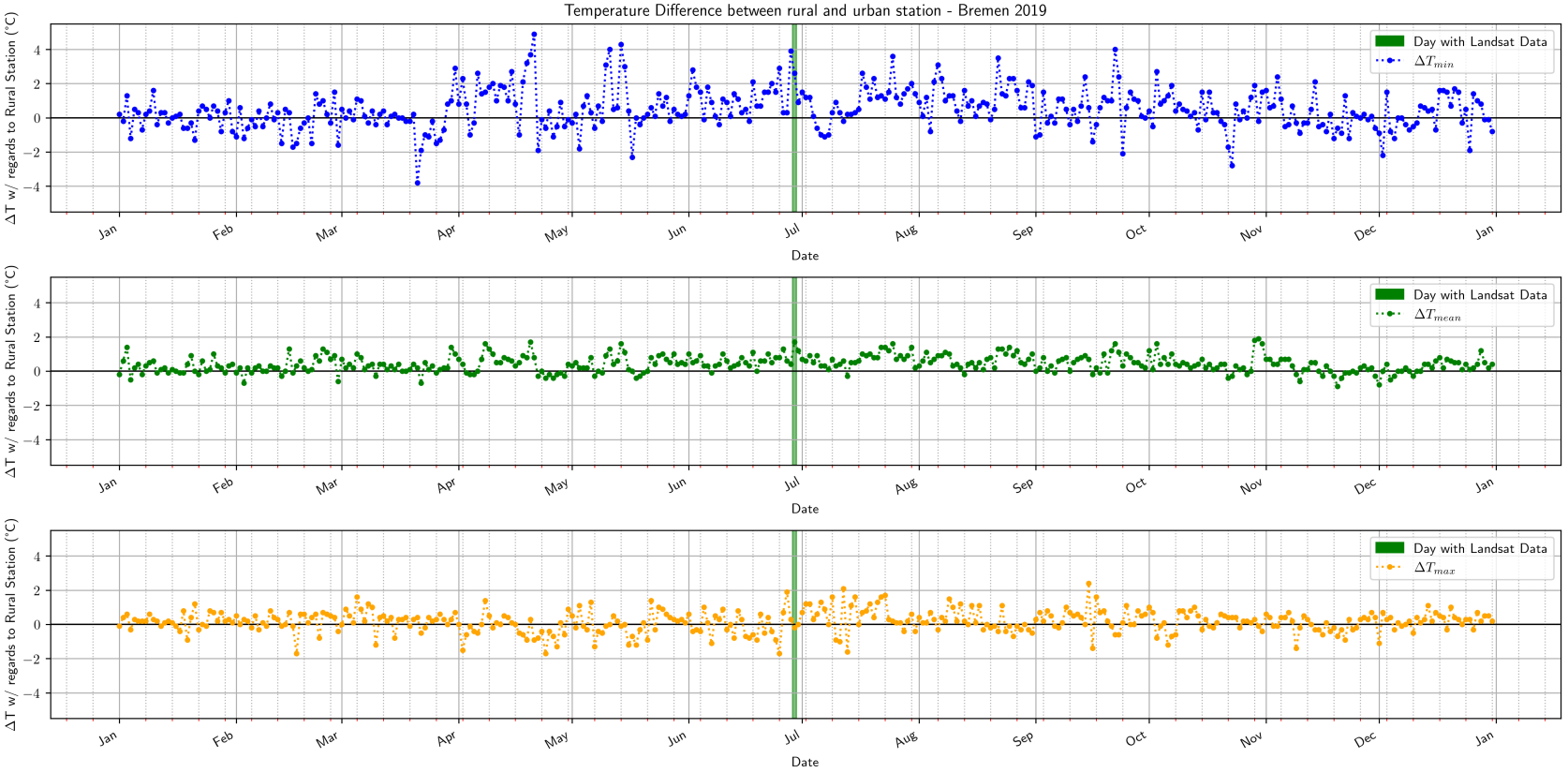

Figure 30: Absolute Differences between measurement stations [°C] and days with satellite coverage (green) in 2015

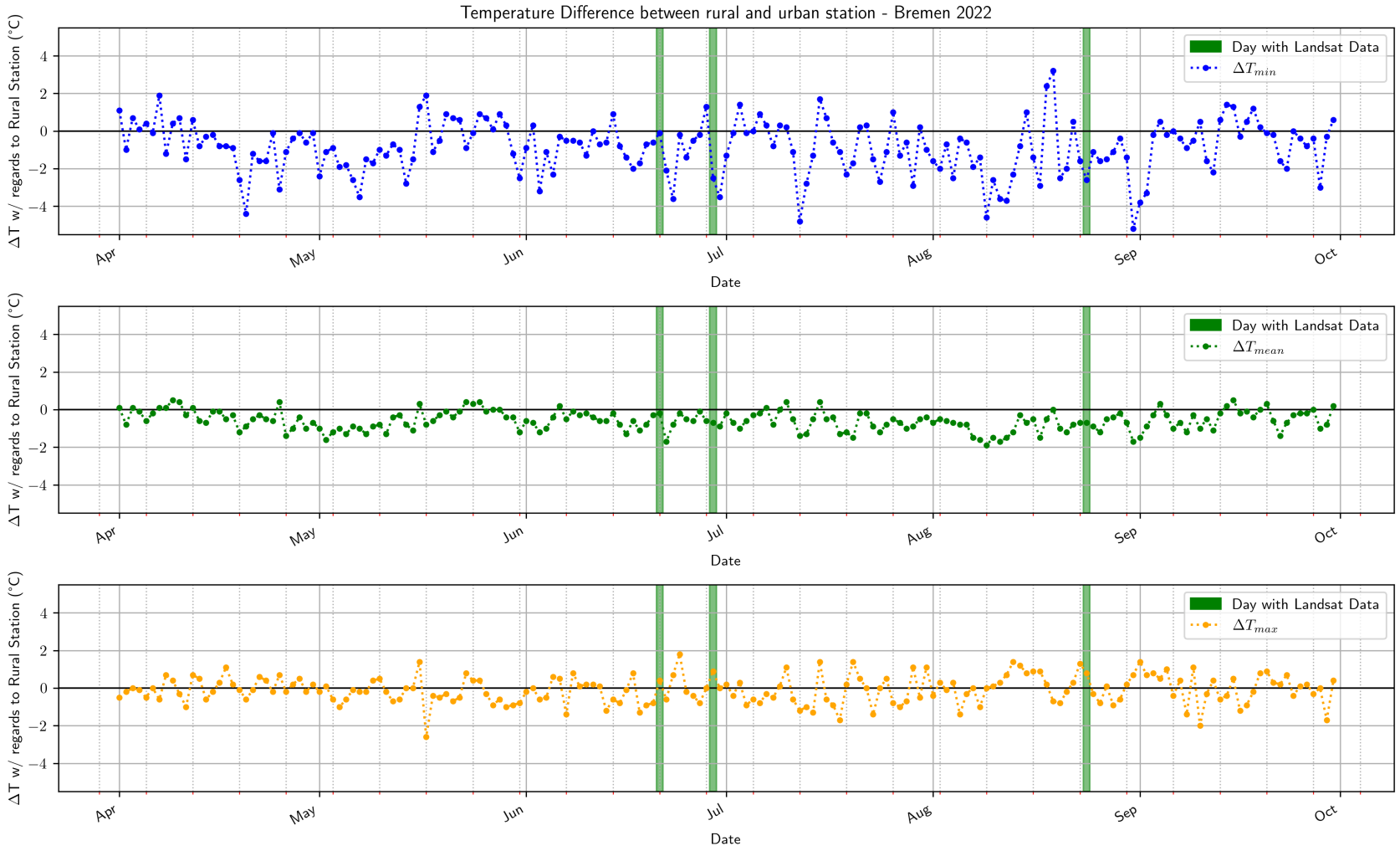

Figure 31: Absolute Differences between measurement stations [°C] and days with satellite coverage (green) in 2022

Figure 19 shows two summer days in Bremen with different temperatures and the influence of temperature onto the UHIs size and shapes. In the image from 2019 (Figure 19a), the average temperature was much higher at the time. It can be seen that the heat islands, while statistically the same difference to the peri urban temperature, increase in size and combine into larger structures. In table 4 the properties of the UHIs for different days within the urban area is shown.

The analysis of the UHIs at the analysed dates, shows a strong increase in maximum and average heat island size, with rising temperatures. UHIs smaller then 5 pixel (4500 m^2) were excluded, to mitigate impact of outliers. Figure 32 shows the distribution of sizes and maximum temperatures within the UHI. Most heat islands are small with a wide range of temperatures, the few very big heat islands are within the mid range of temperatures.

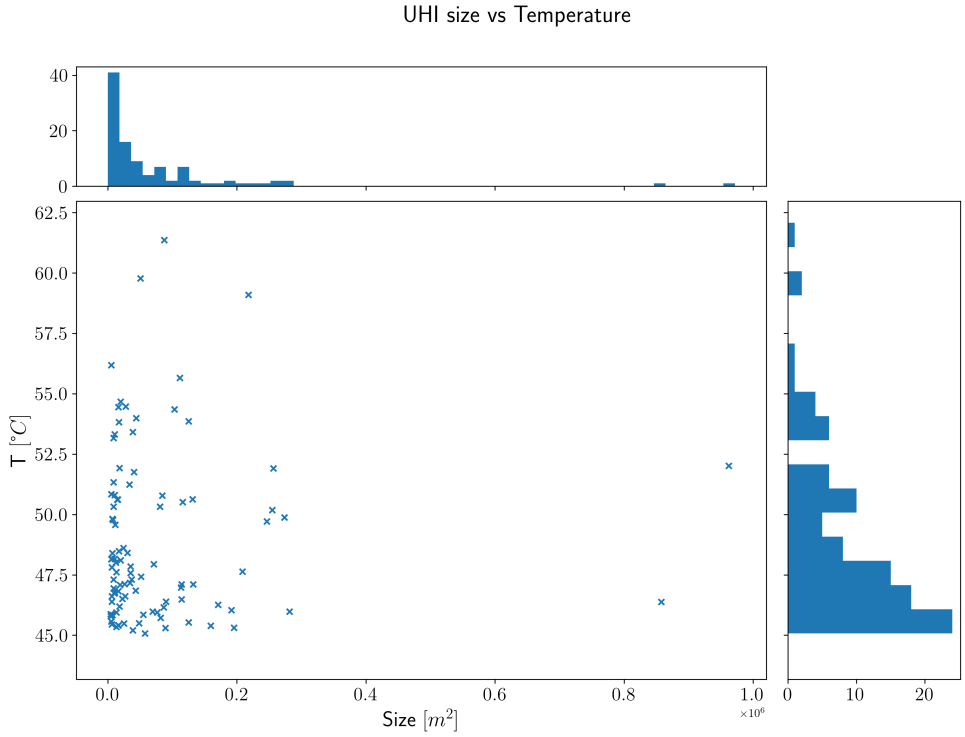

(a) 2019

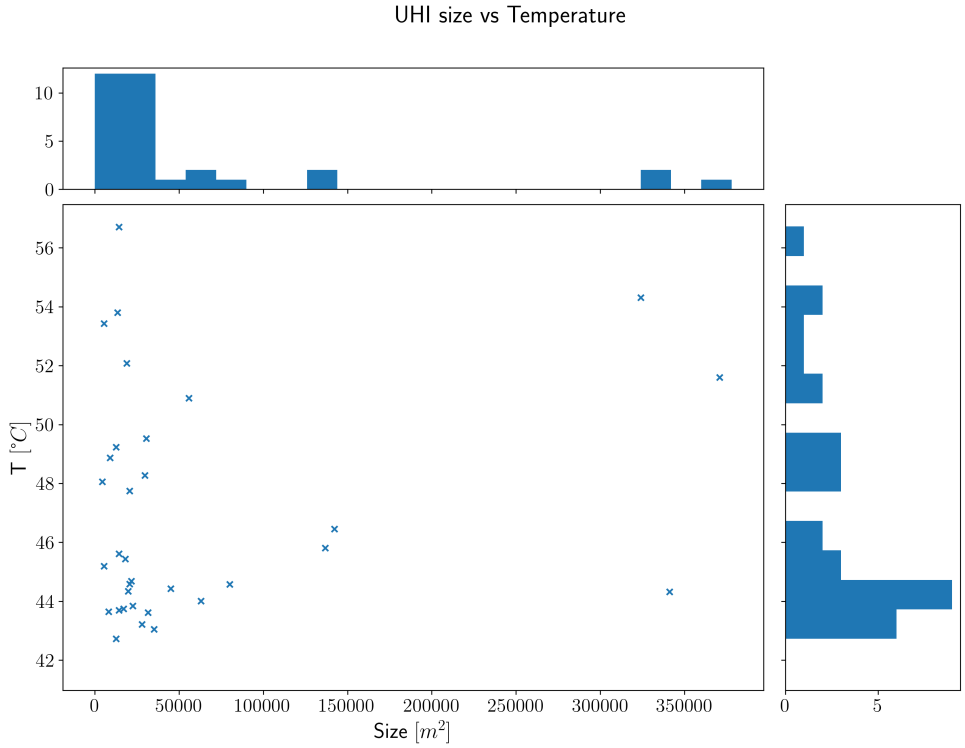

(b) 2022

Figure 32: Maximum Temperatures of the detected UHIs and area above threshold

Table 3: Comparison of Air Temperature, LST and UHI size for Bremen

	Air Temperature							**LST**					
Date	**Urban**			**Rural**			ΔT	**Urban**			**Rural**		
	$T_{\min}$	T_{mean}	$T_{\max}$	$T_{\min}$	T_{mean}	$T_{\max}$		$T_{\min}$	T_{mean} (std)	$T_{\max}$	Num. UHIs	$T_{\min}$	$T_{mean}(std)$	$T_{\max}$
2019–06–29	15.9	24.7	31.9	17.7	25.4	30.7	-0.7	22.9	34.2 (3.5)	61.4	102	22.92	35.2(3.77)	61.4
2022–06–21	6.9	15.7	22.3	7.6	15.6	23.0	-1.0	4.4	29.0 (4.4)	56.7	34	4.7	29.7 (4.4)	56.7

Table 4: Comparison of Urban Heat Islands in Bremen over time

Date	Number UHIs	min area $[m^2]$	mean area $[m^2]$	max area $[m^2]$	$\text{UHI}_{\max}$ T_{mean} [°C]	UHI_{max} T_{max} [°C]
2019–06–29	102	4500	74691	962100	47.7	52.0
2022–06–21	34	4500	58950	370800	46.4	51.6

7 Conclusion

Due to the limited remote sensing data availability at summer dates with similar weather, statistical analysis is not conclusive. There is an increase in number, mean size and maximum size visible with rising average temperatures. The maximum temperatures are very similar and do not increase linearly with average temperatures. Analysing each UHI for more parameter and using measurements from different sources, e.g. ground measurement campaigns to refine and verify measurements. The data indicates size increases of SUHIs with rising temperatures, due to lack of measurement stations there is no data on the impact of the inner city air temperature distribution. In the following sections the answers to the research questions are recapitulated.

7.1 What definition can be used to define UHIs comparably?

An SUHI is an area with increased surface temperature within an urban space. It is defined as having a temperature at least 3 standard deviations above the average temperature of the adjacent rural buffer zone. This measurement is corrected for larger settlements. This definition can be used to compare urban areas in different settings and surroundings.

7.2 What is the influence of LU/LC change on the size of urban heat islands?

A strong correlation exists between dominant surface types and urban heat island size. Surfaces with high NDVI and low surface sealing tend to have lower temperatures. Consequently, these areas feature few, if any, urban heat islands.

7.3 How significant is the impact of urbanisation on UHIs, both in terms of absolute and relative temperature changes?

Sealed surfaces and industrialized areas are most impacted by and are major sources of urban heat islands, regardless of average reference temperature. Surface types typically associated with urbanisation and human activity, are most affected by UHIs. These Surfaces are bare, sealed areas (parking lots, runways, bare ground and industry lots), industrial areas and high density residential and commercial zones, commonly found within city centres. The study area did not allow to investigate areas impacted by surface type changes, due to lack of a large enough change within the observed time frame. The strong correlation and other studies show that urbanization without mitigations is a strong driver for UHIs formation.

7.4 What is the effect of rising average temperatures on the UHIs effect?

The weather data from the DWD shows an increase of average temperature from 1990 to 2020 of 1.4 °C average yearly temperature. Combined with the findings of the influence of average temperature on UHIs size increase, this subject could be investigated further. To answer this question with a significant statistical analysis, additional satellite imagery is needed (e.g. Landsat-7 or Sentinel-3 footage, if enhanced with a super resolution algorithm)

7.5 What indices can be used or created to categorize and rate UHI intensity?

The use of indices like the HI (see section 2.4.2) and WBGT (see section 2.5) are useful tools to measure and predict the danger and risk of UHI. One requirement for the use of these are either weather stations within areas affected by UHIs or a model transforming LST to air temperature values.

7.6 Summary

The study shows that even in higher latitudes the surface temperatures caused by anthropogenic surface modification causes high surface temperatures. The impact of climate change indicates an increase of hot days and tropical nights in temperate climate zones, increasing the risk of negative health effects and dangerous air temperatures during summer and heat waves.
It was also shown that Landsat data can independently be used for surface classification with high accuracy compared for single day classification, when combined with feature engineering such as Gabor filters using unsupervised machine learning. At time of the study the availability of cloud free remote sensing data posed a severe hurdle. The proposed statistical definition could be helpful to compare UHIs in different climate zones and seasons. Urban area extraction, adapted from the suggestion of *Sobrino and Irakulis 2020* approach, has shown to follow the natural borders of the city well. All posed questions were answered but the results where inconclusive due to the lack of data or land cover change. The work showed that there are insides to be gained by the study of UHIs, even in cities at higher latitudes. Rising global temperatures show the need for scientific understanding and pose multiple opportunities for modelling and investigating the UHI phenomena further. The results may help future research by showing what areas are to be investigated and what approaches and indices can be used to measure health impact and danger of UHI.

7.7 Limitations and Challenges

While the connection of ground based sensor stations with remote imagery works well, a direct reliable conversion from land surface temperatures to air temperature, since there is a temporal and seasonally different energy transport between surfaces and surrounding air. Another limiting factor was the availability of suitable cloud free satellite footage of the area of study. While with the introduction of Landsat 9, the amount of footage doubled, in regions with high cloud cover (like Bremen) and due to the not evenly distributed coverage times of the satellites (2d apart), this resulted in very few images that were useable for the statistical analysis. Due to the low numbers, the results are not statistically relevant and another satellite product or future results need to be used to come to a significant outcome. Observing the impact of land cover change another study area is needed, where significant land cover changes are done. This could be areas that have high growths or construction (see section 7.8) or areas that were impacted by catastrophes or war, artificially changing the surface properties

7.7.1 Data

Another limiting factor was the availability of suitable cloud free satellite footage of the area of study. While with the introduction of Landsat 9, the amount of footage doubled, in regions with a lot of cloud cover like Bremen, the amount of usable footage is very limited.

7.7.2 Software

For the analysis of the Area Of Interest, a python application and script assortment was developed. It has was developed with adaptability in mind so that the The software was written in python code used for generating the data, the documentation of the code is located within the doc folder. The main.py is documented using the –help option. This file provides download and classification of Landsat data.
The LST2.py file can be run to detect urban heat islands when the classification was done previously. The integration of this part into the main.py functionality is still outstanding.

7.8 Outlook and Future Work

The overall results of this work allowed to identify many further areas of studies. The classification part could be improved by using a widely available product that has a suitable resolution. During development a 300 m and 10 m reference product were used (see section 5.2), the first was considered not precise enough for these measurements. The second reference product used had 10-m resolution, but was limited by the available temporal resolution of one year, with yearly averages. Since the selected Area Of Interest did not contain sufficiently large LU/LC changes within the urban area, multiple sides where selected that could be of interest for future studies using the same methodology.

Leipzig 416 is a construction project within the city center of Leipzig. The construction started in 2021 and a significant land use change was observed in that area.
One interesting area of study would be the Leipzig 416 Project, an urban district development project, currently being constructed in the city centre of Leipzig, designed to be environmentally friendly, vegetation rich and designed after sponge city concepts. Monitoring the development of UHIs in the area and surrounding could show how effective modern urban planning is compared to the previous situation.

Another interesting non-urban area of study could be large construction projects in previously rural areas, like the Tesla Factory in Grünheide, the Berlin Brandenburg Airport in Germany, the ITER (International Thermonuclear Experimental Reactor) near Marseilles in France and the impact on the surrounding micro climate and fauna caused by the LU/LC change.
Another topic of interest could be the scientific study and monitoring of implemented mitigating techniques. Allowing rating of effectiveness for installed countermeasures to find optimized, cost effective solutions for the mitigation of UHIs, adapted to the local conditions.

Using the same methodology on other European cities, affected by high heat or pollution gives the opportunity to verify the methodology and the findings of this work and investigate if patterns and differences exists when comparing similar cities. Cities of interest found during this work are:

- Frankfurt am Main
- Valencia
- Stuttgart
- Essen
- Karlsruhe
- Berlin
- Madrid

8 Appendix

8.1 Use of AI based tools (Nutzung KI basierte Anwendungen)

According to the *Eigenständigkeitserklärung* section 8.2.3 the use of so called AI tools needs to be declared. During this work the following tools were used:

- OpenAIs ChatGPT (*OpenAI 2023*) for aid during programming, help with formulations, getting topic overviews and aid in finding keywords for further research.
- Kagi's summerizer (*Kagi Inc. 2024*), to deem papers relevant.

All informations from these tools were used as an aid and were always cross-checked with primary sources.

8.2 Content of the Data Storage device

All data and the software used to create the figures and images for this document are available on the storage device. The software is also available online in the linked GitHub repository. The software version last used for this document is tagged with the name: `master-submission` The following artefacts can be found in these locations.

8.2.1 Additional Figures

Additional Figures can be found in the "Image" folder on the storage Medium.

8.2.2 Data

The data is stored in multiple subfolders. The `Data` folder contains the different cities as subfolders, within each of these folders, there is a `dataset` folder, containing a `xarray` dataset named *dataXarrayCITY_NAME.nc* of the used area of interest, including all bands and the classifiction at all times analysed during this project. The `dataXarrayCITY_NAME_feat.nc` contains the extracted feature bands from the Gabor feature extraction. The `ML_Model` folder contains a "pickeled" k-means model, a file containing a numpy array with cluster centres for the label assignment.

8.2.3 Code

The src.zip contains the python code used for generating the data, the documentation of the code is located within the doc folder. For the description and starting point of the software see Section 7.7.2. The following folder structure was used for the code artefacts:

- The main folder contains scripts that run and process data directly
- The folder *preprocessing* contains scripts for processing and preparing land sat images

- The *processing* folder contains scripts to calculate different indices and prepare the surface classification of the Landsat Data
- The *visualisation* folder contains helper functions for plotting images

References

Alkan-Bala, Havva and Taner Üstüntaş (Mar. 2014). "Modelling the Urban Interface by Using Fuzzy Logic". en. In: *Journal of Building Construction and Planning Research* 2.1, pp. 59–73. DOI: 10.4236/jbcpr.2014.21006. URL: https://www.scirp.org/journal/paperinformation.aspx?paperid=44262 (visited on 02/25/2024).

Andrae, Linus (Oct. 2023). *Automated detection of Urban Heat Islands using remote sensing data.*

AutoGluon (2024). en. URL: https://auto.gluon.ai/index.html (visited on 02/21/2024).

Baccini, Michela et al. (Sept. 2008). "Heat Effects on Mortality in 15 European Cities". en-US. In: *Epidemiology* 19.5, p. 711. ISSN: 1044-3983. DOI: 10.1097/EDE.0b013e318176bfcd. URL: https://journals.lww.com/epidem/fulltext/2008/09000/The_Time_Course_of_Weather_Related_Deaths.00013.aspx?casa_token=eNZv8dUc69AAAAAA:0LbPhhgrywnV-JSUqxMyilUw8cGaojk5G5aDIFH_utCeBduijlHOCFs6nufZ7K7idcT6daDFqJM8DxuLg6NcgkGoolVHN4mjZ (visited on 04/25/2024).

Bador, Margot, Laurent Terray, and Julien Boé (May 2016). "Detection of anthropogenic influence on the evolution of record-breaking temperatures over Europe". en. In: *Climate Dynamics* 46.9, pp. 2717–2735. ISSN: 1432-0894. DOI: 10.1007/s00382-015-2725-8. URL: https://doi.org/10.1007/s00382-015-2725-8 (visited on 05/02/2024).

Bell, Michelle L, Devra L Davis, and Tony Fletcher (Jan. 2004). "A retrospective assessment of mortality from the London smog episode of 1952: the role of influenza and pollution." In: *Environmental Health Perspectives* 112.1, pp. 6–8. ISSN: 0091-6765. URL: https://www.ncbi.nlm.nih.gov/pmc/articles/PMC1241789/ (visited on 05/03/2024).

Block, Ronald (July 1978). "Development of Thermal Infrared Imagery to the Detection of Urban Heat Islands". In: *Open Access Master's Theses (through 2010)*. URL: https://digitalcommons.unl.edu/opentheses/16.

Burrough, P. A., P. F. M. van Gaans, and R. A. MacMillan (July 2000). "High-resolution landform classification using fuzzy k-means". In: *Fuzzy Sets and Systems* 113.1, pp. 37–52. ISSN: 0165-0114. DOI: 10.1016/S0165-0114(99)00011-1. URL: https://www.sciencedirect.com/science/article/pii/S0165011499000111 (visited on 05/05/2024).

Camps-Valls, Gustau and Lorenzo Bruzzone (Sept. 2009). *Kernel Methods for Remote Sensing Data Analysis*. en. Google-Books-ID: _KhUMXQQkmQC. John Wiley & Sons. ISBN: 9780470749005.

Carlson, T. N., J. A. Augustine, and F. E. Boland (1977). "Potential Application of Satellite Temperature Measurements in the Analysis of Land Use over Urban Areas". In:

Bulletin of the American Meteorological Society 58.12, pp. 1301–1303. ISSN: 0003-0007. URL: https://www.jstor.org/stable/26218022 (visited on 01/04/2024).

Cassano, John (2010). *Heat Index Calculator*. URL: https://atoc.colorado.edu/~cassano/wx_calculator/formulas/heatIndex.html.

CEOS (Mar. 2024). *Sentinel LSTM-A*. online. URL: https://database.eohandbook.com/database/missionsummary.aspx?missionID=1041.

Cerdan, R. (1993). "Image Ultracompactification Mathematical Model". In: *WIT Transactions on Information and Communication Technologies*. Vol. 2, p. 12. DOI: 10.2495/AIENG930322.

Chandler, T. J. (1961). "The Changing Form of London's Heat-island". In: *Geography* 46.4, pp. 295–307. ISSN: 0016-7487. URL: https://www.jstor.org/stable/40565541 (visited on 01/04/2024).

Dask Development Team (2022). *Dask: Library for dynamic task scheduling*. URL: http://dask.org.

Deutscher Wetter Dienst (Mar. 2024a). *Wetter und Klima - Deutscher Wetterdienst - Bremen*. en. online. URL: https://www.dwd.de/EN/weather/weather_climate_local/lower-saxony_bremen/bremen/_node.html (visited on 03/17/2024).

– (Mar. 2024b). *Wetter- und Klimalexikon*. en. online. URL: https://www.dwd.de/DE/service/lexikon/Functions/glossar.html?lv3=101162&lv2=101094 (visited on 03/17/2024).

Dimoudi, Argiro and Marialena Nikolopoulou (Jan. 2003). "Vegetation in the urban environment: microclimatic analysis and benefits". In: *Energy and Buildings*. Special issue on urban research 35.1, pp. 69–76. ISSN: 0378-7788. DOI: 10.1016/S0378-7788(02)00081-6. URL: https://www.sciencedirect.com/science/article/pii/S0378778802000816 (visited on 02/25/2024).

Duckworth, Fowler S. and James S. Sandberg (May 1954). "The Effect of Cities upon Horizontal and Vertical Temperature Gradients". en. In: *Bulletin of the American Meteorological Society* 35.5, pp. 198–207. ISSN: 0003-0007, 1520-0477. DOI: 10.1175/1520-0477-35.5.198. URL: https://journals.ametsoc.org/view/journals/bams/35/5/1520-0477-35_5_198.xml (visited on 01/04/2024).

Earth Resources Observation And Science (EROS) Center (2013). *Collection-2 Landsat 8-9 OLI (Operational Land Imager) and TIRS (Thermal Infrared Sensor) Level-2 Science Products*. Type: dataset. DOI: 10.5066/P9OGBGM6. URL: https://www.usgs.gov/centers/eros/science/usgs-eros-archive-landsat-archives-landsat-8-9-olitirs-collection-2-level-2 (visited on 09/16/2023).

Ebi, Kristie L. and Glenn McGregor (Nov. 2008). "Climate Change, Tropospheric Ozone and Particulate Matter, and Health Impacts". In: *Environmental Health Perspectives* 116.11, pp. 1449–1455. ISSN: 1552-9924. DOI: 10.1289/ehp.11463.

ESRI LULC (2024). *Impact Observatory | Sentinel-2 10m land cover time series of the world from 2017-2021*. en. URL: https://www.esri.com/partners/impact-observatory-a2T5x0000084pJXEAY/sentinel-2-10m-land--a2d5x000005jw9NAAQ (visited on 04/22/2024).

Extreme heat (Oct. 2022). *Extreme heat: Preparing for the heat waves of the future | IFRC*. en. URL: https://www.ifrc.org/document/extreme-heat-preparing-heat-waves-future (visited on 04/25/2024).

Fabrizi, Roberto, Stefania Bonafoni, and Riccardo Biondi (May 2010). "Satellite and Ground-Based Sensors for the Urban Heat Island Analysis in the City of Rome". en. In: *Remote Sensing* 2.5, pp. 1400–1415. ISSN: 2072-4292. DOI: 10.3390/rs2051400. URL: https://www.mdpi.com/2072-4292/2/5/1400 (visited on 05/03/2024).

Fallmann, Joachim, Renate Forkel, and Stefan Emeis (Jan. 2016). "Secondary effects of urban heat island mitigation measures on air quality". In: *Atmospheric Environment* 125, pp. 199–211. ISSN: 1352-2310. DOI: 10.1016/j.atmosenv.2015.10.094. URL: https://www.sciencedirect.com/science/article/pii/S1352231015305094 (visited on 05/06/2024).

Fayad, Fadye Al, Wahid Maref, and Mohamed M. Awad (Jan. 2021). "Review of White Roofing Materials and Emerging Economies with Focus on Energy Performance Cost-Benefit, Maintenance, and Consumer Indifference". en. In: *Sustainability* 13.17, p. 9967. ISSN: 2071-1050. DOI: 10.3390/su13179967. URL: https://www.mdpi.com/2071-1050/13/17/9967 (visited on 02/25/2024).

Feyisa, Gudina Legese, Klaus Dons, and Henrik Meilby (Mar. 2014). "Efficiency of parks in mitigating urban heat island effect: An example from Addis Ababa". In: *Landscape and Urban Planning* 123, pp. 87–95. ISSN: 0169-2046. DOI: 10.1016/j.landurbplan.2013.12.008. URL: https://www.sciencedirect.com/science/article/pii/S0169204613002399 (visited on 02/25/2024).

Foster, J. L., J. P. Ormsby, and R. J. Gurney (1981). "Satellite Observations of England and North-Western Europe". en. In: *Weather* 36.9, pp. 252–259. ISSN: 1477-8696. DOI: 10.1002/j.1477-8696.1981.tb05416.x. URL: https://onlinelibrary.wiley.com/doi/abs/10.1002/j.1477-8696.1981.tb05416.x (visited on 01/04/2024).

Gabriel, Katharina M. A. and Wilfried R. Endlicher (Aug. 2011). "Urban and rural mortality rates during heat waves in Berlin and Brandenburg, Germany". In: *Environmental Pollution*. Selected papers from the conference Urban Environmental Pollution: Overcom-

ing Obstacles to Sustainability and Quality of Life (UEP2010), 20-23 June 2010, Boston, USA 159.8, pp. 2044–2050. ISSN: 0269-7491. DOI: 10.1016/j.envpol.2011.01.016. URL: https://www.sciencedirect.com/science/article/pii/S0269749111000388 (visited on 04/25/2024).

Gartland, Lisa Mummery (2008). *Heat Islands. Understanding and Mitigating Heat in Urban Areas*. Description based on publisher supplied metadata and other sources. London. URL: http://katalog.suub.uni-bremen.de/DB=1/LNG=DU/CMD?ACT=SRCHA%5C&IKT=8000%5C&TRM=88877316*.

Ghazvinian, Hamidreza et al. (Nov. 2021). "Introducing affordable and accessible physical covers to reduce evaporation from agricultural water reservoirs and pools (field study, statistics, and intelligent methods)". en. In: *Arabian Journal of Geosciences* 14.23, p. 2543. ISSN: 1866-7538. DOI: 10.1007/s12517-021-08735-3. URL: https://doi.org/10.1007/s12517-021-08735-3 (visited on 05/07/2024).

Guenther, Alex et al. (Jan. 2000). "Natural emissions of non-methane volatile organic compounds, carbon monoxide, and oxides of nitrogen from North America". In: *Atmospheric Environment* 34.12, pp. 2205–2230. ISSN: 1352-2310. DOI: 10.1016/S1352-2310(99)00465-3. URL: https://www.sciencedirect.com/science/article/pii/S1352231099004653 (visited on 02/24/2024).

Haeger-Eugensson, Marie and Björn Holmer (1999). "Advection caused by the urban heat island circulation as a regulating factor on the nocturnal urban heat island". en. In: *International Journal of Climatology* 19.9, pp. 975–988. ISSN: 1097-0088. DOI: 10.1002/(SICI)1097-0088(199907)19:9<975::AID-JOC399>3.0.CO;2-J. URL: https://onlinelibrary.wiley.com/doi/abs/10.1002/%28SICI%291097-0088%28199907%2919%3A9%3C975%3A%3AAID-JOC399%3E3.0.CO%3B2-J (visited on 09/10/2023).

He, Bao-Jie et al. (July 2019). "Co-benefits approach: Opportunities for implementing sponge city and urban heat island mitigation". In: *Land Use Policy* 86, pp. 147–157. ISSN: 0264-8377. DOI: 10.1016/j.landusepol.2019.05.003. URL: https://www.sciencedirect.com/science/article/pii/S0264837718308111 (visited on 04/02/2024).

Howard, Luke (1833). *The Climate of London: Deduced from Meteorological Observations Made in the Metropolis and at Various Places Around it*. en. Google-Books-ID: L0g0AQAAMAAJ. Harvey, Darton, J., and A. Arch, Longman, Hatchard, S. Highley [and] R. Hunter.

Hoyer, S. and J. Hamman (2017). "xarray: N-D labeled arrays and datasets in Python". In: *Journal of Open Research Software* 5.1. DOI: 10.5334/jors.148. URL: https://doi.org/10.5334/jors.148.

ISO (2024). *ISO 7243:2017*. en. URL: https://www.iso.org/standard/67188.html (visited on 01/04/2024).

Kagi Inc. (2024). *Kagi Summerizer*. URL: https://kagi.com/summarizer/index.html.

Kanakidou, Maria et al. (Feb. 2011). "Megacities as hot spots of air pollution in the East Mediterranean". In: *Atmospheric Environment* 45.6, pp. 1223–1235. ISSN: 1352-2310. DOI: 10.1016/j.atmosenv.2010.11.048. URL: https://www.sciencedirect.com/science/article/pii/S1352231010010162 (visited on 01/03/2024).

Kansal, Ankur (July 2009). "Sources and reactivity of NMHCs and VOCs in the atmosphere: A review". In: *Journal of Hazardous Materials* 166.1, pp. 17–26. ISSN: 0304-3894. DOI: 10.1016/j.jhazmat.2008.11.048. URL: https://www.sciencedirect.com/science/article/pii/S0304389408017391 (visited on 02/24/2024).

Karakuş, Can Bülent (Nov. 2019). "The Impact of Land Use/Land Cover (LULC) Changes on Land Surface Temperature in Sivas City Center and Its Surroundings and Assessment of Urban Heat Island". en. In: *Asia-Pacific Journal of Atmospheric Sciences* 55.4, pp. 669–684. ISSN: 1976-7951. DOI: 10.1007/s13143-019-00109-w. URL: https://doi.org/10.1007/s13143-019-00109-w (visited on 04/04/2024).

Keras Development Team (2024). *Keras documentation: Code examples*. en. URL: https://keras.io/examples/ (visited on 02/21/2024).

Köppen, Wladimir and Rudolf Geiger (1930). *Handbuch der klimatologie*. Vol. 1. Gebrüder Borntraeger Berlin.

Landsberg, Helmut E. (May 1979). "Atmospheric changes in a growing community (the Columbia, Maryland experience)". In: *Urban Ecology* 4.1, pp. 53–81. ISSN: 0304-4009. DOI: 10.1016/0304-4009(79)90023-8. URL: https://www.sciencedirect.com/science/article/pii/0304400979900238 (visited on 01/04/2024).

Launching a Cross-Agency Temperature Network (2024). en-US. URL: https://fas.org/publication/cross-agency-heat-monitoring/ (visited on 04/25/2024).

LES (2024). *PT-100 Accuracy*. online. URL: %7Bhttps://www.epicsensors.com/en/faq/what-are-the-pt100-accuracy-classes/%7D.

Leung, Dennis Y. C. (Jan. 2015). "Outdoor-indoor air pollution in urban environment: challenges and opportunity". In: *Frontiers in Environmental Science* 2. ISSN: 2296-665X. DOI: 10.3389/fenvs.2014.00069. URL: https://www.frontiersin.org/articles/10.3389/fenvs.2014.00069.

"Chapter 7 - Land surface temperature and thermal infrared emissivity" (Jan. 2020). In: ed. by Shunlin Liang and Jindi Wang. Academic Press, pp. 251–295. ISBN: 9780128158265.

DOI: 10.1016/B978-0-12-815826-5.00007-6. URL: https://www.sciencedirect.com/science/article/pii/B9780128158265000076 (visited on 09/19/2023).

Ljungberg, Sven-Ake and R Norberg (1980). "Use of aerial thermography in urban areas". In: *Proc. 14th International Congress for Photogrammetry (Hamburg.*

Matson, Michael et al. (1978). "Satellite Detection of Urban Heat Islands". In: *Monthly Weather Review* 106.12, pp. 1725–1734. DOI: https://doi.org/10.1175/1520-0493(1978)106<1725:SDOUHI>2.0.CO;2. URL: https://journals.ametsoc.org/view/journals/mwre/106/12/1520-0493_1978_106_1725_sdouhi_2_0_co_2.xml.

Maxwell, Aaron E., Timothy A. Warner, and Fang Fang (May 2018). "Implementation of machine-learning classification in remote sensing: an applied review". In: *International Journal of Remote Sensing* 39.9, pp. 2784–2817. ISSN: 0143-1161. DOI: 10.1080/01431161.2018.1433343. URL: https://doi.org/10.1080/01431161.2018.1433343 (visited on 05/09/2024).

McDuffie, Erin E. et al. (June 2021). "Source sector and fuel contributions to ambient PM2.5 and attributable mortality across multiple spatial scales". en. In: *Nature Communications* 12.1, p. 3594. ISSN: 2041-1723. DOI: 10.1038/s41467-021-23853-y. URL: https://www.nature.com/articles/s41467-021-23853-y (visited on 05/03/2024).

Mudway, I. S. and F. J. Kelly (Mar. 2000). "Ozone and the lung: a sensitive issue". In: *Molecular Aspects of Medicine* 21.1, pp. 1–48. ISSN: 0098-2997. DOI: 10.1016/S0098-2997(00)00003-0. URL: https://www.sciencedirect.com/science/article/pii/S0098299700000030 (visited on 04/01/2024).

Nemery, Benoit, Peter HM Hoet, and Abderrahim Nemmar (Mar. 2001). "The Meuse Valley fog of 1930: an air pollution disaster". English. In: *The Lancet* 357.9257, pp. 704–708. ISSN: 0140-6736, 1474-547X. DOI: 10.1016/S0140-6736(00)04135-0. URL: https://www.thelancet.com/journals/lancet/article/PIIS0140-6736(00)04135-0/abstract (visited on 04/23/2024).

Nichol, Janet (Jan. 1994). "A GIS-Based Approach to Microclimate Monitoring in Singapore's High-Rise Housing Estates". In: *Photogrammetric Engineering & Remote Sensing* 60, pp. 1225–1232.

Oke, T. (1968). "-1 - TOWARDS A MORE RATIONAL UNDERSTANDING OF THE URBAN HEAT ISLAND". In.

OpenAI (2023). *ChatGPT*. Accessed: 2024-05-09. URL: https://www.openai.com/chatgpt.

Otero, Noelia, Henning W. Rust, and Tim Butler (May 2021). "Temperature dependence of tropospheric ozone under NOx reductions over Germany". In: *Atmospheric Environment*

253, p. 118334. ISSN: 1352-2310. DOI: 10.1016/j.atmosenv.2021.118334. URL: https://www.sciencedirect.com/science/article/pii/S1352231021001527 (visited on 04/01/2024).

Pedregosa, F. et al. (2011). "Scikit-learn: Machine Learning in Python". In: *Journal of Machine Learning Research* 12, pp. 2825–2830.

Peppler, Albert (1929). "Das auto als hilfsmittel der meteorologischen forschung". In: *Das Wetter* 46, pp. 305–308.

Piracha, Awais and Muhammad Tariq Chaudhary (2022). "Urban Air Pollution, Urban Heat Island and Human Health: A Review of the Literature". In: DOI: .org/10.3390/su14159234.

Pontes, Renan Hatakeyama et al. (Mar. 2022). "Adapting the Olgyay bioclimatic chart to assess local thermal comfort levels in urban regions". en. In: *Clean Technologies and Environmental Policy* 24.2, pp. 661–675. ISSN: 1618-9558. DOI: 10.1007/s10098-021-02158-0. URL: https://doi.org/10.1007/s10098-021-02158-0 (visited on 05/06/2024).

Ramamurthy, P. and E. Bou-Zeid (2017). "Heatwaves and urban heat islands: A comparative analysis of multiple cities". en. In: *Journal of Geophysical Research: Atmospheres* 122.1, pp. 168–178. ISSN: 2169-8996. DOI: 10.1002/2016JD025357. URL: https://onlinelibrary.wiley.com/doi/abs/10.1002/2016JD025357 (visited on 09/03/2023).

Ramamurthy, Prathap et al. (Sept. 2014). "Influence of Subfacet Heterogeneity and Material Properties on the Urban Surface Energy Budget". EN. In: *Journal of Applied Meteorology and Climatology* 53.9, pp. 2114–2129. ISSN: 1558-8424, 1558-8432. DOI: 10.1175/JAMC-D-13-0286.1. URL: https://journals.ametsoc.org/view/journals/apme/53/9/jamc-d-13-0286.1.xml (visited on 09/03/2023).

Renou, E (1862). "Différences de température entre, Paris et Choisy-le-Roi". In: *Annuaire Société Météorologique de France* 10, pp. 105–109.

Rodrigues, Francisco A. (Nov. 2023). "Machine learning in physics: A short guide". en. In: *Europhysics Letters* 144.2, p. 22001. ISSN: 0295-5075. DOI: 10.1209/0295-5075/ad0575. URL: https://dx.doi.org/10.1209/0295-5075/ad0575 (visited on 05/09/2024).

Romps, David M. and Yi-Chuan Lu (Aug. 2022). "Chronically underestimated: a reassessment of US heat waves using the extended heat index". en. In: *Environmental Research Letters* 17.9, p. 094017. ISSN: 1748-9326. DOI: 10.1088/1748-9326/ac8945. URL: https://dx.doi.org/10.1088/1748-9326/ac8945 (visited on 05/04/2024).

Sachindra, D. A. et al. (2016). "Impact of climate change on urban heat island effect and extreme temperatures: a case-study". en. In: *Quarterly Journal of the Royal Meteorological Society* 142.694, pp. 172–186. ISSN: 1477-870X. DOI: 10.1002/qj.2642. URL: https://onlinelibrary.wiley.com/doi/abs/10.1002/qj.2642 (visited on 09/16/2023).

Santamouris, M. (Jan. 2020). "Recent progress on urban overheating and heat island research. Integrated assessment of the energy, environmental, vulnerability and health impact. Synergies with the global climate change". In: *Energy and Buildings* 207, p. 109482. ISSN: 0378-7788. DOI: 10.1016/j.enbuild.2019.109482. URL: https://www.sciencedirect.com/science/article/pii/S0378778819326696 (visited on 10/08/2023).

Schoen, Carl (Sept. 2005). "A New Empirical Model of the Temperature–Humidity Index". EN. In: *Journal of Applied Meteorology and Climatology* 44.9, pp. 1413–1420. ISSN: 1520-0450, 0894-8763. DOI: 10.1175/JAM2285.1. URL: https://journals.ametsoc.org/view/journals/apme/44/9/jam2285.1.xml (visited on 05/06/2024).

Sinaga, Kristina P. and Miin-Shen Yang (2020). "Unsupervised K-Means Clustering Algorithm". In: *IEEE Access* 8, pp. 80716–80727. ISSN: 2169-3536. DOI: 10.1109/ACCESS.2020.2988796. URL: https://ieeexplore.ieee.org/document/9072123#:~:text=The%20k-means%20algorithm%20is%20generally%20the%20most%20known%20and%20used%20clustering%20method (visited on 02/22/2024).

Smith, Randall P. (Jan. 2012). *Introduction to Hyperspectral Imageing*. online. URL: https://www.microimages.com/documentation/Tutorials/hyprspec.pdf.

Sobrino, José Antonio and Itziar Irakulis (June 2020). "A Methodology for Comparing the Surface Urban Heat Island in Selected Urban Agglomerations Around the World from Sentinel-3 SLSTR Data". In: *Remote Sensing* 12.12, p. 2052. ISSN: 2072-4292. DOI: 10.3390/rs12122052.

Steadman, R. G. (July 1979). "The Assessment of Sultriness. Part I: A Temperature-Humidity Index Based on Human Physiology and Clothing Science". EN. In: *Journal of Applied Meteorology and Climatology* 18.7, pp. 861–873. ISSN: 1520-0450. DOI: 10.1175/1520-0450(1979)018<0861:TAOSPI>2.0.CO;2. URL: https://journals.ametsoc.org/view/journals/apme/18/7/1520-0450_1979_018_0861_taospi_2_0_co_2.xml (visited on 01/31/2024).

Stewart, I. D. (Jan. 2011). "A systematic review and scientific critique of methodology in modern urban heat island literature". en. In: *International Journal of Climatology* 31.2, pp. 200–217. ISSN: 1097-0088. DOI: 10.1002/joc.2141. URL: https://onlinelibrary.wiley.com/doi/abs/10.1002/joc.2141 (visited on 10/08/2023).

Tollner, Hanns (1932). *Untersuchungen über die Temperaturverteilung in der Stadt Wien im Sommer 1931*. Hölder-Pichler-Tempsky.

U.S. Environmental Protection Agency (EPA) (2008). "Reducing urban heat islands: Compendium of strategies". In: URL: https://www.epa.gov/heatislands/heat-island-compendium.

U.S. Geological Survey (Feb. 2024). *Landsat Archive Dashboard*. online. URL: https://landsat.usgs.gov/landsat-archive-dashboard.

Uhe, P. et al. (2016). "Comparison of methods: Attributing the 2014 record European temperatures to human influences". en. In: *Geophysical Research Letters* 43.16, pp. 8685–8693. ISSN: 1944-8007. DOI: 10.1002/2016GL069568. URL: https://onlinelibrary.wiley.com/doi/abs/10.1002/2016GL069568 (visited on 04/23/2024).

USGS (2014). *Landsat Sensor Spectral Coverage*. Tech. rep. USGS. URL: https://www.usgs.gov/media/images/spectral-bandpasses-all-landsat-sensors.

Van Oldenborgh, Geert Jan et al. (2022). "Attributing and Projecting Heatwaves Is Hard: We Can Do Better". en. In: *Earth's Future* 10.6, e2021EF002271. ISSN: 2328-4277. DOI: 10.1029/2021EF002271. URL: https://onlinelibrary.wiley.com/doi/abs/10.1029/2021EF002271 (visited on 04/23/2024).

Vanos, Jennifer K. et al. (Feb. 2022). "Evaporative misters for urban cooling and comfort: effectiveness and motivations for use". en. In: *International Journal of Biometeorology* 66.2, pp. 357–369. ISSN: 1432-1254. DOI: 10.1007/s00484-020-02056-y. URL: https://doi.org/10.1007/s00484-020-02056-y (visited on 05/04/2024).

Walt, Stéfan van der et al. (June 2014). "scikit-image: image processing in Python". In: *PeerJ* 2, e453. ISSN: 2167-8359. DOI: 10.7717/peerj.453. URL: https://doi.org/10.7717/peerj.453.

Wang, Z., E.P. Simoncelli, and A.C. Bovik (Nov. 2003). "Multiscale structural similarity for image quality assessment". In: *The Thrity-Seventh Asilomar Conference on Signals, Systems & Computers, 2003*. Vol. 2, 1398–1402 Vol.2. DOI: 10.1109/ACSSC.2003.1292216. URL: https://ieeexplore.ieee.org/document/1292216 (visited on 05/10/2024).

Wang, Zhou et al. (Apr. 2004). "Image quality assessment: from error visibility to structural similarity". In: *IEEE Transactions on Image Processing* 13.4, pp. 600–612. ISSN: 1941-0042. DOI: 10.1109/TIP.2003.819861. URL: https://ieeexplore.ieee.org/document/1284395 (visited on 04/29/2024).

Watson, K. (Jan. 1975). "Geologic applications of thermal infrared images". In: *Proceedings of the IEEE* 63.1, pp. 128–137. ISSN: 1558-2256. DOI: 10.1109/PROC.1975.9712.

URL: https://ieeexplore.ieee.org/abstract/document/1451642 (visited on 01/04/2024).

Weng, Qihao (May 2003). "Fractal Analysis of Satellite-Detected Urban Heat Island Effect". In: *Photogrammetric Engineering & Remote Sensing* 69.5, pp. 555–566. DOI: 10.14358/pers.69.5.555.

Weng, Qihao, Dengsheng Lu, and Jacquelyn Schubring (Feb. 2004). "Estimation of land surface temperature–vegetation abundance relationship for urban heat island studies". en. In: *Remote Sensing of Environment* 89.4, pp. 467–483. ISSN: 0034-4257. DOI: 10.1016/j.rse.2003.11.005. URL: https://www.sciencedirect.com/science/article/pii/S0034425703003390 (visited on 01/15/2023).

Wilby, Robert L (Oct. 2008). "Constructing Climate Change Scenarios of Urban Heat Island Intensity and Air Quality". en. In: *Environment and Planning B: Planning and Design* 35.5, pp. 902–919. ISSN: 0265-8135. DOI: 10.1068/b33066t. URL: https://journals.sagepub.com/doi/abs/10.1068/b33066t (visited on 09/16/2023).

Wilke, Sibylle (Sept. 2023). *Indicator: Hot days*. en. URL: https://www.umweltbundesamt.de/en/data/environmental-indicators/indicator-hot-days (visited on 05/03/2024).

Zanter, K. (Nov. 2019). *Landsat 8 (L8) Data User Handbook*. 5.0. LSDS-1574. U.S. Geological Survey. Siux Falls, South Dakota.

Zhang, Jinnan (2024). *Esri | Sentinel-2 Land Cover Explorer*. URL: https://livingatlas.arcgis.com/landcoverexplorer/ (visited on 02/22/2024).

Eigenständigkeitserklärung

Universität Bremen

Nachname **Andrae** Matrikelnr. **6015384**

Vorname **Linus**

Hinweise zu den offiziellen Erklärungen

1. Die folgende Seite mit den offiziellen Erklärungen
   A) Eigenständigkeitserklärung
   B) Erklärung zur Veröffentlichung von Bachelor- oder Masterarbeiten
   C) Einverständniserklärung über die Bereitstellung und Nutzung der Bachelorarbeit / Masterarbeit in elektronischer Form zur Überprüfung durch eine Plagiatssoftware

   ist entweder direkt in jedes Exemplar der Bachelor- oder Masterarbeit fest mit einzubinden oder unverändert im Wortlaut in jedes Exemplar der Bachelor- oder Masterarbeit zu übernehmen.

   Bitte achten Sie darauf, jede Erklärung in allen drei Exemplaren der Arbeit zu unterschreiben.

2. In der digitalen Fassung kann auf die Unterschrift verzichtet werden. Die Angaben und Entscheidungen müssen jedoch enthalten sein.

Zu B)

Die Einwilligung kann jederzeit durch Erklärung gegenüber der Universität Bremen, mit Wirkung für die Zukunft, widerrufen werden.

Zu C)

Das Einverständnis der dauerhaften Speicherung des Textes ist freiwillig.

Die Einwilligung kann jederzeit durch Erklärung gegenüber der Universität Bremen, mit Wirkung für die Zukunft, widerrufen werden.

Weitere Informationen zur Überprüfung von schriftlichen Arbeiten durch die Plagiatsoftware sind im Nutzungs- und Datenschutzkonzept enthalten. Diese finden Sie auf der Internetseite der Universität Bremen.

Universität Bremen

Nachname Andrae Matrikelnr. 6015384

Vorname Linus

A) Eigenständigkeitserklärung

Ich versichere, dass ich die vorliegende Arbeit selbstständig verfasst und keine anderen als die angegebenen Quellen und Hilfsmittel verwendet habe. Alle Teile meiner Arbeit, die wortwörtlich oder dem Sinn nach anderen Werken entnommen sind, wurden unter Angabe der Quelle kenntlich gemacht. Gleiches gilt auch für Zeichnungen, Skizzen, bildliche Darstellungen sowie für Quellen aus dem Internet, dazu zählen auch KI-basierte Anwendungen oder Werkzeuge. Die Arbeit wurde in gleicher oder ähnlicher Form noch nicht als Prüfungsleistung eingereicht. Die elektronische Fassung der Arbeit stimmt mit der gedruckten Version überein. Mir ist bewusst, dass wahrheitswidrige Angaben als Täuschung behandelt werden.

☒ Ich habe KI-basierte Anwendungen und/oder Werkzeuge genutzt und diese im Anhang "Nutzung KI basierte Anwendungen" dokumentiert.

B) Erklärung zur Veröffentlichung von Bachelor- oder Masterarbeiten

Die Abschlussarbeit wird zwei Jahre nach Studienabschluss dem Archiv der Universität Bremen zur dauerhaften Archivierung angeboten. Archiviert werden:

1) Masterarbeiten mit lokalem oder regionalem Bezug sowie pro Studienfach und Studienjahr 10 % aller Abschlussarbeiten
2) Bachelorarbeiten des jeweils ersten und letzten Bachelorabschlusses pro Studienfach und Jahr.

☒ Ich bin damit einverstanden, dass meine Abschlussarbeit im Universitätsarchiv für wissenschaftliche Zwecke von Dritten eingesehen werden darf.

☒ Ich bin damit einverstanden, dass meine Abschlussarbeit nach 30 Jahren (gem. §7 Abs. 2 BremArchivG) im Universitätsarchiv für wissenschaftliche Zwecke von Dritten eingesehen werden darf.

☐ Ich bin nicht damit einverstanden, dass meine Abschlussarbeit im Universitätsarchiv für wissenschaftliche Zwecke von Dritten eingesehen werden darf.

C) Einverständniserklärung zur Überprüfung der elektronischen Fassung der Bachelorarbeit / Masterarbeit durch Plagiatssoftware

Eingereichte Arbeiten können nach § 18 des Allgemeinen Teil der Bachelor- bzw. der Master-prüfungsordnungen der Universität Bremen mit qualifizierter Software auf Plagiatsvorwürfe untersucht werden.
Zum Zweck der Überprüfung auf Plagiate erfolgt das Hochladen auf den Server der von der Universität Bremen aktuell genutzten Plagiatssoftware.

☒ Ich bin damit einverstanden, dass die von mir vorgelegte und verfasste Arbeit zum oben genannten Zweck dauerhaft auf dem externen Server der aktuell von der Universität Bremen genutzten Plagiatssoftware, in einer institutionseigenen Bibliothek (Zugriff nur durch die Universität Bremen), gespeichert wird.

☐ Ich bin nicht damit einverstanden, dass die von mir vorgelegte und verfasste Arbeit zum o.g. Zweck dauerhaft auf dem externen Server der aktuell von der Universität Bremen genutzten Plagiatssoftware, in einer institutionseigenen Bibliothek (Zugriff nur durch die Universität Bremen), gespeichert wird.

PDFSigning Certificate
Signiert von : PDFSigningCertificate
Datum: 2024-05-09 11:23:06 CEST

09.05.2024

Datum Unterschrift